Wave regimes and mass transfer in two-layer falling films

by

Gökçen Çekiç

A thesis submitted to
The University of Birmingham
for the degree of
Doctor of Philosophy

School of Mathematics
The University of Birmingham
September 2014

Abstract

In this thesis, two-layer film flows down a vertical wall are studied. The integral method is used to derive an approximate system of evolution equations modelling long-wave flows of the film. Then, families of nonlinear steady-travelling periodic waves are computed. Computed waves have qualitatively similar behaviour to those found in one-layer films but the quantitative characteristics of the waves strongly depend on additional similarity parameters in the two-layer films. In particular, the average location of the interface between the layers affects the bifurcation scheme of the waves. To select the wave regimes which can be used to compare with experiments, systematic transient computations have been carried out to create a map of the attracting wave regimes, so-called dominating waves. For dominating wave regimes, the mass transfer problem for a weakly soluble gas is solved. In particularly, the absorption problem is systematically studied.

Dedicated to three magnificent women in my life:

my grandmother, mother and sister.

Acknowledgements

Above all, I would like to state my special thanks and appreciation to Dr. Grigory Sisoev for his splendid supervision and patience. I will be forever grateful to him for the time which he has spent educating me.

A special thanks to my mother and sister for their love and encouragement. Words cannot express how indebted I am to them. The support of my mother and sister has enabled me to fulfil my ambitions. I would also like to thank the rest of my family who supported me to come abroad for doing PhD.

I would like to thank my co-supervisor Prof. Yulii Shikhmurzaev for his fruitful discussions. I would also like to thank all of my friends and colleagues at the School of Mathematics at the University of Birmingham who made my time here interesting and enjoyable.

I am very lucky to have good friends in Birmingham, special and best friends in Turkey, who make me feel like at home in Birmingham. I feel gratitude to all of them for cheering me up through all times.

Finally I gratefully acknowledge the financial support of the IDB.

Contents

List of Figures

List of Tables

Chapter 1

Introduction

Hydrodynamics of one-layer films and immiscible two-layer films are intensively studied as they hold practical interest for many applications in environmental flows. It is also a key element of technological processes in chemical engineering, bioengineering, pharmaceutical industry and others. In particular, two-layer films are used in many technologies which facilitate mass and heat transfer between two viscous liquids which have different physical properties.

In previous theoretical studies of two-layer film flows, linear and weakly nonlinear models are exploited due to the complexity of the nonlinear problem. In this thesis, developed from [8], a strongly nonlinear model is used to solve the hydrodynamical problem and diffusion problem.

Hydrodynamics of a two-layer film flowing down a vertical wall is investigated under the assumptions that liquids in the layers are viscous, immiscible and incompressible. The superposition of the first layer adjacent to the second layer indicates a liquid-liquid interface. A sketch of the studied flow is demonstrated in Fig. 1.1.

A review of the theoretical and experimental works relevant to the problem studied in the thesis is discussed in this chapter. Then, the thesis is organized as follows: In Chapter 2, the approximate evolution equations modelling flows at real-life values of the

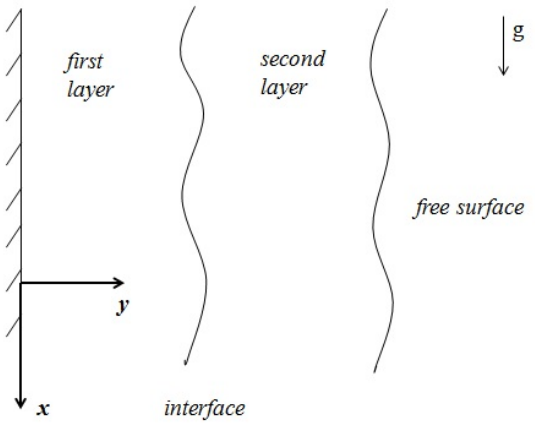

Figure 1.1: Physical picture of two-layer flow.

similarity parameters are derived. Linear stability of the waveless flow is analysed in the framework of the evolution equations and the generalized Orr-Sommerfeld problem to verify the model. After this, in Chapter 3, the method used to compute steady-travelling waves is given, and examples of the waves are shown. Attracting flow regimes are computed in numerous transient computations and these regimes are compared with found steady-travelling waves in Chapter 4. Then, in Chapter 5, mass transfer in regimes of dominating waves is studied. Finally, conclusions are provided in Chapter 6.

1.1 One-layer film flows

Modelling two-layer film flows is based on theoretical models for one-layer films which have been developing for a few decades starting from seminal works [34] and [35]. For this reason, we begin from a short review of the theory developed for the one-layer films.

Film flow down a vertical wall at moderate flow rates, or "falling films" have been considered later in numerous experimental and theoretical investigations [3]. In experiments, falling films demonstrate a wide variety of flow regimes, which are very sensitive to flow conditions. The systematic experimental investigation firstly carried out in [35] demonstrates that there is some critical flow rate at which waves on the liquid surface start to

appear or, at least, to be observed. If the flow rate is less than the critical one, the wave regime does not exist, or cannot be measured since its small amplitude. In addition to this, it was demonstrated that there is existence of two principal wave types: periodic sinusoidal waves and solitary waves, each is travelling with its own constant velocity. These so-called regular waves can take on different shapes, amplitudes and velocities depending on flow conditions.

[34] analysed linear and weakly nonlinear flows of a one-layer film down an inclined plane in the framework of the boundary layer approximation (unfortunately, a convective term was mistakenly omitted in the momentum equation). Linear stability analysis was first formulated comprehensively by [75] where the Orr-Sommerfeld problem [14] was solved by Yih with an expansion in powers of αRe where Re is the Reynolds number and α is the wavenumber. Yih's numerical results showed that the flow down a vertical plane is unstable for $\mathrm{Re} > 1.5$. However, it was proved in [5] that showed the neutral stability curve and values of the wave velocity were incorrect.

In his revision of Yih's formulation and method, Benjamin [5] calculated the neutral stability curves, and he obtained the critical Reynolds number $\mathrm{Re}_{cr} = (5\cot\theta)/6$ where θ is the inclination angle. In particular, it means that the vertical flow is always unstable since $\mathrm{Re}_{cr} = 0$ in this case. Nevertheless, when Re is small, the unstable waves' amplification factors become very small and that of wavelengths become very big. Benjamin's study provided to estimate the value of Re at which observable waves should first develop on a vertical water film as well as the length and the velocity of the waves.

Dependence of the neutral curves on the similarity parameters in the one-layer films was studied in [76] using the asymptotic method. In particular, there are two important outcomes:

a) The $\alpha = 0$ axis is always a part of the neutral curve,

b) When $\mathrm{Re} = (5\cot\theta)/6$, the bifurcation point exists on $\alpha = 0$ for the neutral stability

curve.

As mentioned above, the principal approach of theoretical investigation based on use of a long-wave approximation was suggested in [34]. The majority of theoretical results used to describe experimental data were reached in the framework of the Kapitza-Shkadov evolution equations derived in [52] by the integral method. This method was used to enable the consideration of the wave flow of the liquid as a non-linear problem, and it allowed to specify the parameters of the wave regime, amplitude, velocity, length and frequency.

In further theoretical papers, it has been found that the Kapitza-Shkadov model possesses a two-parametric manifold of solutions in the form of steady-travelling periodic waves, and this manifold includes wave regimes observed in experiments [65, 53].

The character of branching periodic steady-travelling wave solutions was analysed in the pioneering work [6] and further publications, see [9] where the review can be found. Stability and bifurcations of the wave families were studied in [68, 67, 69]. Studies of evolution of waves on a vertical falling film were carried out in many works, see [10] and references in there. In [65, 55, 56, 57], the families of the steady-travelling space-periodic waves and their bifurcations were revealed. In addition to these analysis, periodic waves in phase space and their mechanical meaning were discussed in [55, 57].

The manifold of steady-travelling space-periodic waves has nonuniqueness of solutions when more than one solutions exist at given values of the similarity parameters and the wavenumber. To use these solutions to describe experimental data, it was necessary to identify theoretical waves observed in experiments. To select such wave regimes theoretically, two principal approaches have been used. The first approach is to study the linear stability analysis of nonlinear waves, see [67, 69] where stable wave regimes or regimes with minimum amplification factor are found for the comparison with experiments. Another approach, see [13, 64, 63], is to find attractors of the evolution equations. The latter

method has led to discovering so-called dominating waves such that each is a solution with fastest velocity and largest amplitude among all steady-travelling space-periodic waves existing at given values of the similarity parameters and the wave frequency. Attracting oscillating regimes were also computed if the wavenumber is in some neighbourhood of fold bifurcations of a family of steady-travelling waves. This approach led to a map of dominating waves [64, 63] corresponding to the experimental data [63, 53].

Since Kapitza & Kapitza's experiments [35] for one-layer films, it has been known that it is impossible to observe steady-travelling periodic waves whose wave lengths exceed some critical value. In other words, existing of maximum finite spacing between principal humps in a sequence of quasi-solitary waves was showed experimentally. It was seen that the space between the humps decreases owing to the hydrodynamic instability for small values of wavenumber, and the critical wavelength was computed in [54].

For many years the Kapitza-Shkadov model [52] has been used as the main tool to explain experimental data and provides modelling possible flow regimes in one-layer film flows despite deriving other models. We just note that there are another approaches to the problem. For example, in [48, 49] weighted-residual method combined with standard long-wavelength expansion was used for film flows down inclined planes. The finite element method was also used to analyse the full Navier-Stokes equations in [50] and comparisons between the long-wave expansion and finite element method for increasing Reynolds number were given for large and small amplitude waves.

Existing knowledge of the wavy flow of falling thin liquid films was summarized in monographs [3] and [9] where numerous examples of flows of one-layer falling films were given.

1.2 Two-layer film flows

Studies on the one-layer film flow discussed in Section 1.1 was extended in [32] to the case of flow of a heterogeneous system which consists of two layers of viscous, incompressible and immiscible liquids. Long wave instability of the two-layer film flow was studied in this paper in the case of equal dynamic viscosities and different densities of the liquids. It was indicated that there are effects of the existence of the film surface and the interface on the hydrodynamic stability of the system. Kao analysed these effects with respect to surface disturbances and shear waves. Furthermore, a relation between the wavenumber α and the Reynolds number Re for given ratios of the densities of the liquids, depth rate and inclined angle was obtained. The axis $\alpha = 0$ in the (α, Re)-plane is part of the neutral stability curve, and it shows that the neutral oscillation can exist when $\mathrm{Re} = 0$ similar to the case of the one-layer film. The bifurcation point of this curve on $\alpha = 0$ was found. The critical Reynolds number for the two-layer flow where the density of the upper liquid is more than that of the lower liquid was calculated. It was also obtained that the stratification may lead to stability or instability depending on whether the density of the second layer is less or higher than that of the first layer. Finally, surface tension has a stabilising influence for long waves and small Reynolds numbers.

The stability of flow down an inclined plane under the role of the interface mode was also analysed in [31]. This mode is significant for the governing of the flow. When the ratio $\rho^{(2)}/\rho^{(1)}$, where $\rho^{(1)}$ and $\rho^{(2)}$ are densities of the first liquid adjoin to the wall and the second liquid with the free surface, respectively, is small, especially 1/10, interface and surface modes of instability were showed to compete each other to control the flow. In particular, if $\rho^{(2)}/\rho^{(1)} = 0.1$ at $(h^{(2)} - h^{(1)})/h^{(1)} < 1.6$, where $h^{(1)}$ and $h^{(2)}$ are thicknesses of the first layer and the film respectively, the stability is governed by the surface mode but for $(h^{(2)} - h^{(1)})/h^{(1)} > 1.6$ the stability is governed by the interface mode and the

similar results at $\rho^{(2)}/\rho^{(1)} = 0.3$ were demonstrated.

The general case of two modes in flow with viscous stratification was presented in [33] using the same method. It was found that the surface mode has a faster velocity than the interface mode in the long wave estimation. The interface instability happens under a critical Reynolds number for the surface mode. For instance, when $\mathrm{Re} \to 0$, the interface mode exists. The interface mode was named as inertialess instability because of the inertialess character of the destabilisation.

Linear stability of two-layer flow down an inclined plane was numerically investigated in the framework of the Orr-Sommerfeld problem in [62]. Two unstable modes associated with the free surface and the interface were computed at moderate values of the Reynolds number. It was shown that the modes have different physical meaning and compete each other depending on values of the similarity parameters. In examples, it was shown that the interface mode demonstrates the property of the Rayleigh-Taylor instability [14] depending on the ratio of the liquids' densities in the case of small wall inclination, and the effect of the density ratio depends on the value of the inclination. On the other hand, the interface mode is unstable if the less viscous liquid is in the region between the wall and interface, and it is stable in the opposite case.

[38] analysed the limit case of zero value of the Reynolds number and absence of the surface and interface tensions by using asymptotic method, and it has been demonstrated that it is not sufficient to investigate the behaviour of the system at all small wavenumbers if a consideration of the wavelength of the unstable mode is necessary. A significant conclusion of this paper is that when the less viscous layer is contiguous to the inclined wall, the flow is unstable at zero value of the Reynolds number. The most reinforced wave was demonstrated to have a wavelength comparable to the second layer thickness. In addition to this, the interface mode is unstable and this instability is owing to a stratification in the liquids' viscosity. The flow was shown to be stable to all disturbance

wavelengths at zero-Reynolds when the more viscous fluid is next to the inclined plane.

The calculations of this paper was extended in [11] to the case of thicker second layers for zero-Reynolds number flows. The Orr-Sommerfeld problem was used to investigate the interface and surface modes in the cases when both interface and surface tensions were zero, or the only surface tension was zero. The roles of the inertia and viscous stratification were illustrated with plots of the amplification factors and neutral curves. When the lower layer is less viscous, the stability of both the surface and interface modes can not occur simultaneously and wavy motion resulting from the instability can happen at any Reynolds number. For the contrary configuration with the more viscous fluid contiguous to the wall, under the certain conditions, the flow can become linearly stable.

[26] studied on the inertialess linear interface instability of inclined two-layer film flows at small inclination angle. The inertialess interface instability under the same zero-Reynolds number approximation as [38] was analysed under neglecting the surface tension effects, and the density stratification effects through a linear temporal approach were studied. It was demonstrated that increasing the density rate $\left(\rho^{(2)}/\rho^{(1)} > 1\right)$ has a destabilising influence but decreasing the density rate from 1 $\left(\rho^{(2)}/\rho^{(1)} < 1\right)$ has unsubstantial influence. Furthermore, the spatio-temporal nature (absolute or convective) of the instability of the two-layer film flow and where the stability is convective were investigated. The study of the properties of the spatially amplifying waves in the region of parameters was focused in [26, 27].

The effect of inertia on the temporal and spatiotemporal instabilities of the two-layer film flow was also studied in [27] and the effects of inertia and density stratification on both interface and surface modes were characterized for different depth and viscous ratios. A transition from convective to absolute instability [51] was appointed for the wall's small inclinations and for increasing inertia, various depth, density and viscosity ratios and the results compared to experimental data. In particular, it was detected that the absolute

instability in the two-layer flow is associated with he Rayleigh-Taylor instability [14] of the second mode as previously shown in [62]. The absolute instability appears in $\rho^{(2)} > \rho^{(1)}$ in the case of relatively small inclination angles.

The effect of viscosity stratification in two-layer flows was studied in [29] to designate the physical mechanism of suppression of the inertialess instability by using a kinetic energy balance approach. The mechanism of the long waves on the surface and interface at zero and very low values of the Reynolds number was discussed in this study. They also found that the shear stress at the unperturbed free surface is necessary to cause the inertialess interfacial instability.

In [18], an explanation of the mechanism for the long wave inertialess instability of a two-layer flow, which was extended the study of [66] for a one-layer film, was clarified. The mechanism was represented by examining the longitudinal perturbation velocity correlated with the surface and interface variations. It was shown that the velocity is stated with the composition of three parts; related to the shear stress at the free surface, the continuity case at the interface, and the pressure induced by gravity.

Another relevant area of research is the interface instability between two viscous flows. This type of instability was first studied in [77] by the asymptotic method [76] in the case of the plane Couette-Poiseulle flow. In a specific case of liquids with equal densities, it was shown that the flow is unstable for any small value of the Reynolds number, and the instability is supplied by either the moving boundary or the pressure gradient. In [24], a parallel flow of two viscous liquids of equal density in infinite domains divided by a flat interface was studied, and it was shown that there exists a short wave instability in the absence of the surface tension. This mechanism of instability is comparatively small, and it can be stabilised by the surface tension. As illustrated in [22], the surface tension at the interface should be unrealistically small to observe the interface instability in the unbounded stratified Couette flow. In the case when one of liquids is bounded by a wall,

and another liquid is unbounded, there were found a long wave interface instability in [23]. In [25], a weakly nonlinear equation modelling the plane Couette-Poiseulle flow of two liquids was derived, and some examples of wave evolution were computed.

A special case of the two-layer Couette flow with high dynamic viscosities ratios was modelled in [45] using an evolution equation derived by the integral method. The integral method was also used to model non-linear solitary waves in two-layer plane flows driven by the gravity [58] and the pressure [59]. Some attention was also paid to stability of interface waves in [44] where a gas-liquid waves were studied. Solitary and periodic waves in an interface between two liquids were observed in a cylindrical Couette flow at high ratio of the dynamic viscosities [17] and in microchannel [79].

In [30], enhancement and suppression of instability in a two-layer film flow on a vertical wall was studied theoretically. The results from this paper show that the instability in a two-layer film could be suppressed by oscillation of suitable frequency and amplitudes to the wall although the stability could be occurred only in particular flow parameters. Except from these parameters, the instability is enhanced. In this area, the wave number and the amplification factors of wave raised considerably. These results can be carried with to improve the mass and heat transfer from the film.

At small Reynolds numbers, spatio-temporal instability of two-layer film was analysed in [70]. In this study, the flow has neutral stability in the limit of zero Reynolds number despite the past studies have showed the flow is unstable in the same limit. New mechanisms of instability related to the convective nature of the disturbance were studied.

[40] analysed the linear stability of two-layer shear-thinning film liquids and studied on the four parameter Carreau inelastic model [7]. It was found that when the viscosity is stronger in the second layer, the changes on the shear-thinning properties in this layer does not strongly affect the stability. On the contrary, the shear-thinning properties affect the long-wave surface instability and the short and long-wave interface instabilities in the

different cases.

[71] examined the van der Waals interfacial instability of two superposed thin layers of fluids on a vertical substrate. The author arrived the evolution equations by using lubrication theory and classified the state of the system into four different cases: first layer rupture, second layer rupture, double layer rupture and mixed layer rupture. The mixed layer rupture is qualitatively different from the double layer rupture. The double layer rupture in which the two fluids rupture together and form compound droplets on the surface of the substrate. The mixed layer rupture where the second layer fills in the gap created when the first layer goes to rupture.

1.3 Mass transfer

In this section, some selected works on mass transfer in flowing liquid films are reviewed.

Mass transfer in one-layer falling films have been intensively studied for decades, see monograph [36] and review [37]. The researches have been stimulated by numerous applications, in particular, there is a principal problem of gas absorption by flowing liquid film.

As has been revealed in experiments [15, 28, 42, 20, 73, 78], wavy films demonstrate larger capacity to absorb a gas in comparison with theoretical predictions for the waveless flow, and this result has been measured for films flowing in different regimes. In particular, the wave frequency affects the developing wave regime and thus the rate of gas absorption.

The amplification of the absorption was found in many other types of flows, for example, a cocurrent film-gas flow [39, 4] and in horizontal wavy films [41, 19].

The gas absorption and its amplification in wavy films have been also studied. The penetration theory [21] and the theory based on surface renewal [12] could not explain this phenomenon. The absorption problem for the waveless flow was solved in [46].

A few approaches used simplified models to solve the mass transfer problem in wavy

regimes. Kapitza's solution [34] was used in [47], and an experimentally observed waves were used in [72] to model the gas absorption.

Systematic computations of the absorption on wavy regimes in falling films were carried out in [60, 43] for a falling film, and in [61] for close problem of flow over a spinning disk. The main result is that there is a strong dependence of the absorption rate on the wave frequency (wavenumber), and this is due to nonuniform distribution of a local gas flux along a wave with maximum at troughs of the wave. A numerical simulations were carried out for a vertical falling film in [74] and the numerical experiments were compared with the previous ones.

The review of the relevant literature can be also found in [2] where the absorption problem was solved by Volume-of-Fluid Method where results of [60, 43] were confirmed.

Chapter 2

Evolution Equations

2.1 Basic Equations

In this section, the Navier-Stokes equations [1, 16] and relevant boundary conditions describing a two-layer film flowing down a vertical wall are given. Then, the dimensionless variables are defined and the system are made dimensionless. The basic solution describing the waveless steady flow is found and properties of this solution in the phase space are studied.

2.1.1 Equations and boundary conditions

We consider a liquid film flowing down a vertical wall. The film consists of two layers of liquids, and the layer attached to the wall will be referred as the first layer and the layer with the free surface will be referred as the second layer. We assume that both liquids are incompressible, viscous and immiscible.

To describe the flow, the Cartesian coordinate system $(\tilde{x}, \tilde{y})$ is introduced such that the $\tilde{x}$-axis coincides the wall and points downstream and the $\tilde{y}$-axis points to the liquid bulk.

Then, the full Navier-Stokes system is written in the form

Liquid	Density, g/cm^3	Viscosity, cm^2/s	Surface tension, g/s^2
Water	0.998	0.0101	72
Benzene	0.879	0.0074	29

Table 2.1: Physical properties of water and benzene.

$$
\begin{aligned}
&\frac{\partial \tilde{u}}{\partial \tilde{x}} + \frac{\partial \tilde{v}}{\partial \tilde{y}} = 0, \qquad (2.1)\\
&\frac{\partial \tilde{u}}{\partial \tilde{t}} + \tilde{u}\frac{\partial \tilde{u}}{\partial \tilde{x}} + \tilde{v}\frac{\partial \tilde{u}}{\partial \tilde{y}} = -\frac{1}{\rho^{(j)}}\frac{\partial \tilde{p}}{\partial \tilde{x}} + \nu^{(j)}\left(\frac{\partial^2 \tilde{u}}{\partial \tilde{x}^2} + \frac{\partial^2 \tilde{u}}{\partial \tilde{y}^2}\right) + g,\\
&\frac{\partial \tilde{v}}{\partial \tilde{t}} + \tilde{u}\frac{\partial \tilde{v}}{\partial \tilde{x}} + \tilde{v}\frac{\partial \tilde{v}}{\partial \tilde{y}} = -\frac{1}{\rho^{(j)}}\frac{\partial \tilde{p}}{\partial \tilde{y}} + \nu^{(j)}\left(\frac{\partial^2 \tilde{v}}{\partial \tilde{x}^2} + \frac{\partial^2 \tilde{v}}{\partial \tilde{y}^2}\right),\\
&\tilde{y} = 0: \quad \tilde{u} = 0, \quad \tilde{v} = 0,\\
&\tilde{y} = \tilde{h}^{(1)}\left(\tilde{x}, \tilde{t}\right): \quad \frac{\partial \tilde{h}^{(1)}}{\partial \tilde{t}} + \tilde{u}\frac{\partial \tilde{h}^{(1)}}{\partial \tilde{x}} = \tilde{v}, \quad [\tilde{p}_{nn}]_1^2 + \sigma^{(1)}\tilde{\varsigma}^{(1)} = 0, \quad [\tilde{p}_{n\tau}]_1^2 = 0,\\
&\qquad\qquad [\tilde{u}]_1^2 = 0, \quad [\tilde{v}]_1^2 = 0,\\
&\tilde{y} = \tilde{h}^{(2)}\left(\tilde{x}, \tilde{t}\right): \quad \frac{\partial \tilde{h}^{(2)}}{\partial \tilde{t}} + \tilde{u}\frac{\partial \tilde{h}^{(2)}}{\partial \tilde{x}} = \tilde{v}, \quad \tilde{p}_{nn} - \sigma^{(2)}\tilde{\varsigma}^{(2)} = 0, \quad \tilde{p}_{n\tau} = 0,
\end{aligned}
$$

where $\tilde{u}\left(\tilde{x}, \tilde{y}, \tilde{t}\right)$ and $\tilde{v}\left(\tilde{x}, \tilde{y}, \tilde{t}\right)$ are the velocity components in $\tilde{x}$ and $\tilde{y}$ directions respectively, $\tilde{p}\left(\tilde{x}, \tilde{y}, \tilde{t}\right)$ is the pressure, $\tilde{h}^{(1)}\left(\tilde{x}, \tilde{t}\right)$ and $\tilde{h}^{(2)}\left(\tilde{x}, \tilde{t}\right)$ are the thicknesses of the first layer and the film, respectively . The notation $[f]_1^2 \equiv f^{(2)} - f^{(1)}$ denotes the jump in quantity f from the value in the first liquid, $f^{(1)}$, to the value in the second liquid, $f^{(2)}$.

The problem includes the following dimensional parameters: the densities $\rho^{(1)}$ and $\rho^{(2)}$, viscosities $\nu^{(1)}$ and $\nu^{(2)}$ of the first and second liquids, and the surface tension $\sigma^{(1)}$ at the interface and the surface tension $\sigma^{(2)}$ at the film surface. Also, the gravity g is contained in the system.

As an example of the similarity parameters of the two-layer film, we consider water and benzene whose physical properties are summarized in Table 2.1. The surface tension

between water and benzene is $\sigma^{(1)} = 33.6$ g/s^2.

The boundary conditions at the interface and the surface in (2.1) contain the normal stresses

$$\tilde{p}_{nn} = -\tilde{p} + 2\rho\nu \left[1 + \left(\frac{\partial \tilde{h}}{\partial \tilde{x}}\right)^2\right]^{-1} \left[\left(\frac{\partial \tilde{h}}{\partial \tilde{x}}\right)^2 \frac{\partial \tilde{u}}{\partial \tilde{x}} + \frac{\partial \tilde{v}}{\partial \tilde{y}} - \frac{\partial \tilde{h}}{\partial \tilde{x}} \left(\frac{\partial \tilde{u}}{\partial \tilde{y}} + \frac{\partial \tilde{v}}{\partial \tilde{x}}\right)\right],$$

the tangential stresses

$$\tilde{p}_{n\tau} = \rho\nu \left[1 + \left(\frac{\partial \tilde{h}}{\partial \tilde{x}}\right)^2\right]^{-1} \left[\left(1 - \left(\frac{\partial \tilde{h}}{\partial \tilde{x}}\right)^2\right) \left(\frac{\partial \tilde{u}}{\partial \tilde{y}} + \frac{\partial \tilde{v}}{\partial \tilde{x}}\right) + 2\frac{\partial \tilde{h}}{\partial \tilde{x}} \left(\frac{\partial \tilde{v}}{\partial \tilde{y}} - \frac{\partial \tilde{u}}{\partial \tilde{x}}\right)\right],$$

and the curvatures

$$\tilde{\varsigma} = \left[1 + \left(\frac{\partial \tilde{h}}{\partial \tilde{x}}\right)^2\right]^{-\frac{3}{2}} \frac{\partial^2 \tilde{h}}{\partial \tilde{x}^2},$$

where $\tilde{h} = \tilde{h}^{(1)}$ or $\tilde{h} = \tilde{h}^{(2)}$ and the values of the corresponding liquids are used.

The problem (2.1) has a solution describing the steady waveless flow denoted by capital letters:

$$\begin{aligned} y \in \left[0, \tilde{H}^{(1)}\right] \quad : \quad & \tilde{U}^{(1)}(\tilde{y}) = \frac{g}{\nu^{(1)}} \left\{ \left[\frac{\rho^{(2)}}{\rho^{(1)}} \tilde{H}^{(2)} + \left(1 - \frac{\rho^{(2)}}{\rho^{(1)}}\right) \tilde{H}^{(1)}\right] \tilde{y} - \frac{1}{2}\tilde{y}^2 \right\}, \qquad (2.2) \\ & \tilde{V}^{(1)}(\tilde{y}) = 0, \\ & \tilde{P}^{(1)}(\tilde{y}) = 0, \\ & \tilde{Q}^{(1)} \equiv \int_0^{\tilde{H}^{(1)}} \tilde{U}^{(1)} d\tilde{y} = \frac{g}{2\nu^{(1)}} \left(\tilde{H}^{(1)}\right)^2 \left[\left(\frac{2}{3} - \frac{\rho^{(2)}}{\rho^{(1)}}\right) \tilde{H}^{(1)} + \frac{\rho^{(2)}}{\rho^{(1)}} \tilde{H}^{(2)}\right], \end{aligned}$$

$$
\begin{aligned}
y \in \left[\tilde{H}^{(1)}, \tilde{H}^{(2)}\right] \quad : \quad \tilde{U}^{(2)}(\tilde{y}) &= \frac{g}{\nu^{(2)}}\left\{\left[\frac{1}{2}\left(1+\frac{\nu^{(2)}}{\nu^{(1)}}\right)-\frac{\rho^{(2)}\nu^{(2)}}{\rho^{(1)}\nu^{(1)}}\right]\left(\tilde{H}^{(1)}\right)^2 - \right. \\
&\left.\left(1-\frac{\rho^{(2)}\nu^{(2)}}{\rho^{(1)}\nu^{(1)}}\right)\tilde{H}^{(1)}\tilde{H}^{(2)}+\tilde{H}^{(2)}\tilde{y}-\frac{1}{2}\tilde{y}^2\right\}, \\
\tilde{V}^{(2)}(\tilde{y}) &= 0, \\
\tilde{P}^{(2)}(\tilde{y}) &= 0, \\
\tilde{Q} &\equiv \int_{\tilde{H}^{(1)}}^{\tilde{H}^{(2)}} \tilde{U}^{(2)} d\tilde{y} \\
&= \frac{g}{\nu^{(2)}}\left(\tilde{H}^{(2)}-\tilde{H}^{(1)}\right)\left\{\left(\frac{1}{3}+\frac{1}{2}\frac{\nu^{(2)}}{\nu^{(1)}}-\frac{\rho^{(2)}\nu^{(2)}}{\rho^{(1)}\nu^{(1)}}\right)\left(\tilde{H}^{(1)}\right)^2 - \right. \\
&\left.\left(\frac{2}{3}-\frac{\rho^{(2)}\nu^{(2)}}{\rho^{(1)}\nu^{(1)}}\right)\tilde{H}^{(1)}\tilde{H}^{(2)}+\frac{1}{3}\left(\tilde{H}^{(2)}\right)^2\right\},
\end{aligned}
$$

where $\tilde{Q}^{(1)}$ and $\tilde{Q}$ are the flow rates of first and second layers, respectively. The first layer thickness $\tilde{H}^{(1)}$ and the second layer thickness $\tilde{H}^{(2)} - \tilde{H}^{(1)}$ are constants. The total flow rate of the film is

$$
\begin{aligned}
\tilde{Q}^{(2)} \equiv \tilde{Q}^{(1)} + \tilde{Q} = \frac{g}{\nu^{(2)}}\left\{\left(1+\frac{1}{2}\frac{\nu^{(2)}}{\nu^{(1)}}-\frac{3}{2}\frac{\rho^{(2)}\nu^{(2)}}{\rho^{(1)}\nu^{(1)}}\right)\left(\tilde{H}^{(1)}\right)^2\left(\tilde{H}^{(2)}-\frac{1}{3}\tilde{H}^{(1)}\right)+ \right. \\
\left.\left[\frac{1}{3}\tilde{H}^{(2)}-\left(1-\frac{\rho^{(2)}\nu^{(2)}}{\rho^{(1)}\nu^{(1)}}\right)\tilde{H}^{(1)}\right]\left(\tilde{H}^{(2)}\right)^2\right\}.
\end{aligned}
$$

2.1.2 Dimensionless variables

If the length scale is chosen as $H_c = \tilde{H}^{(2)}$, and the velocity scale is denoted as U_c and defined below, then, new dimensionless variables can be introduced:

$$
\begin{aligned}
&\tilde{t} = \frac{H_c}{U_c}t, \ \tilde{x} = H_c x, \ \tilde{y} = H_c y, \\
&\tilde{u} = U_c u, \ \tilde{v} = U_c v, \ \tilde{p} = \rho^{(2)} U_c^2 p, \\
&\tilde{h}^{(1)} = H_c h^{(1)}, \ \tilde{h}^{(2)} = H_c h^{(2)}.
\end{aligned} \tag{2.3}
$$

Using the dimensionless variables, the equations and boundary conditions (2.1), can be rewritten in the following form

$$
\begin{aligned}
&\frac{\partial u}{\partial x}+\frac{\partial v}{\partial y}=0, \qquad (2.4)\\
&\frac{\partial u}{\partial t}+u\frac{\partial u}{\partial x}+v\frac{\partial u}{\partial y}=-\frac{1}{\rho_0^{(j)}}\frac{\partial p}{\partial x}+\frac{\nu_0^{(j)}}{\mathrm{Re}}\left(\frac{\partial^2 u}{\partial x^2}+\frac{\partial^2 u}{\partial y^2}\right)+\frac{1}{\mathrm{Fr}^2},\\
&\frac{\partial v}{\partial t}+u\frac{\partial v}{\partial x}+v\frac{\partial v}{\partial y}=-\frac{1}{\rho_0^{(j)}}\frac{\partial p}{\partial y}+\frac{\nu_0^{(j)}}{\mathrm{Re}}\left(\frac{\partial^2 v}{\partial x^2}+\frac{\partial^2 v}{\partial y^2}\right),\\
&y=0: \quad u=0, \quad v=0,\\
&y=h^{(1)}(x,t): \quad \frac{\partial h^{(1)}}{\partial t}+u\frac{\partial h^{(1)}}{\partial x}=v, \quad [p_{nn}]_1^2+\frac{\sigma_0}{\mathrm{We}}\varsigma^{(1)}=0, \quad [p_{n\tau}]_1^2=0,\\
&\qquad\qquad [u]_1^2=0, \quad [v]_1^2=0,\\
&y=h^{(2)}(x,t): \quad \frac{\partial h^{(2)}}{\partial t}+u\frac{\partial h^{(2)}}{\partial x}=v, \quad p_{nn}-\frac{1}{\mathrm{We}}\varsigma^{(2)}=0, \quad p_{n\tau}=0,
\end{aligned}
$$

where

$$
\begin{aligned}
p_{nn}&=\frac{2\rho_0^{(j)}\nu_0^{(j)}}{\mathrm{Re}}\left[1+\left(\frac{\partial h}{\partial x}\right)^2\right]^{-1}\left[\left(1-\left(\frac{\partial h}{\partial x}\right)^2\right)\frac{\partial v}{\partial y}-\frac{\partial h}{\partial x}\left(\frac{\partial u}{\partial y}+\frac{\partial v}{\partial x}\right)\right]-p,\\
p_{n\tau}&=\frac{\rho_0^{(j)}\nu_0^{(j)}}{\mathrm{Re}}\left[1+\left(\frac{\partial h}{\partial x}\right)^2\right]^{-1}\left[\left(1-\left(\frac{\partial h}{\partial x}\right)^2\right)\left(\frac{\partial u}{\partial y}+\frac{\partial v}{\partial x}\right)+4\frac{\partial h}{\partial x}\frac{\partial v}{\partial y}\right],\\
\varsigma&=\left[1+\left(\frac{\partial h}{\partial x}\right)^2\right]^{-\frac{3}{2}}\frac{\partial^2 h}{\partial x^2}
\end{aligned}
$$

for $h=h^{(1)}$ or $h=h^{(2)}$. The system contains 6 similarity parameters:

$$
\begin{aligned}
&\mathrm{Re}=\frac{U_c H_c}{\nu^{(2)}}, \quad \mathrm{We}=\frac{\rho^{(2)}U_c^2 H_c}{\sigma^{(2)}}, \quad \mathrm{Fr}^2=\frac{U_c^2}{gH_c},\\
&\rho_0=\frac{\rho^{(1)}}{\rho^{(2)}}, \quad \nu_0=\frac{\nu^{(1)}}{\nu^{(2)}}, \quad \sigma_0=\frac{\sigma^{(1)}}{\sigma^{(2)}},
\end{aligned}
$$

and additional notations: $\rho_0^{(2)}=1$, $\rho_0^{(1)}=\rho_0$, $\nu_0^{(2)}=1$ and $\nu_0^{(1)}=\nu_0$.

For example, Table 2.2 shows values of the similarity parameters ρ_0, ν_0 and σ_0 which

System	ρ_0	ν_0	σ_0	Ka
Water (1) – Benzene (2)	1.13538	1.36486	1.15862	2302.56
Benzene (1) – Water (2)	0.880762	0.732673	0.466667	3325.71

Table 2.2: Parameters of water-benzene and benzene-water systems.

only depend on the properties of liquids in water-benzene and benzene-water systems.

In the dimensionless form, the steady flow (2.2) is

$$
\begin{aligned}
y \in [0, H] \quad : \quad & U^{(1)}(y) = \frac{\mathrm{Re}}{\nu_0 \mathrm{Fr}^2} \left(a^{(1)} y - \frac{y^2}{2} \right), \\
& V^{(1)}(y) = 0, \\
& P^{(1)}(y) = 0, \\
& Q^{(1)} = \int_0^H U^{(1)} dy = \frac{\mathrm{Re}}{2\nu_0 \mathrm{Fr}^2} H^2 \left[\frac{1}{\rho_0} + \left(\frac{2}{3} - \frac{1}{\rho_0} \right) H \right], \\
y \in [H, 1] \quad : \quad & U^{(2)}(y) = \frac{\mathrm{Re}}{\mathrm{Fr}^2} \left(a^{(2)} + y - \frac{y^2}{2} \right), \\
& V^{(2)}(y) = 0, \\
& P^{(2)}(y) = 0, \\
& Q = \int_H^1 U^{(2)} dy \\
& \quad = \frac{\mathrm{Re}}{\mathrm{Fr}^2} (1 - H) \left[\frac{1}{3} + \left(\frac{1}{\rho_0 \nu_0} - \frac{2}{3} \right) H + \left(\frac{1}{3} + \frac{1}{2\nu_0} - \frac{1}{\rho_0 \nu_0} \right) H^2 \right],
\end{aligned}
\tag{2.5}
$$

where the coefficients have been introduced:

$$
\begin{aligned}
a^{(1)} &= \frac{1}{\rho_0} + \left(1 - \frac{1}{\rho_0} \right) H, \\
a^{(2)} &= \left(\frac{1 + \nu_0}{2\nu_0} - \frac{1}{\rho_0 \nu_0} \right) H^2 + \left(\frac{1}{\rho_0 \nu_0} - 1 \right) H.
\end{aligned}
$$

The total flow rate in the film is

$$Q^{(2)} = Q^{(1)} + Q = \varphi \frac{\mathrm{Re}}{\mathrm{Fr}^2},$$

where

$$\varphi(\rho_0, \nu_0, H) = \frac{H^2}{2\nu_0}\left[\frac{1}{\rho_0} + \left(\frac{2}{3} - \frac{1}{\rho_0}\right) H\right] + (1-H)\left[\frac{1}{3} + \left(\frac{1}{\rho_0\nu_0} - \frac{2}{3}\right) H + \left(\frac{1}{3} + \frac{1}{2\nu_0} - \frac{1}{\rho_0\nu_0}\right) H^2\right].$$

If the velocity scale, U_c, is chosen as the average velocity then $Q^{(2)} = 1$ and thus

$$\varphi \frac{\mathrm{Re}}{\mathrm{Fr}^2} = 1. \tag{2.6}$$

That relation allows us to calculate the velocity scale

$$U_c = \frac{\varphi g H_c^2}{\nu^{(2)}}.$$

2.1.3 Parameters and basic solution

Formula (2.6) allows us to eliminate the Froude number $\mathrm{Fr}^2 = \varphi \mathrm{Re}$. On the other hand, flow depends on the first layer thickness H determining flow rates in the layers. Thus, the problem (2.4) contains the following 6 similarity parameters:

$$\mathrm{Re} = \frac{U_c H_c}{\nu^{(2)}}, \quad \mathrm{We} = \frac{\rho^{(2)} U_c^2 H_c}{\sigma^{(2)}},$$
$$\rho_0 = \frac{\rho^{(1)}}{\rho^{(2)}}, \quad \nu_0 = \frac{\nu^{(1)}}{\nu^{(2)}}, \quad \sigma_0 = \frac{\sigma^{(1)}}{\sigma^{(2)}}, \quad H.$$

We can also use another set of the parameters:

$$\mathrm{Ka} \equiv \frac{\sigma^{(2)}}{\rho^{(2)}\left(g\left(\nu^{(2)}\right)^4\right)^{\frac{1}{3}}}, \quad \delta \equiv \frac{1}{45\left(\nu^{(2)}\right)^2}\left(\frac{\rho^{(2)}g^4H_c^{11}}{\sigma^{(2)}}\right)^{\frac{1}{3}},$$
$$\rho_0 = \frac{\rho^{(1)}}{\rho^{(2)}}, \quad \nu_0 = \frac{\nu^{(1)}}{\nu^{(2)}}, \quad \sigma_0 = \frac{\sigma^{(1)}}{\sigma^{(2)}}, \quad H,$$

where the Reynolds number Re and the Froude number Fr have been replaced for the Kapitza number Ka depending on gravity and the properties of the second liquid only, and δ is the film parameter. Values of the Kapitza number for benzene and water are given in Table 2.2.

Then, we can calculate the dimensional scales:

$$H_c = \left[\frac{(45\delta)^3\left(\nu^{(2)}\right)^6\sigma^{(2)}}{\rho^{(2)}g^4}\right]^{\frac{1}{11}},$$
$$U_c = \varphi\left[(45\delta)^6\frac{g^3\nu^{(2)}\left(\sigma^{(2)}\right)^2}{\left(\rho^{(2)}\right)^2}\right]^{\frac{1}{11}}$$

Hence, the Reynolds number and the Weber number are expressed by the δ and Ka as follows:

$$\mathrm{Re} = \frac{\varphi g H_c^3}{\left(\nu^{(2)}\right)^2} = \varphi\left(45\delta\right)^{\frac{9}{11}}\mathrm{Ka}^{\frac{3}{11}},$$
$$\mathrm{We} = \frac{\varphi^2\rho^{(2)}g^2H_c^5}{\sigma^{(2)}\left(\nu^{(2)}\right)^2} = \varphi^2\frac{(45\delta)^{\frac{15}{11}}}{\mathrm{Ka}^{\frac{6}{11}}}.$$

Let's calculate the inverse transformation from Re and We to δ and Ka. First,

$$\mathrm{Ka}^{\frac{3}{11}} = \frac{\mathrm{Re}}{\varphi\left(45\delta\right)^{\frac{9}{11}}},$$

and so the Weber number is expressed as

$$\mathrm{We} = \varphi^2 \frac{(45\delta)^{\frac{15}{11}}}{\mathrm{Ka}^{\frac{6}{11}}} = \varphi^2 (45\delta)^{\frac{15}{11}} \left(\frac{\varphi (45\delta)^{\frac{9}{11}}}{\mathrm{Re}} \right)^2 = \frac{\varphi^4 (45\delta)^3}{\mathrm{Re}^2}.$$

Therefore, we calculate δ and then Ka:

$$\delta = \frac{1}{45} \left(\frac{\mathrm{Re}^2 \mathrm{We}}{\varphi^4} \right)^{\frac{1}{3}}, \quad \mathrm{Ka} = \frac{\left(\mathrm{Re}^5 \varphi\right)^{\frac{1}{3}}}{\mathrm{We}}.$$

The dimensionless form of the steady flow (2.5) is rewritten as

$$\begin{aligned}
y \in [0, H] \quad : \quad & U^{(1)}(y) = \frac{1}{\varphi \nu_0} \left(a^{(1)} y - \frac{y^2}{2} \right), \\
& V^{(1)}(y) = 0, \\
& P^{(1)}(y) = 0, \\
& Q^{(1)} = \int_0^H U^{(1)} dy = \frac{H^2}{2\varphi\nu_0} \left[\frac{1}{\rho_0} + \left(\frac{2}{3} - \frac{1}{\rho_0} \right) H \right], \\
y \in [H, 1] \quad : \quad & U^{(2)}(y) = \frac{1}{\varphi} \left(a^{(2)} + y - \frac{y^2}{2} \right), \\
& V^{(2)}(y) = 0, \\
& P^{(2)}(y) = 0, \\
& Q = \int_H^1 U^{(2)} dy \\
& \quad = \frac{1 - H}{\varphi} \left[\frac{1}{3} + \left(\frac{1}{\rho_0 \nu_0} - \frac{2}{3} \right) H + \left(\frac{1}{3} + \frac{1}{2\nu_0} - \frac{1}{\rho_0 \nu_0} \right) H^2 \right].
\end{aligned} \tag{2.7}$$

To analyse flows in the layers, we can also introduce the Reynolds numbers in each layer as follows:

$$\mathrm{Re}^{(1)} \equiv \frac{\tilde{Q}^{(1)}}{\nu^{(1)}} = \frac{\mathrm{Re}\, Q^{(1)}}{\nu_0}, \quad \mathrm{Re}^{(2)} \equiv \frac{\tilde{Q}}{\nu^{(2)}} = \mathrm{Re}\, Q.$$

2.2 Linear stability of the waveless flow

In this section, we follow [62]. To analyse the linear stability of the waveless flow, the eigenvalue problem is formulated. Then, the numerical method in order to solve the eigenvalue problem is examined, and numerical results are presented at the end of this section.

To investigate linear stability of the steady flow (2.7), a non-steady solution of (2.4) is looked for in the form

$$
\begin{aligned}
&u(x,y,t) = U(y) + \hat{u}(x,y,t), \quad v(x,y,t) = \hat{v}(x,y,t),\\
&p(x,y,t) = \hat{p}(x,y,t),\\
&h^{(1)}(x,t) = H + \hat{h}^{(1)}(x,t), \quad h^{(2)}(x,t) = 1 + \hat{h}^{(2)}(x,t),
\end{aligned}
$$

where cups denote small perturbations. After substituting in (2.4) and linearising we arrive at

$$
\begin{aligned}
&\frac{\partial \hat{u}}{\partial x} + \frac{\partial \hat{v}}{\partial y} = 0,\\
&\frac{\partial \hat{u}}{\partial t} + U\frac{\partial \hat{u}}{\partial x} + U'\hat{v} = -\frac{1}{\rho_0^{(j)}}\frac{\partial \hat{p}}{\partial x} + \frac{\nu_0^{(j)}}{\mathrm{Re}}\left(\frac{\partial^2 \hat{u}}{\partial x^2} + \frac{\partial^2 \hat{u}}{\partial y^2}\right),\\
&\frac{\partial \hat{v}}{\partial t} + U\frac{\partial \hat{v}}{\partial x} = -\frac{1}{\rho_0^{(j)}}\frac{\partial \hat{p}}{\partial y} + \frac{\nu_0^{(j)}}{\mathrm{Re}}\left(\frac{\partial^2 \hat{v}}{\partial x^2} + \frac{\partial^2 \hat{v}}{\partial y^2}\right),\\
&y = 0: \quad \hat{u} = 0, \quad \hat{v} = 0,\\
&y = H: \quad \frac{\partial \hat{h}^{(1)}}{\partial t} + U\frac{\partial \hat{h}^{(1)}}{\partial x} = \hat{v},\\
&\qquad \left[U'\hat{h}^{(1)} + \hat{u}\right]_1^2 = 0, \quad [\hat{v}]_1^2 = 0,\\
&\qquad \left[-\hat{p} + \frac{2\rho_0^{(j)}\nu_0^{(j)}}{\mathrm{Re}}\left(\frac{\partial \hat{v}}{\partial y} - U'\frac{\partial \hat{h}^{(1)}}{\partial x}\right)\right]_1^2 + \frac{\sigma_0}{\mathrm{We}}\frac{\partial^2 \hat{h}^{(1)}}{\partial x^2} = 0,\\
&\qquad \left[\rho_0^{(j)}\nu_0^{(j)}\left(\frac{\partial \hat{u}}{\partial y} + \frac{\partial \hat{v}}{\partial x} + U''\hat{h}^{(1)}\right)\right]_1^2 = 0,
\end{aligned}
$$

$$
\begin{aligned}
y=1: \quad & \frac{\partial \hat{h}^{(2)}}{\partial t}+U\frac{\partial \hat{h}^{(2)}}{\partial x}=\hat{v}, \\
& -\hat{p}+\frac{2}{\mathrm{Re}}\left(\frac{\partial \hat{v}}{\partial y}-U'\frac{\partial \hat{h}^{(2)}}{\partial x}\right)-\frac{1}{\mathrm{We}}\frac{\partial^2 \hat{h}^{(2)}}{\partial x^2}=0, \\
& \frac{\partial \hat{u}}{\partial y}+\frac{\partial \hat{v}}{\partial x}+U''\hat{h}^{(2)}=0.
\end{aligned}
$$

where the primes denote derivatives with respect to y.

Then, solution in the form of normal mode is used

$$
\begin{aligned}
&\left(\hat{u}(x,y,t),\hat{v}(x,y,t),\hat{p}(x,y,t),\hat{h}^{(1)}(x,t),\hat{h}^{(2)}(x,t)\right)= \\
&\qquad\left(\breve{u}(y),\breve{v}(y),\breve{p}(y),\breve{h}^{(1)},\breve{h}^{(2)}\right)\exp\left(i\alpha\left(x-ct\right)\right),
\end{aligned}
$$

where α is the x-wavenumber, and $c=c_r+ic_i$ (here and below the lower index r denotes the real part of the corresponding variable, and the lower index i denotes its imaginary part) is the complex wave velocity to be found and the sign of the imaginary part c_i indicates the stability, $c_i<0$, or instability, $c_i>0$, of the steady waveless flow. System for the amplitude functions is

$$
\begin{aligned}
& i\alpha\breve{u}+\breve{v}'=0, \\
& i\alpha(U-c)\breve{u}+U'\breve{v}=-\frac{i\alpha}{\rho_0^{(j)}}\breve{p}+\frac{\nu_0^{(j)}}{\mathrm{Re}}\left(\breve{u}''-\alpha^2\breve{u}\right), \\
& i\alpha(U-c)\breve{v}=-\frac{1}{\rho_0^{(j)}}\breve{p}'+\frac{\nu_0^{(j)}}{\mathrm{Re}}(\breve{v}''-\alpha^2\breve{v}), \\
& y=0: \quad \breve{u}=0, \quad \breve{v}=0,
\end{aligned}
$$

$$
\begin{aligned}
y = H: \quad & i\alpha(U-c)\breve{h}^{(1)} = \breve{v}, \\
& \left[U'\breve{h}^{(1)} + \breve{u}\right]_1^2 = 0, \quad [\breve{v}]_1^2 = 0, \\
& \left[-\breve{p} + \frac{2\rho_0^{(j)}\nu_0^{(j)}}{\mathrm{Re}}\left(\breve{v}' - i\alpha U'\breve{h}^{(1)}\right)\right]_1^2 - \frac{\alpha^2\sigma_0}{\mathrm{We}}\breve{h}^{(1)} = 0, \\
& \left[\rho_0^{(j)}\nu_0^{(j)}\left(\breve{u}' + i\alpha\breve{v} + U''\breve{h}^{(1)}\right)\right]_1^2 = 0, \\
y = 1: \quad & i\alpha(U-c)\breve{h}^{(2)} = \breve{v}, \\
& -\breve{p} + \frac{2}{\mathrm{Re}}\left(\breve{v}' - i\alpha U'\breve{h}^{(2)}\right) + \frac{\alpha^2}{\mathrm{We}}\breve{h}^{(2)} = 0, \\
& \breve{u}' + i\alpha\breve{v} + U''\breve{h}^{(2)} = 0.
\end{aligned}
$$

Eliminating perturbation of the longitudinal velocity from the continuity equation

$$\breve{u} = \frac{i}{\alpha}\breve{v}',$$

and the pressure perturbation from x-axis momentum equation

$$\breve{p} = \frac{\rho_0^{(j)}\nu_0^{(j)}}{\alpha^2\mathrm{Re}}\breve{v}''' - \rho_0^{(j)}\left[\frac{i}{\alpha}(U-c) + \frac{\nu_0^{(j)}}{\mathrm{Re}}\right]\breve{v}' + \frac{i\rho_0^{(j)}}{\alpha}U'\breve{v},$$

and perturbation of the interface thickness from kinematic condition at the interface

$$i\alpha\left(U\left(H\right) - c\right)\breve{h}^{(1)} = \breve{v}\left(H\right),$$

and perturbation of film thickness from the kinematic condition at the free surface

$$i\alpha(U(1) - c)\breve{h}^{(2)} = \breve{v}(1)$$

leads to the following eigenvalue problem for perturbation of the y-axis velocity compo-

nent:

$$
\begin{aligned}
&\breve{v}'''' - 2\alpha^2\breve{v}'' + \alpha^4\breve{v} - \frac{i\alpha\mathrm{Re}}{\nu_0^{(j)}}\left[(U-c)(\breve{v}''-\alpha^2\breve{v}) - U''\breve{v}\right] = 0, \qquad (2.8)\\
&y = 0: \quad \breve{v} = 0, \quad \breve{v}' = 0,\\
&y = H: \quad [\breve{v}]_1^2 = 0,\\
&\qquad \left[\breve{v}' - \frac{U'}{U-c}\breve{v}\right]_1^2 = 0,\\
&\qquad \left[\rho_0^{(j)}\nu_0^{(j)}\left\{\breve{v}''' - \left(3\alpha^2 + \frac{i\alpha\mathrm{Re}}{\nu_0^{(j)}}(U-c)\right)\breve{v}' + \right.\right.\\
&\qquad\qquad \left.\left.\left(\frac{i\alpha\mathrm{Re}U'}{\nu_0^{(j)}} + \frac{2\alpha^2U'}{U-c}\right)\breve{v}\right\}\right]_1^2 - \frac{i\sigma_0\alpha^3\mathrm{Re}}{\mathrm{We}(U-c)}\breve{v} = 0,\\
&\qquad \left[\rho_0^{(j)}\nu_0^{(j)}\left\{\breve{v}'' + \left(\alpha^2 - \frac{U''}{U-c}\right)\breve{v}\right\}\right]_1^2 = 0,\\
&y = 1: \quad \breve{v}'' + \left(\alpha^2 - \frac{U''}{U-c}\right)\breve{v} = 0,\\
&\qquad \breve{v}''' - \left[3\alpha^2 + i\alpha\mathrm{Re}(U-c)\right]\breve{v}'\\
&\qquad\quad + \left[\frac{i\alpha}{U-c}\frac{\alpha^2\mathrm{Re}}{\mathrm{We}} + \left(i\alpha\mathrm{Re} + \frac{2\alpha^2}{U-c}\right)U'\right]\breve{v} = 0.
\end{aligned}
$$

The problem (2.8) is a generalized Orr-Sommerfeld problem studied in [62]. To solve (2.8) numerically, the differential sweep method is applied. If new variables

$$w_1 = \breve{v}, \quad w_2 = \breve{v}', \quad w_3 = \breve{v}'', \quad w_4 = \breve{v}''',$$

are introduced, then the problem is rewritten in the form

$$
\begin{aligned}
&\frac{dw_1}{dy} = w_2, \quad \frac{dw_2}{dy} = w_3, \quad \frac{dw_3}{dy} = w_4, \qquad (2.9)\\
&\frac{dw_4}{dy} = 2\alpha^2w_3 - \alpha^4w_1 + \frac{i\alpha\mathrm{Re}}{\nu_0^{(j)}}\left[(U-c)(w_3-\alpha^2w_1) - U''w_1\right],\\
&y = 0: \quad w_1 = 0, \quad w_2 = 0,
\end{aligned}
$$

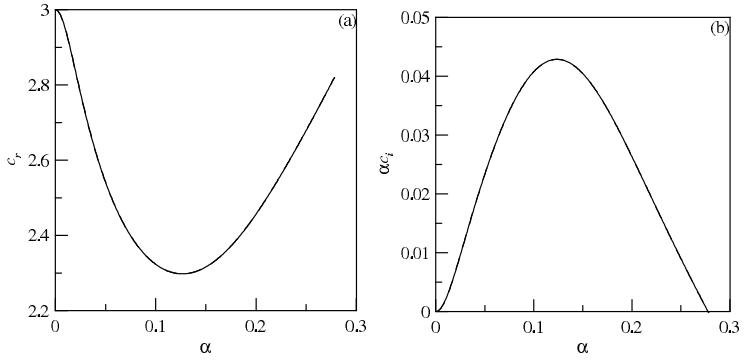

Figure 2.1: Wave velocities (a) and amplification factors (b) in the case of the one-layer film at $\mathrm{Re} = 18.37, \mathrm{We} = 0.026$ when $\delta = 0.2$. The results do not depend on the value of H.

$$
\begin{aligned}
y = H: \quad & [w_1]_1^2 = 0, \\
& \left[w_2 - \frac{U'}{U-c} w_1 \right]_1^2 = 0, \\
& \left[\rho_0^{(j)} \nu_0^{(j)} \left\{ w_4 - \left(3\alpha^2 + \frac{i\alpha \mathrm{Re}}{\nu_0^{(j)}} (U-c) \right) w_2 + \right. \right. \\
& \qquad \left. \left. \left(\frac{i\alpha \mathrm{Re} U'}{\nu_0^{(j)}} + \frac{2\alpha^2 U'}{U-c} \right) w_1 \right\} \right]_1^2 - \frac{i\alpha^3 \sigma_0 \mathrm{Re}}{\mathrm{We}(U-c)} w_1 = 0, \\
& \left[\rho_0^{(j)} \nu_0^{(j)} \left\{ w_3 + \left(\alpha^2 - \frac{U''}{U-c} \right) w_1 \right\} \right]_1^2 = 0, \\
y = 1: \quad & w_3 + \left(\alpha^2 - \frac{U''}{U-c} \right) w_1 = 0, \\
& w_4 - \left[3\alpha^2 + i\alpha \mathrm{Re}(U-c) \right] w_2 \\
& \quad + \left[\frac{i\alpha}{U-c} \frac{\alpha^2 \mathrm{Re}}{\mathrm{We}} + \left(i\alpha \mathrm{Re} + \frac{2\alpha^2}{U-c} \right) U' \right] w_1 = 0.
\end{aligned}
$$

The numerical algorithm to solve the eigenvalue problem (2.9) is given in Appendix A. To test the code, calculations have been carried out in the case of a one-layer film, see Fig. 2.1 showing the wave velocities and amplification factors. In particular, results do not depend on value of the first layer thickness as expected. Numerical solutions of (2.9) are used in Section 2.3.4 below to verify an approximate model derived in Section 2.3.3.

2.3 Evolution equations

In this section, the evolution equations approximating the full Navier-Stokes problem are derived. To do this, firstly an approximate long-wave model is formulated. Then, the integral method is applied to state the evolution equations.

2.3.1 New variables

To describe the long wave motions, new variables are introduced as

$$x_\kappa = \kappa x, \quad t_\kappa = \kappa t, \quad v_\kappa = \frac{v}{\kappa}, \tag{2.10}$$

where κ is a stretching parameter defined below. Then, the system (2.4) is rewritten in the form

$$\begin{aligned}
&\frac{\partial u}{\partial x_\kappa} + \frac{\partial v_\kappa}{\partial y} = 0, \qquad (2.11)\\
&\frac{\partial u}{\partial t_\kappa} + u\frac{\partial u}{\partial x_\kappa} + v_\kappa\frac{\partial u}{\partial y} = -\frac{1}{\rho_0^{(j)}}\frac{\partial p}{\partial x_\kappa} + \frac{\nu_0^{(j)}}{\kappa \mathrm{Re}}\left(\kappa^2\frac{\partial^2 u}{\partial x_\kappa^2} + \frac{\partial^2 u}{\partial y^2}\right) + \frac{1}{\kappa\varphi\mathrm{Re}},\\
&\kappa^2\left(\frac{\partial v_\kappa}{\partial t_\kappa} + u\frac{\partial v_\kappa}{\partial x_\kappa} + v_\kappa\frac{\partial v_\kappa}{\partial y}\right) = -\frac{1}{\rho_0^{(j)}}\frac{\partial p}{\partial y} + \frac{\kappa^2\nu_0^{(j)}}{\kappa \mathrm{Re}}\left(\kappa^2\frac{\partial^2 v_\kappa}{\partial x_\kappa^2} + \frac{\partial^2 v_\kappa}{\partial y^2}\right),\\
&y = 0: \quad u = 0, \quad v_\kappa = 0,\\
&y = h^{(1)}(x_\kappa, t_\kappa): \quad \frac{\partial h^{(1)}}{\partial t_\kappa} + u\frac{\partial h^{(1)}}{\partial x_\kappa} = v_\kappa, \quad [p_{nn}]_1^2 + \frac{\kappa^2\sigma_0}{\mathrm{We}}\varsigma_\kappa^{(1)} = 0, \quad [p_{n\tau}]_1^2 = 0,\\
&\qquad\qquad [u]_1^2 = 0, \quad [v_\kappa]_1^2 = 0,\\
&y = h^{(2)}(x_\kappa, t_\kappa): \quad \frac{\partial h^{(2)}}{\partial t_\kappa} + u\frac{\partial h^{(2)}}{\partial x_\kappa} = v_\kappa, \quad p_{nn} - \frac{\kappa^2}{\mathrm{We}}\varsigma_\kappa^{(2)} = 0, \quad p_{n\tau} = 0,
\end{aligned}$$

where

$$p_{nn} = -p + \frac{2\kappa^2 \rho_0^{(j)} \nu_0^{(j)}}{\kappa \mathrm{Re}} \left[1 + \kappa^2 \left(\frac{\partial h}{\partial x_\kappa}\right)^2\right]^{-1} \times \left[\left(1 - \kappa^2 \left(\frac{\partial h}{\partial x_\kappa}\right)^2\right) \frac{\partial v_\kappa}{\partial y} - \frac{\partial h}{\partial x_\kappa} \left(\frac{\partial u}{\partial y} + \kappa^2 \frac{\partial v_\kappa}{\partial x_\kappa}\right)\right],$$

$$p_{n\tau} = \frac{\rho_0^{(j)} \nu_0^{(j)}}{\mathrm{Re}} \left[1 + \kappa^2 \left(\frac{\partial h}{\partial x_\kappa}\right)^2\right]^{-1} \times \left[\left(1 - \kappa^2 \left(\frac{\partial h}{\partial x_\kappa}\right)^2\right) \left(\frac{\partial u}{\partial y} + \kappa^2 \frac{\partial v_\kappa}{\partial x_\kappa}\right) + 4\kappa^2 \frac{\partial h}{\partial x_\kappa} \frac{\partial v_\kappa}{\partial y}\right],$$

$$\varsigma_\kappa = \left[1 + \kappa^2 \left(\frac{\partial h}{\partial x_\kappa}\right)^2\right]^{-\frac{3}{2}} \frac{\partial^2 h}{\partial x_\kappa^2}$$

with $h = h^{(1)}$ at $j = 1$ and $h = h^{(2)}$ at $j = 2$.

The capillary waves in liquid films appear in the case of a balance of gravity, viscosity and capillarity that can be written in the form as

$$\frac{1}{\kappa \varphi \mathrm{Re}} = \frac{\kappa^2}{\mathrm{We}}.$$

Here the left-hand side is the gravity term in the first momentum equation. At the same time, this term express the balance of the viscosity and gravity leading to the existence of the waveless flow. The right-hand side shows the scale of capillarity at the film surface. This equation allows us to find the stretching parameter κ:

$$\kappa = \left(\frac{\rho^{(2)} g H_c^2}{\sigma^{(2)}}\right)^{\frac{1}{3}} = \left(\frac{(45\delta)^2}{\mathrm{Ka}^3}\right)^{\frac{1}{11}}.$$

It is worthy to note that the parameter κ can be written by using the capillary number

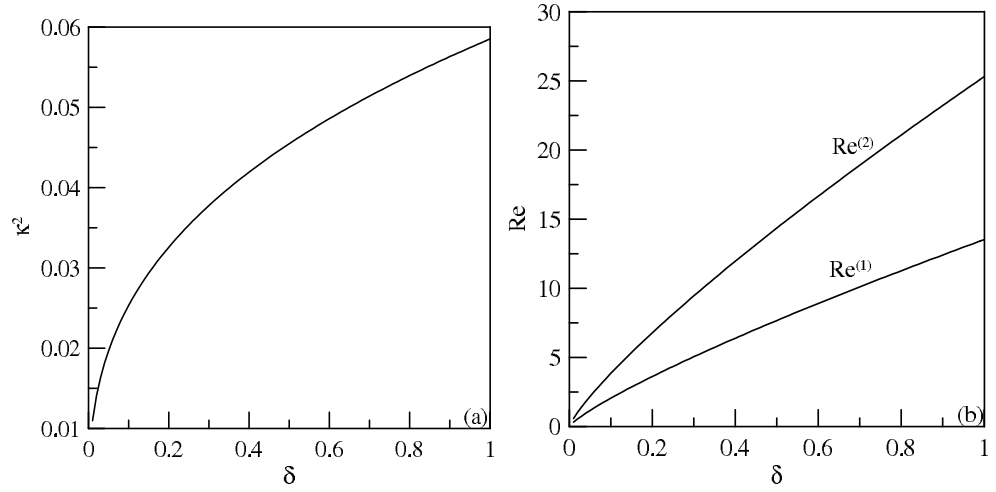

Figure 2.2: The stretching parameter κ^2 (a) and the Reynolds numbers $\mathrm{Re}^{(1)}$ and $\mathrm{Re}^{(2)}$ (b) at $H = 0.6$ for water-benzene system.

Ca used in many theoretical and experimental works

$$\kappa^3 = \frac{\mathrm{Ca}}{\varphi}, \quad \mathrm{Ca} \equiv \frac{\rho^{(2)}\nu^{(2)}U_c}{\sigma^{(2)}} = \frac{\mathrm{We}}{\mathrm{Re}}.$$

As an example of two-layer film, we consider the case of water (liquid 1) and benzene (liquid 2) whose physical properties are summarized in Table 2.1 and the similarity parameters are given in Table 2.2. Henceforth this case is called 'water-benzene' and the opposite one is called 'benzene-water' in this thesis. The properties of water and benzene were used in [62] and these liquids could be exploited in future experiments.

Typical values of the parameters are shown in Fig. 2.2 for water-benzene system at $H = 0.6$. It is seen that κ^2 is small value for moderate values of the Reynolds numbers in the layers.

Fig. 2.3 demonstrates another example of values κ^2 and Re in the case $H = 0.3$. It is seen that $\kappa^2 < 0.05$ if $\delta \leq 0.4$. For the same interval of δ, the Reynolds number $\mathrm{Re} < 25$ which is typical for observed regular waves in film flows.

Fig. 2.4 and Fig. 2.5 illustrate the dependencies of the stretching parameter κ^2 and

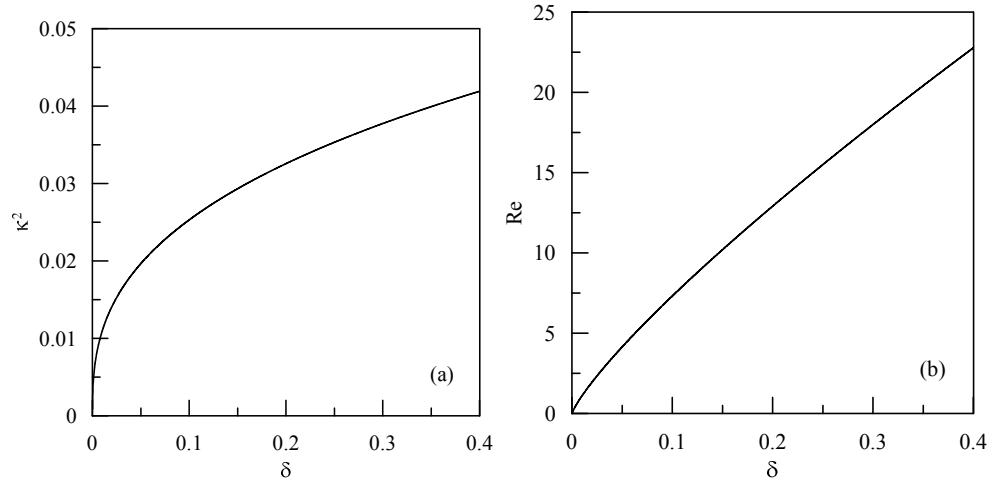

Figure 2.3: Dependencies of the stretching parameter κ^2 (a) and the Reynolds number Re (b) on the film parameter δ in the case water-benzene system at $H = 0.3$.

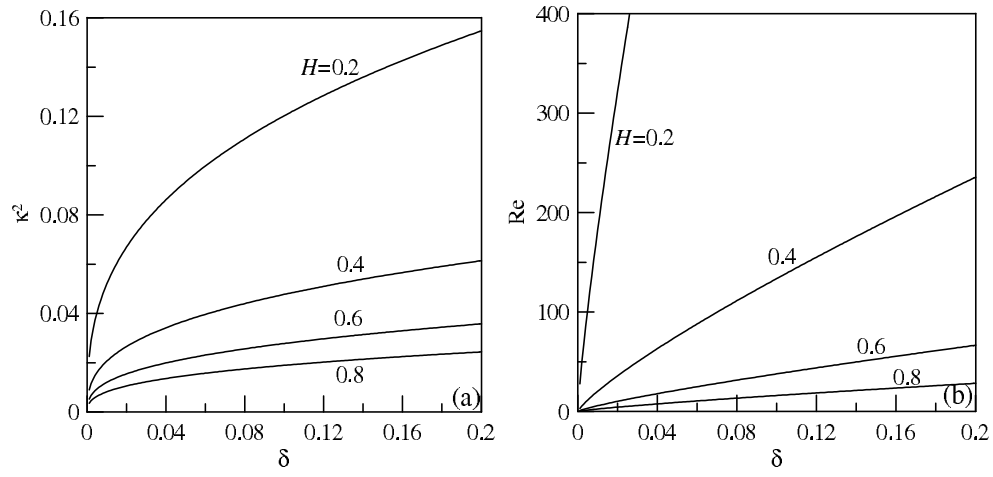

Figure 2.4: Dependencies of the stretching parameter κ^2 (a) and the Reynolds number Re (b) on the film parameter δ in the case water-benzene system at $H = 0.2, 0.4, 0.6, 0.8$.

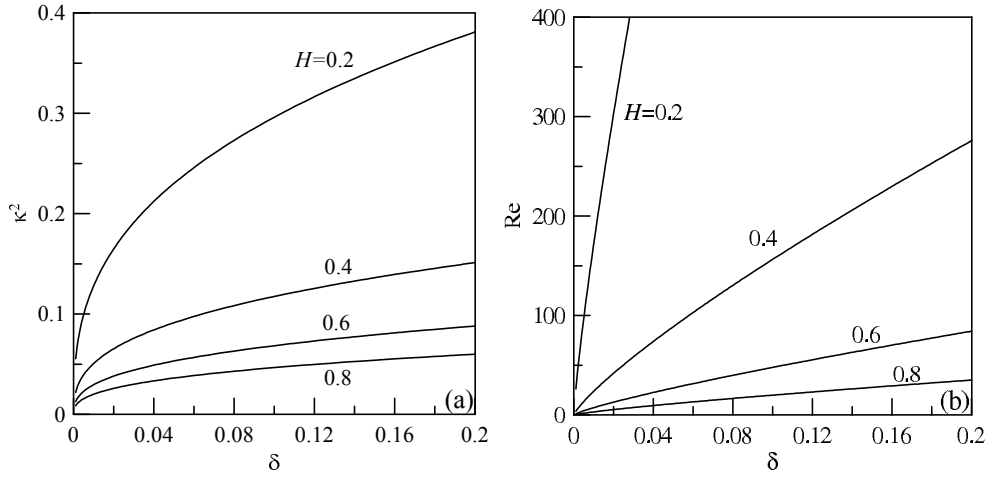

Figure 2.5: Dependencies of the stretching parameter κ^2 (a) and the Reynolds number Re (b) on the film parameter δ in the case benzene-water system at $H = 0.2, 0.4, 0.6, 0.8$.

the Reynolds number Re on the film parameter $\delta \in (0, 0.2)$ in the case water-benzene and benzene-water systems, respectively at different values of H. It is seen that decreasing the first layer thickness leads to growth of κ^2, or shorter longitudinal scale. Thus, accuracy of the approximation become worse. It is worthy to note that Fig. 2.4a contains Fig. 2.2a at $\delta \in [0, 0.2]$.

2.3.2 Approximate equations

The system (2.11) includes the following 5 parameters:

$$\kappa^2, \quad \delta = \frac{\kappa\varphi \mathrm{Re}}{5}, \quad \rho_0, \quad \nu_0, \quad \sigma_0. \tag{2.12}$$

As shown above, the stretching parameter $\kappa^2 \ll 1$ and we can neglect the terms of order κ^2:

$$\begin{aligned} &\frac{\partial u}{\partial x_\kappa} + \frac{\partial v_\kappa}{\partial y} = 0, \\ &\frac{\partial u}{\partial t_\kappa} + u\frac{\partial u}{\partial x_\kappa} + v_\kappa \frac{\partial u}{\partial y} = -\frac{1}{\rho_0^{(j)}}\frac{\partial p}{\partial x_\kappa} + \frac{\varphi \nu_0^{(j)}}{5\delta}\frac{\partial^2 u}{\partial y^2} + \frac{1}{5\delta}, \end{aligned} \tag{2.13}$$

$$
\begin{aligned}
&\frac{1}{\rho_0^{(j)}}\frac{\partial p}{\partial y}=0,\\
&y=0: \quad u=0, \quad v_\kappa=0,\\
&y=h^{(1)}(x_\kappa,t_\kappa): \quad \frac{\partial h^{(1)}}{\partial t_\kappa}+u\frac{\partial h^{(1)}}{\partial x_\kappa}=v_\kappa, \quad [u]_1^2=0, \quad [v_\kappa]_1^2=0,\\
&\qquad\qquad \left[\rho_0^{(j)}\nu_0^{(j)}\frac{\partial u}{\partial y}\right]_1^2=0, \quad [-p]_1^2+\frac{\sigma_0}{5\delta}\frac{\partial^2 h^{(1)}}{\partial x_\kappa^2}=0,\\
&y=h^{(2)}(x_\kappa,t_\kappa): \quad \frac{\partial h^{(2)}}{\partial t_\kappa}+u\frac{\partial h^{(2)}}{\partial x_\kappa}=v_\kappa, \quad \frac{\partial u}{\partial y}=0, \quad p+\frac{1}{5\delta}\frac{\partial^2 h^{(2)}}{\partial x_\kappa^2}=0.
\end{aligned}
$$

This is so-called long-wave approximation of the full Navier-Stokes problem in the film theory. The third equation and the balances of the normal stresses at the interface and free surface in (2.13) allow us to find the pressure in both layers:

$$
\begin{aligned}
y\in\left[0,h^{(1)}\right]: \quad & p=-\frac{1}{5\delta}\left(\sigma_0\frac{\partial^2 h^{(1)}}{\partial x_\kappa^2}+\frac{\partial^2 h^{(2)}}{\partial x_\kappa^2}\right),\\
y\in\left[h^{(1)},h^{(2)}\right]: \quad & p=-\frac{1}{5\delta}\frac{\partial^2 h^{(2)}}{\partial x_\kappa^2}.
\end{aligned}
$$

Having eliminated the pressure, we can rewrite the system in the form as

$$
\begin{aligned}
y=0: \quad & u=0, \quad v_\kappa=0,\\
y\in\left[0,h^{(1)}\right]: \quad & \frac{\partial u}{\partial x_\kappa}+\frac{\partial v_\kappa}{\partial y}=0,\\
& \frac{\partial u}{\partial t_\kappa}+u\frac{\partial u}{\partial x_\kappa}+v_\kappa\frac{\partial u}{\partial y}=\frac{1}{5\delta}\left(\frac{\sigma_0}{\rho_0}\frac{\partial^3 h^{(1)}}{\partial x_\kappa^3}+\frac{1}{\rho_0}\frac{\partial^3 h^{(2)}}{\partial x_\kappa^3}+\varphi\nu_0\frac{\partial^2 u}{\partial y^2}+1\right)\\
y=h^{(1)}: \quad & \frac{\partial h^{(1)}}{\partial t_\kappa}+u\frac{\partial h^{(1)}}{\partial x_\kappa}=v_\kappa, \quad [u]_1^2=0, \quad [v_\kappa]_1^2=0, \quad \left[\rho_0^{(j)}\nu_0^{(j)}\frac{\partial u}{\partial y}\right]_1^2=0,\\
y\in\left[h^{(1)},h^{(2)}\right]: \quad & \frac{\partial u}{\partial x_\kappa}+\frac{\partial v_\kappa}{\partial y}=0,\\
& \frac{\partial u}{\partial t_\kappa}+u\frac{\partial u}{\partial x_\kappa}+v_\kappa\frac{\partial u}{\partial y}=\frac{1}{5\delta}\left(\frac{\partial^3 h^{(2)}}{\partial x_\kappa^3}+\varphi\frac{\partial^2 u}{\partial y^2}+1\right),\\
y=h^{(2)}: \quad & \frac{\partial h^{(2)}}{\partial t_\kappa}+u\frac{\partial h^{(2)}}{\partial x_\kappa}=v_\kappa, \quad \frac{\partial u}{\partial y}=0.
\end{aligned}
$$

This is a nonlinear system with dispersion and viscosity that is stated in two adjacent domains with unknown boundaries.

2.3.3 Integral method

To simplify the approximate system, the continuity equations and momentum equations are integrated across thicknesses in each layer:

$$\frac{\partial h^{(1)}}{\partial t_\kappa} + \frac{\partial q^{(1)}}{\partial x_\kappa} = 0, \quad q^{(1)} \equiv \int_0^{h^{(1)}} u \, dy,$$

$$\frac{\partial q^{(1)}}{\partial t_\kappa} + \frac{\partial}{\partial x_\kappa} \int_0^{h^{(1)}} u^2 \, dy = \frac{1}{5\delta} \left[\frac{\sigma_0 h^{(1)}}{\rho_0} \frac{\partial^3 h^{(1)}}{\partial x_\kappa^3} + \frac{h^{(1)}}{\rho_0} \frac{\partial^3 h^{(2)}}{\partial x_\kappa^3} + \varphi \nu_0 \left(\left. \frac{\partial u}{\partial y} \right|_{h^{(1)}} - \left. \frac{\partial u}{\partial y} \right|_0 \right) + h^{(1)} \right],$$

$$\frac{\partial \left(h^{(2)} - h^{(1)} \right)}{\partial t_\kappa} + \frac{\partial q}{\partial x_\kappa} = 0, \quad q \equiv \int_{h^{(1)}}^{h^{(2)}} u \, dy,$$

$$\frac{\partial q}{\partial t_\kappa} + \frac{\partial}{\partial x_\kappa} \int_{h^{(1)}}^{h^{(2)}} u^2 \, dy = \frac{1}{5\delta} \left[\left(h^{(2)} - h^{(1)} \right) \frac{\partial^3 h^{(2)}}{\partial x_\kappa^3} + \varphi \left(\left. \frac{\partial u}{\partial y} \right|_{h^{(2)}} - \left. \frac{\partial u}{\partial y} \right|_{h^{(1)}} \right) + h^{(2)} - h^{(1)} \right],$$

where $q^{(1)}(x_\kappa, t_\kappa)$ and $q(x_\kappa, t_\kappa)$ are the local flow rates in the layers.

After summations of the continuity equations and the momentum equations we can replace the third and fourth equations, and rewrite the system as follows:

$$\frac{\partial h^{(1)}}{\partial t_\kappa} + \frac{\partial q^{(1)}}{\partial x_\kappa} = 0, \quad q^{(1)} \equiv \int_0^{h^{(1)}} u \, dy,$$

$$\frac{\partial q^{(1)}}{\partial t_\kappa} + \frac{\partial}{\partial x_\kappa} \int_0^{h^{(1)}} u^2 \, dy = \frac{1}{5\delta} \left[\frac{\sigma_0 h^{(1)}}{\rho_0} \frac{\partial^3 h^{(1)}}{\partial x_\kappa^3} + \frac{h^{(1)}}{\rho_0} \frac{\partial^3 h^{(2)}}{\partial x_\kappa^3} + \varphi \nu_0 \left(\left. \frac{\partial u}{\partial y} \right|_{h^{(1)}} - \left. \frac{\partial u}{\partial y} \right|_0 \right) + h^{(1)} \right],$$

$$\frac{\partial h^{(2)}}{\partial t_\kappa} + \frac{\partial q^{(2)}}{\partial x_\kappa} = 0, \quad q^{(2)} \equiv \int_0^{h^{(2)}} u \, dy,$$

$$\frac{\partial q^{(2)}}{\partial t_\kappa} + \frac{\partial}{\partial x_\kappa} \int\limits_0^{h^{(2)}} u^2 \, dy = \frac{1}{5\delta} \left[\frac{\sigma_0 h^{(1)}}{\rho_0} \frac{\partial^3 h^{(1)}}{\partial x_\kappa^3} + \left(h^{(2)} + \left(\frac{1}{\rho_0} - 1 \right) h^{(1)} \right) \frac{\partial^3 h^{(2)}}{\partial x_\kappa^3} \right]$$
$$+ \frac{\varphi}{5\delta} \left[\left. \frac{\partial u}{\partial y} \right|_{h^{(2)}} - \left. \frac{\partial u}{\partial y} \right|_{h^{(1)}+0} + \nu_0 \left(\left. \frac{\partial u}{\partial y} \right|_{h^{(1)}-0} - \left. \frac{\partial u}{\partial y} \right|_0 \right) \right] + \frac{h^{(2)}}{5\delta}.$$

To complete the system, we have to know how the velocity u depends on the thicknesses $h^{(1)}$ and $h^{(2)}$, and the flow rates $q^{(1)}$ and $q^{(2)}$. We assume that this dependence is similar to one for the waveless flow. So, the velocity profiles satisfy to the following boundary conditions

$$\begin{aligned} y = 0: \quad & u = 0, \\ y = h^{(1)}: \quad & [u]_1^2 = 0, \quad \left[\rho_0^{(j)} \nu_0^{(j)} \frac{\partial u}{\partial y} \right]_1^2 = 0, \\ y = h^{(2)}: \quad & \frac{\partial u}{\partial y} = 0, \end{aligned}$$

and we look for a solution in the form

$$\begin{aligned} y \in \left[0, h^{(1)}\right] \quad &: \quad u = U_{11} y + U_{12} y^2, \\ y \in \left[h^{(1)}, h^{(2)}\right] \quad &: \quad u = U_{20} + U_{22} \left(y^2 - 2h^{(2)} y \right). \end{aligned} \tag{2.14}$$

These velocity profiles satisfy the boundary conditions at $y = 0$ and $y = h^{(2)}$. Then, the boundary conditions at the interface $y = h^{(1)}$ and the definitions of the flow rates give us the following linear system for functions U_{11}, U_{12}, U_{20} and U_{22} :

$$\begin{aligned} & h^{(1)} U_{11} + \left(h^{(1)}\right)^2 U_{12} - U_{20} - h^{(1)} \left(h^{(1)} - 2h^{(2)}\right) U_{22} = 0, \\ & \rho_0 \nu_0 U_{11} + 2\rho_0 \nu_0 U_{12} h^{(1)} - 2U_{22} \left(h^{(1)} - h^{(2)}\right) = 0, \end{aligned} \tag{2.15}$$

$$\frac{\left(h^{(1)}\right)^2}{2}U_{11}+\frac{\left(h^{(1)}\right)^3}{3}U_{12}=q^{(1)},$$
$$\left(h^{(2)}-h^{(1)}\right)U_{20}+\left[\frac{\left(h^{(2)}\right)^3-\left(h^{(1)}\right)^3}{3}-h^{(2)}\left(\left(h^{(2)}\right)^2-\left(h^{(1)}\right)^2\right)\right]U_{22}=q^{(2)}-q^{(1)}.$$

The system (2.15) for these coefficients can be explicitly solved. First, we find the following coefficients depending on U_{12}:

$$\begin{aligned}
U_{11}&=\frac{2q^{(1)}}{\left(h^{(1)}\right)^2}-\frac{2h^{(1)}U_{12}}{3},\\
U_{22}&=-\frac{\rho_0\nu_0}{2}\frac{U_{11}+2U_{12}h^{(1)}}{h^{(2)}-h^{(1)}},\\
U_{20}&=\frac{q^{(2)}-q^{(1)}}{h^{(2)}-h^{(1)}}+\frac{1}{3}\left[2\left(h^{(2)}\right)^2+2h^{(1)}h^{(2)}-\left(h^{(1)}\right)^2\right]U_{22},
\end{aligned}$$

and then calculate this coefficient from the first equation of (2.15):

$$\begin{aligned}
U_{12}=&\frac{3}{h^{(1)}\left[\left(3-4\rho_0\nu_0\right)h^{(1)}+4\rho_0\nu_0h^{(2)}\right]}\\
&\times\left\{\frac{3q^{(2)}}{h^{(2)}-h^{(1)}}-\left[\frac{3}{h^{(2)}-h^{(1)}}+\frac{2}{\left(h^{(1)}\right)^2}\left[\left(3-\rho_0\nu_0\right)h^{(1)}+\rho_0\nu_0h^{(2)}\right]\right]q^{(1)}\right\}.
\end{aligned}$$

Thus, the coefficients U_{11}, U_{12}, U_{20} and U_{22} are found as

$$\begin{aligned}
U_{12}=&\frac{3}{h^{(1)}\left[\left(3-4\rho_0\nu_0\right)h^{(1)}+4\rho_0\nu_0h^{(2)}\right]}\\
&\times\left\{\frac{3q^{(2)}}{h^{(2)}-h^{(1)}}-\left[\frac{3}{h^{(2)}-h^{(1)}}+\frac{2}{\left(h^{(1)}\right)^2}\left[\left(3-\rho_0\nu_0\right)h^{(1)}+\rho_0\nu_0h^{(2)}\right]\right]q^{(1)}\right\},\\
U_{11}=&\frac{2q^{(1)}}{\left(h^{(1)}\right)^2}-\frac{2h^{(1)}U_{12}}{3},\\
U_{22}=&-\frac{\rho_0\nu_0}{2}\frac{U_{11}+2U_{12}h^{(1)}}{h^{(2)}-h^{(1)}},\\
U_{20}=&\frac{q^{(2)}-q^{(1)}}{h^{(2)}-h^{(1)}}+\frac{1}{3}\left[2\left(h^{(2)}\right)^2+2h^{(1)}h^{(2)}-\left(h^{(1)}\right)^2\right]U_{22}.
\end{aligned}\tag{2.16}$$

Finally, the system of differential equations for the functions $h^{(1)}$, $q^{(1)}$, $h^{(2)}$ and $q^{(2)}$ is stated:

$$\begin{aligned}
&\frac{\partial h^{(1)}}{\partial t_\kappa}+\frac{\partial q^{(1)}}{\partial x_\kappa}=0, \\
&\frac{\partial q^{(1)}}{\partial t_\kappa}+\frac{\partial J^{(1)}}{\partial x_\kappa}=\frac{h^{(1)}}{5\delta}\left(\frac{\sigma_0}{\rho_0}\frac{\partial^3 h^{(1)}}{\partial x_\kappa^3}+\frac{1}{\rho_0}\frac{\partial^3 h^{(2)}}{\partial x_\kappa^3}+2\varphi\nu_0 U_{12}+1\right), \\
&\frac{\partial h^{(2)}}{\partial t_\kappa}+\frac{\partial q^{(2)}}{\partial x_\kappa}=0, \\
&\frac{\partial q^{(2)}}{\partial t_\kappa}+\frac{\partial J^{(2)}}{\partial x_\kappa}=\frac{1}{5\delta}\left[\frac{\sigma_0 h^{(1)}}{\rho_0}\frac{\partial^3 h^{(1)}}{\partial x_\kappa^3}+\left(h^{(2)}+\left(\frac{1}{\rho_0}-1\right)h^{(1)}\right)\frac{\partial^3 h^{(2)}}{\partial x_\kappa^3}\right] \\
&\quad+\frac{\varphi}{5\delta}\left[2\nu_0 U_{12}h^{(1)}+2U_{22}\left(h^{(2)}-h^{(1)}\right)\right]+\frac{h^{(2)}}{5\delta},
\end{aligned} \tag{2.17}$$

where

$$J^{(1)}\equiv\int\limits_0^{h^{(1)}}u^2\,dy=\frac{U_{11}^2}{3}\left(h^{(1)}\right)^3+\frac{U_{11}U_{12}}{2}\left(h^{(1)}\right)^4+\frac{U_{12}^2}{5}\left(h^{(1)}\right)^5, \tag{2.18}$$

$$\begin{aligned}
J^{(2)}\equiv\int\limits_0^{h^{(2)}}u^2\,dy&=J^{(1)}+U_{20}^2\left(h^{(2)}-h^{(1)}\right)-2U_{20}U_{22}h^{(2)}\left[\left(h^{(2)}\right)^2-\left(h^{(1)}\right)^2\right]+ \\
&\frac{2}{3}\left[2U_{22}^2\left(h^{(2)}\right)^2+U_{20}U_{22}\right]\left[\left(h^{(2)}\right)^3-\left(h^{(1)}\right)^3\right]- \\
&U_{22}^2h^{(2)}\left[\left(h^{(2)}\right)^4-\left(h^{(1)}\right)^4\right]+\frac{U_{22}^2}{5}\left[\left(h^{(2)}\right)^5-\left(h^{(1)}\right)^5\right],
\end{aligned}$$

and U_{11}, U_{12}, U_{20} and U_{22} are given by (2.16). The system includes the parameters δ, σ_0, ρ_0 and ν_0.

The system (2.17) has the steady flow satisfying the following equations:

$$2\varphi\nu_0U_{12}+1=0,\quad \varphi\left[2\nu_0U_{12}h^{(1)}\left(1-\rho_0\right)-\rho_0\nu_0U_{11}\right]+h^{(2)}=0.$$

Its solution is

$$H^{(1)} = H, \quad Q^{(1)} = \frac{H^2}{2\varphi\nu_0}\left[\frac{1}{\rho_0} + \left(\frac{2}{3} - \frac{1}{\rho_0}\right)H\right], \tag{2.19}$$
$$H^{(2)} = 1, \quad Q^{(2)} = 1.$$

that coincides with (2.7).

Thus, we have derived the evolution system (2.17) whose coefficients are calculated from (2.16) and (2.18).

2.3.4 Linear stability

To verify whether the evolution equations approximate the full Navier-Stokes system, we can compare spectra of the linear stability of both models. To analyse the linear stability of the steady flow (2.19) in the framework of the system (2.17), we look for solution in the form

$$h^{(1)}(x_\kappa, t_\kappa) = h_f^{(1)} + \hat{h}^{(1)}(x_\kappa, t_\kappa), \quad h^{(2)}(x_\kappa, t_\kappa) = h_f^{(2)} + \hat{h}^{(2)}(x_\kappa, t_\kappa),$$
$$q^{(1)}(x_\kappa, t_\kappa) = q_f^{(1)} + \hat{q}^{(1)}(x_\kappa, t_\kappa), \quad q^{(2)}(x_\kappa, t_\kappa) = q_f^{(2)} + \hat{q}^{(2)}(x_\kappa, t_\kappa),$$

where

$$h_f^{(1)} = H, \quad h_f^{(2)} = 1, \quad q_f^{(1)} = Q^{(1)}, \quad q_f^{(2)} = Q^{(2)} = 1,$$

and the variables with hats are small perturbations.

Then, we linearise the coefficients in (2.17):

$$J^{(k)} = J_0^{(k)} + J_1^{(k)}\hat{h}^{(1)} + J_2^{(k)}\hat{h}^{(2)} + J_3^{(k)}\hat{q}^{(1)} + J_4^{(k)}\hat{q}^{(2)}, \quad k = 1, 2, \tag{2.20}$$

$$J_0^{(k)} = J^{(k)}\Big|_{h_f^{(1)},h_f^{(2)},q_f^{(1)},q_f^{(2)}}, \quad J_1^{(k)} = \frac{\partial J^{(k)}}{\partial h^{(1)}}\Big|_{h_f^{(1)},h_f^{(2)},q_f^{(1)},q_f^{(2)}}, \quad J_2^{(k)} = \frac{\partial J^{(k)}}{\partial h^{(2)}}\Big|_{h_f^{(1)},h_f^{(2)},q_f^{(1)},q_f^{(2)}},$$

$$J_3^{(k)} = \frac{\partial J^{(k)}}{\partial q^{(1)}}\Big|_{h_f^{(1)},h_f^{(2)},q_f^{(1)},q_f^{(2)}}, \quad J_4^{(k)} = \frac{\partial J^{(k)}}{\partial q^{(2)}}\Big|_{h_f^{(1)},h_f^{(2)},q_f^{(1)},q_f^{(2)}},$$

$$U_{kj} = U_{kj,0} + U_{kj,1}\hat{h}^{(1)} + U_{kj,2}\hat{h}^{(2)} + U_{kj,3}\hat{q}^{(1)} + U_{kj,4}\hat{q}^{(2)}, \quad (kj) = (11), (12), (20), (22),$$

$$U_{kj,0} = U_{kj}\Big|_{h_f^{(1)},h_f^{(2)},q_f^{(1)},q_f^{(2)}}, \quad U_{kj,1} = \frac{\partial U_{kj}}{\partial h^{(1)}}\Big|_{h_f^{(1)},h_f^{(2)},q_f^{(1)},q_f^{(2)}}, \quad U_{kj,2} = \frac{\partial U_{kj}}{\partial h^{(2)}}\Big|_{h_f^{(1)},h_f^{(2)},q_f^{(1)},q_f^{(2)}},$$

$$U_{kj,3} = \frac{\partial U_{kj}}{\partial q^{(1)}}\Big|_{h_f^{(1)},h_f^{(2)},q_f^{(1)},q_f^{(2)}}, \quad U_{kj,4} = \frac{\partial U_{kj}}{\partial q^{(2)}}\Big|_{h_f^{(1)},h_f^{(2)},q_f^{(1)},q_f^{(2)}}.$$

Now we return to the evolution equations. First, we write the continuity equations for perturbations:

$$\begin{aligned} &\frac{\partial \hat{h}^{(1)}}{\partial t_\kappa} + \frac{\partial \hat{q}^{(1)}}{\partial x_\kappa} = 0, \\ &\frac{\partial \hat{h}^{(2)}}{\partial t_\kappa} + \frac{\partial \hat{q}^{(2)}}{\partial x_\kappa} = 0. \end{aligned} \tag{2.21}$$

Then, the linearised momentum equations in both layers are written:

$$\begin{aligned} &\frac{\partial \hat{q}^{(1)}}{\partial t_\kappa} - \frac{h_f^{(1)}}{5\delta}\frac{\sigma_0}{\rho_0}\frac{\partial^3 \hat{h}^{(1)}}{\partial x_\kappa^3} + J_1^{(1)}\frac{\partial \hat{h}^{(1)}}{\partial x_\kappa} - \frac{1}{5\delta}\left(2\nu_0\varphi h_f^{(1)}U_{12,1} + 2\varphi\nu_0 U_{12,0} + 1\right)\hat{h}^{(1)} \\ &\quad + J_3^{(1)}\frac{\partial \hat{q}^{(1)}}{\partial x_\kappa} - \frac{2\varphi\nu_0 h_f^{(1)}U_{12,3}}{5\delta}\hat{q}^{(1)} - \frac{h_f^{(1)}}{5\delta\rho_0}\frac{\partial^3 \hat{h}^{(2)}}{\partial x_\kappa^3} + J_2^{(1)}\frac{\partial \hat{h}^{(2)}}{\partial x_\kappa} - \frac{2\varphi\nu_0 h_f^{(1)}U_{12,2}}{5\delta}\hat{h}^{(2)} \\ &\quad + J_4^{(1)}\frac{\partial \hat{q}^{(2)}}{\partial x_\kappa} - \frac{2\varphi\nu_0 h_f^{(1)}U_{12,4}}{5\delta}\hat{q}^{(2)} = 0, \end{aligned} \tag{2.22}$$

and

$$\begin{aligned}
&\frac{\partial \hat{q}^{(2)}}{\partial t_\kappa} - \frac{\sigma_0 h_f^{(1)}}{5\delta\rho_0}\frac{\partial^3 \hat{h}^{(1)}}{\partial x_\kappa^3} + J_1^{(2)}\frac{\partial \hat{h}^{(1)}}{\partial x_\kappa} \\
&\quad -\frac{\varphi}{5\delta}\left[2\nu_0\left(1-\rho_0\right)h_f^{(1)}U_{12,1} - \rho_0\nu_0 U_{11,1} + 2\nu_0\left(1-\rho_0\right)U_{12,0}\right]\hat{h}^{(1)} \\
&\quad +J_3^{(2)}\frac{\partial \hat{q}^{(1)}}{\partial x_\kappa} - \frac{\varphi}{5\delta}\left[2\nu_0\left(1-\rho_0\right)h_f^{(1)}U_{12,3} - \rho_0\nu_0 U_{11,3}\right]\hat{q}^{(1)} \\
&\quad -\frac{1}{5\delta}\left[h_f^{(2)} + \left(\frac{1}{\rho_0}-1\right)h_f^{(1)}\right]\frac{\partial^3 \hat{h}^{(2)}}{\partial x_\kappa^3} + J_2^{(2)}\frac{\partial \hat{h}^{(2)}}{\partial x_\kappa} \\
&\quad -\frac{1}{5\delta}\left[2\varphi\nu_0\left(1-\rho_0\right)h_f^{(1)}U_{12,2} - \rho_0\nu_0\varphi U_{11,2} + 1\right]\hat{h}^{(2)} \\
&\quad +J_4^{(2)}\frac{\partial \hat{q}^{(2)}}{\partial x_\kappa} - \frac{\varphi}{5\delta}\left[2\nu_0\left(1-\rho_0\right)h_f^{(1)}U_{12,4} - \rho_0\nu_0 U_{11,4}\right]\hat{q}^{(2)} = 0.
\end{aligned} \tag{2.23}$$

Equations (2.21), (2.22) and (2.23) have solution in the form of normal mode

$$\begin{aligned}
&\left(\hat{h}^{(1)}(x_\kappa,t_\kappa), \hat{h}^{(2)}(x_\kappa,t_\kappa), \hat{q}^{(1)}(x_\kappa,t_\kappa), \hat{q}^{(2)}(x_\kappa,t_\kappa)\right) = \\
&\qquad \left(\breve{h}^{(1)}, \breve{h}^{(2)}, \breve{q}^{(1)}, \breve{q}^{(2)}\right)\exp\left(i\alpha_\kappa\left(x_\kappa - ct_\kappa\right)\right),
\end{aligned}$$

where α_κ is the x_κ-axis wavenumber and $c = c_r + ic_i$ is the complex wave velocity whose imaginary part c_i determine stability of the waveless flow.

After substituting this solution, the continuity equations (2.21) give us

$$\breve{q}^{(1)} = c\breve{h}^{(1)}, \quad \breve{q}^{(2)} = c\breve{h}^{(2)},$$

and the linearised momentum equations (2.22) and (2.23) are reduced to the following linear algebraic system for amplitudes $\breve{h}^{(1)}$ and $\breve{h}^{(2)}$

$$\begin{aligned}
&\left(b_{11,2}c^2 + b_{11,1}c + b_{11,0}\right)\breve{h}^{(1)} + \left(b_{12,1}c + b_{12,0}\right)\breve{h}^{(2)} = 0, \\
&\left(b_{21,1}c + b_{21,0}\right)\breve{h}^{(1)} + \left(b_{22,2}c^2 + b_{22,1}c + b_{22,0}\right)\breve{h}^{(2)} = 0,
\end{aligned} \tag{2.24}$$

where the coefficients have the forms

$$
\begin{aligned}
b_{11,2} &= -i\alpha_\kappa, \\
b_{11,1} &= i\alpha_\kappa J_3^{(1)} - \frac{2\varphi\nu_0 h_f^{(1)} U_{12,3}}{5\delta}, \\
b_{11,0} &= i\alpha_\kappa^3 \frac{h_f^{(1)}}{5\delta}\frac{\sigma_0}{\rho_0} + i\alpha_\kappa J_1^{(1)} - \frac{1}{5\delta}\left(2\varphi\nu_0 h_f^{(1)} U_{12,1} + 2\varphi\nu_0 U_{12,0} + 1\right), \\
b_{12,1} &= i\alpha_\kappa J_4^{(1)} - \frac{2\varphi\nu_0 h_f^{(1)} U_{12,4}}{5\delta}, \\
b_{12,0} &= \frac{i\alpha_\kappa^3}{\rho_0}\frac{h_f^{(1)}}{5\delta} + J_2^{(1)} i\alpha_\kappa - \frac{2\varphi\nu_0 h_f^{(1)} U_{12,2}}{5\delta}, \\
b_{21,1} &= J_3^{(2)} i\alpha_\kappa - \frac{\varphi}{5\delta}\left[2\nu_0\left(1-\rho_0\right) h_f^{(1)} U_{12,3} - \rho_0\nu_0 U_{11,3}\right], \\
b_{21,0} &= i\alpha_\kappa^3 \frac{\sigma_0 h_f^{(1)}}{5\delta\rho_0} + J_1^{(2)} i\alpha_\kappa \\
&\quad -\frac{\varphi}{5\delta}\left[2\nu_0\left(1-\rho_0\right) h_f^{(1)} U_{12,1} - \rho_0\nu_0 U_{11,1} + 2\nu_0\left(1-\rho_0\right) U_{12,0}\right], \\
b_{22,2} &= -i\alpha_\kappa, \\
b_{22,1} &= J_4^{(2)} i\alpha_\kappa - \frac{\varphi}{5\delta}\left[2\nu_0\left(1-\rho_0\right) h_f^{(1)} U_{12,4} - \rho_0\nu_0 U_{11,4}\right], \\
b_{22,0} &= \frac{i\alpha_\kappa^3}{5\delta}\left[h_f^{(2)} + \left(\frac{1}{\rho_0} - 1\right) h_f^{(1)}\right] + J_2^{(2)} i\alpha_\kappa \\
&\quad -\frac{1}{5\delta}\left[2\varphi\nu_0\left(1-\rho_0\right) h_f^{(1)} U_{12,2} - \rho_0\nu_0\varphi U_{11,2} + 1\right].
\end{aligned}
\tag{2.25}
$$

The characteristic equation for the eigenvalue c is toward from the condition that there is a nontrivial solution of the linear algebraic system (2.24):

$$
b_4 c^4 + b_3 c^3 + b_2 c^2 + b_1 c + b_0 = 0 \tag{2.26}
$$

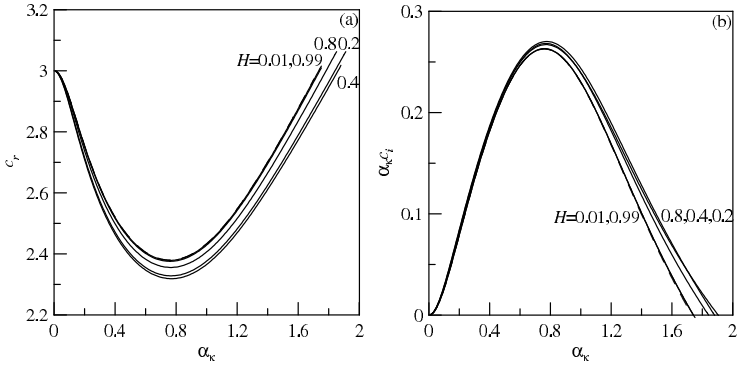

Figure 2.6: Wave velocities (a) and amplification factors (b) in the case when the same liquid is in both layers at $\delta = 0.2$ and different values of H.

where the coefficients are

$$
\begin{aligned}
b_4 &= b_{11,2}b_{22,2}, \qquad (2.27)\\
b_3 &= b_{11,2}b_{22,1} + b_{11,1}b_{22,2},\\
b_2 &= b_{11,2}b_{22,0} + b_{11,1}b_{22,1} + b_{11,0}b_{22,2} - b_{12,1}b_{21,1},\\
b_1 &= b_{11,1}b_{22,0} + b_{11,0}b_{22,1} - b_{12,1}b_{21,0} - b_{12,0}b_{21,1},\\
b_0 &= b_{11,0}b_{22,0} - b_{12,0}b_{21,0}.
\end{aligned}
$$

Finally, an eigenvalue c is a root of polynomial equation (2.26) whose coefficients are computed in (2.25) and (2.27).

2.3.5 Results

To verify the method, we start from the case when the same liquid is in both layers, and there is no surface tension on the interface. Fig. 2.6 shows the wave velocities and amplification factors. At small, $H = 0.01$, and large, $H = 0.99$, values of the interface thickness H, the values c_r and $\alpha_\kappa c_i$ are coincides with the case of the one-layer film (these curves are also shown in the figures). At intermediate values of H, there is some discrepancy since the linear analysis of the two-layer film flow includes independent perturbations of

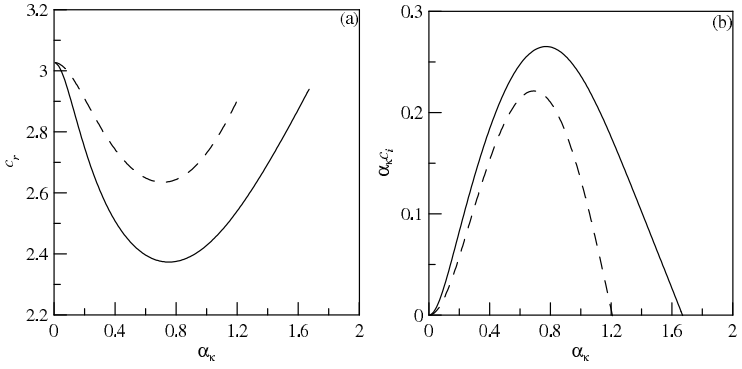

Figure 2.7: Wave velocity (a) and amplification factors (b) for the surface mode in the case of water-benzene system at $\delta = 0.2$ and $H = 0.6$. The solutions of the Orr-Sommerfeld problem and the integral method are shown by dashed curves and solid curves, respectively.

the interface in the contrast to the one-layer film.

To be able to compare spectra computed from (2.8) and (2.26), we need to recalculate wavenumbers and amplification factors in both models:

$$\alpha_\kappa = \frac{2\pi}{L_\kappa} = \frac{2\pi}{\kappa L} = \frac{\alpha}{\kappa},$$
$$c = \frac{dx_\kappa}{dt_\kappa} = \frac{\kappa\, dx}{\kappa\, dt} = \frac{dx}{dt},$$

where L_κ and L are wavelengths along x_κ-axis and x-axis, respectively. In other words, the complex velocity is the same in both models, and the wavenumbers have the coefficients of proportionality κ.

The two-layer film flow has two unstable modes at moderate flow rates [32, 31, 33, 62]. Examples of eigenvalues of the surface mode and the interface mode in the case of water-benzene system at $\delta = 0.2$ and $H = 0.6$ are shown in Figs. 2.7 and 2.8, respectively. It is seen that the integral method provides good approximation of the wave velocity and the amplification factor in the case of the surface mode. The wave velocities of the interface mode in both methods are very close but the amplification factors of the interface mode

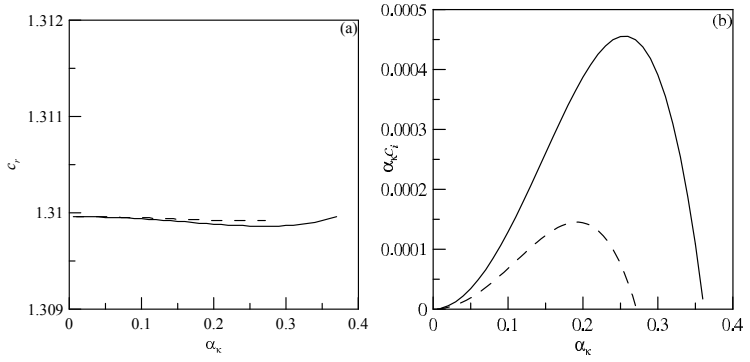

Figure 2.8: Wave velocity (a) and amplification factors (b) for the interface mode in the case of water-benzene system at $\delta = 0.2$ and $H = 0.6$. The solutions of the Orr-Sommerfeld problem and the integral method are shown by dashed curves and solid curves, respectively.

differ. The reason is its very small value in comparison with the one of the surface mode.

Fig. 2.9 and Fig. 2.10 show the wave velocity c_r and amplification factor $\alpha_\kappa c_i$ in the case of water-benzene system at $H = 0.3$ and $\delta = 0.1$. In dimensional terms, this example corresponds to the film thickness $H_c = 0.116$ mm and the average velocity $U_c = 4.66$ cm/s when Re $= 7.3$. In parallel, Figs. 2.9 and 2.10 also show the results of the Orr-Sommerfeld problem (2.8).

It is seen that the model (2.17) provides a good approximation of the intervals of instability and wave velocities of both modes. This is a typical case for one-layer film flows, and successful applications of the integral method are explained by the fact that real-life waves are usually observed for $\alpha_\kappa \leq \alpha_{\kappa,n}/2$ where $\alpha_{\kappa,n}$ is the neutral wavenumber of the surface mode. In the considered case, eigenvalues of the surface mode computed in both models are also close but there is some discrepancy of the amplification factors of two models for the interface mode. However, we note that the scale of amplification factors of the interface mode is about one thousand times smaller than ones of the surface mode. Even for such small values lying on the border of the method accuracy, the approximate model gives sufficiently good results, in particular as $\alpha_\kappa \to 0$.

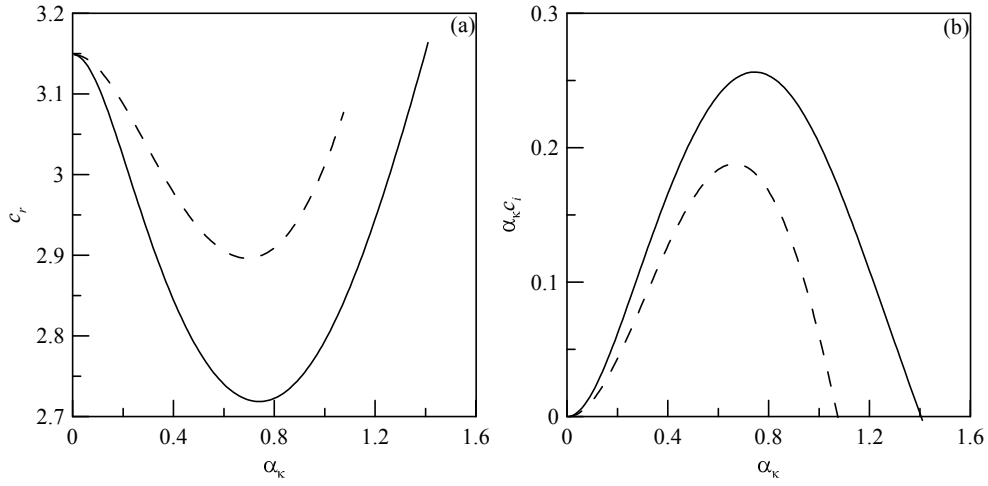

Figure 2.9: Wave velocity (a) and amplification factors (b) for the surface mode in the case of water-benzene system at $\delta = 0.1$ and $H = 0.3$. The solutions of the Orr-Sommerfeld problem and the integral method are shown by dashed curves and solid curves, respectively.

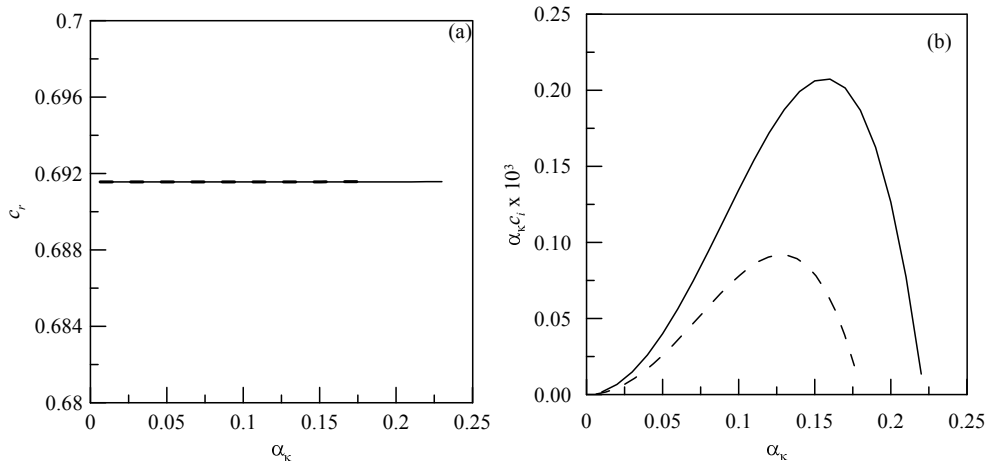

Figure 2.10: Wave velocity (a) and amplification factors (b) for the interface mode in the case of water-benzene system at $\delta = 0.1$ and $H = 0.3$. The solutions of the Orr-Sommerfeld problem and the integral method are shown by dashed curves and solid curves, respectively.

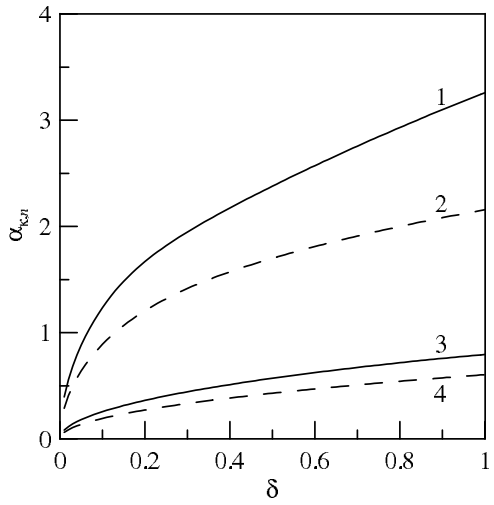

Figure 2.11: Neutral curves of the surface mode (curves 1 and 2) and the interface mode (3 and 4) in the case of water-benzene system at $H = 0.6$. Curves 1 and 3 corresponds to solutions of the integral method, and curves 2 and 4 denote solutions of the Orr-Sommerfeld problem.

Neutral curves for water-benzene system are shown in Fig. 2.11 and Fig. 2.12 at $H = 0.6$ and 0.3, respectively. It is seen that the neutral curves computed by the integral method are in a good agreement with the solutions of the Orr-Sommerfeld problem at relatively small values of δ, and the interface mode is unstable at relatively small values of the wavenumber. It indicates that the unstable interface modes can affect only very long waves.

It is worthy to note that amplification factors of the interface mode can be comparable with that of the surface mode in films flowing down an inclined wall whose inclination is relatively small [62].

2.4 Asymptotic behaviour of very long waves

In this section, we analytically and numerically study asymptotic properties of very long waves to compare below with shapes of non-linear periodic waves at small wavenumber which are computed in Chapter 3.

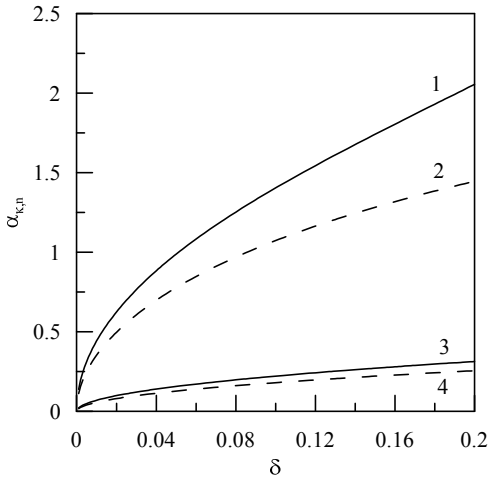

Figure 2.12: Neutral curves of the surface mode (curves 1 and 2) and the interface mode (3 and 4) in the case of water-benzene system at $H = 0.3$. Curves 1 and 3 corresponds to solutions of the integral method, and curves 2 and 4 denote solutions of the Orr-Sommerfeld problem.

2.4.1 Equations

To find a steady-travelling wave, we look for solution of (2.17) in the form

$$h^{(1)}(\xi), \quad h^{(2)}(\xi), \quad q^{(1)}(\xi), \quad q^{(2)}(\xi), \quad \xi = x_\kappa - ct_\kappa,$$

where c is the wave velocity to be found. Having substituted this solution in the system, we arrive at the following ordinary differential equations:

$$\begin{aligned}
&-c\frac{dh^{(1)}}{d\xi} + \frac{dq^{(1)}}{d\xi} = 0,\\
&-c\frac{dq^{(1)}}{d\xi} + \frac{dJ^{(1)}}{d\xi} = h^{(1)}\left[\frac{1}{5\delta}\left(\frac{\sigma_0}{\rho_0}\frac{d^3h^{(1)}}{d\xi^3} + \frac{1}{\rho_0}\frac{d^3h^{(2)}}{d\xi^3} + 2\varphi\nu_0 U_{12} + 1\right)\right],\\
&-c\frac{dh^{(2)}}{d\xi} + \frac{dq^{(2)}}{d\xi} = 0,
\end{aligned}$$

$$-c\frac{dq^{(2)}}{d\xi}+\frac{dJ^{(2)}}{d\xi}=\frac{1}{5\delta}\left[\frac{\sigma_0 h^{(1)}}{\rho_0}\frac{d^3h^{(1)}}{d\xi^3}+\left(h^{(2)}+\left(\frac{1}{\rho_0}-1\right)h^{(1)}\right)\frac{d^3h^{(2)}}{d\xi^3}\right]$$
$$+\frac{\varphi}{5\delta}\left[2\nu_0 U_{12}h^{(1)}\left(1-\rho_0\right)-\rho_0\nu_0 U_{11}\right]+\frac{h^{(2)}}{5\delta}.$$

Integrating the continuity equations gives us:

$$q^{(1)}=ch^{(1)}+q_\infty^{(1)},\quad q^{(2)}=ch^{(2)}+q_\infty^{(2)} \tag{2.28}$$

where the constants $q_\infty^{(1)}$ and $q_\infty^{(2)}$ have to be found.

Then, the system for $h^{(1)}(\xi)$ and $h^{(2)}(\xi)$ is rewritten in the form:

$$-c^2\frac{dh^{(1)}}{d\xi}+\frac{dJ^{(1)}}{d\xi}=h^{(1)}\left[\frac{1}{5\delta}\left(\frac{\sigma_0}{\rho_0}\frac{d^3h^{(1)}}{d\xi^3}+\frac{1}{\rho_0}\frac{d^3h^{(2)}}{d\xi^3}+2\varphi\nu_0U_{12}+1\right)\right], \tag{2.29}$$
$$-c^2\frac{dh^{(2)}}{d\xi}+\frac{dJ^{(2)}}{d\xi}=\frac{1}{5\delta}\left[\frac{\sigma_0 h^{(1)}}{\rho_0}\frac{d^3h^{(1)}}{d\xi^3}+\left(h^{(2)}+\left(\frac{1}{\rho_0}-1\right)h^{(1)}\right)\frac{d^3h^{(2)}}{d\xi^3}\right]$$
$$+\frac{\varphi}{5\delta}\left[2\nu_0 U_{12}h^{(1)}\left(1-\rho_0\right)-\rho_0\nu_0 U_{11}\right]+\frac{h^{(2)}}{5\delta},$$
$$q^{(1)}=ch^{(1)}+q_\infty^{(1)},\quad q^{(2)}=ch^{(2)}+q_\infty^{(2)}.$$

2.4.2 Fixed points

The system (2.29) possesses a fixed point, $h^{(1)}=h_f^{(1)}=$ constant and $h^{(2)}=h_f^{(2)}=$ constant, if the values of $h_f^{(1)}$ and $h_f^{(2)}$ satisfy the nonlinear algebraic equations

$$2\varphi\nu_0U_{12}+1=0,\quad \varphi\left[2\nu_0U_{12}h^{(1)}\left(1-\rho_0\right)-\rho_0\nu_0U_{11}\right]+h^{(2)}=0.$$

These equations have at least one solution that is (2.19):

$$h_f^{(1)}=H,\quad q_f^{(1)}=Q^{(1)}=\frac{H^2}{2\varphi\nu_0}\left[\frac{1}{\rho_0}+\left(\frac{2}{3}-\frac{1}{\rho_0}\right)H\right],$$
$$h_f^{(2)}=1,\quad q_f^{(2)}=Q^{(2)}=1.$$

Thus, we can calculate the constants in (2.28)

$$q_\infty^{(1)} = Q^{(1)} - cH, \quad q_\infty^{(2)} = Q^{(2)} - c,$$

to obtain the flow rates in the form

$$q^{(1)} = c\left(h^{(1)} - H\right) + Q^{(1)}, \quad q^{(2)} = c\left(h^{(2)} - 1\right) + Q^{(2)}.$$

Finally, we have arrived to the following problem to find an one-parametric set of fixed points $\left(h_f^{(1)}, h_f^{(2)}, c_f\right)$:

$$\begin{aligned}
&2\varphi\nu_0 U_{12} + 1 = 0, \quad \varphi\left[2\nu_0 U_{12} h^{(1)}\left(1-\rho_0\right) - \rho_0\nu_0 U_{11}\right] + h^{(2)} = 0, \qquad (2.30)\\
&\varphi = \frac{H^2}{2\nu_0}\left[\frac{1}{\rho_0} + \left(\frac{2}{3} - \frac{1}{\rho_0}\right)H\right]\\
&\quad + (1-H)\left[\frac{1}{3} + \left(\frac{1}{\rho_0\nu_0} - \frac{2}{3}\right)H + \left(\frac{1}{3} + \frac{1}{2\nu_0} - \frac{1}{\rho_0\nu_0}\right)H^2\right],\\
&q^{(1)} = c\left(h^{(1)} - H\right) + Q^{(1)}, \quad q^{(2)} = c\left(h^{(2)} - 1\right) + Q^{(2)},
\end{aligned}$$

where the functions U_{11} and U_{12} are given by the equations (2.16).

Equations (2.30) can be formally rewritten as

$$f_1\left(h^{(1)}, h^{(2)}, c; \rho_0, \nu_0, H\right) = 0, \quad f_2\left(h^{(1)}, h^{(2)}, c; \rho_0, \nu_0, H\right) = 0.$$

In 3D space $\left(h^{(1)}, h^{(2)}, c\right)$, these equations describe curves, and one of the curves is the line $h^{(1)} = H,\ h^{(2)} = 1$, see examples in Fig. 2.13 for water-benzene and benzene-water systems at $H = 0.6$. It is shown that there are bifurcation points B_I and B_S for the bifurcating fixed points of the first type and the second type, respectively. The same example is also shown in plane (c, h) in Fig. 2.14 for water-benzene system.

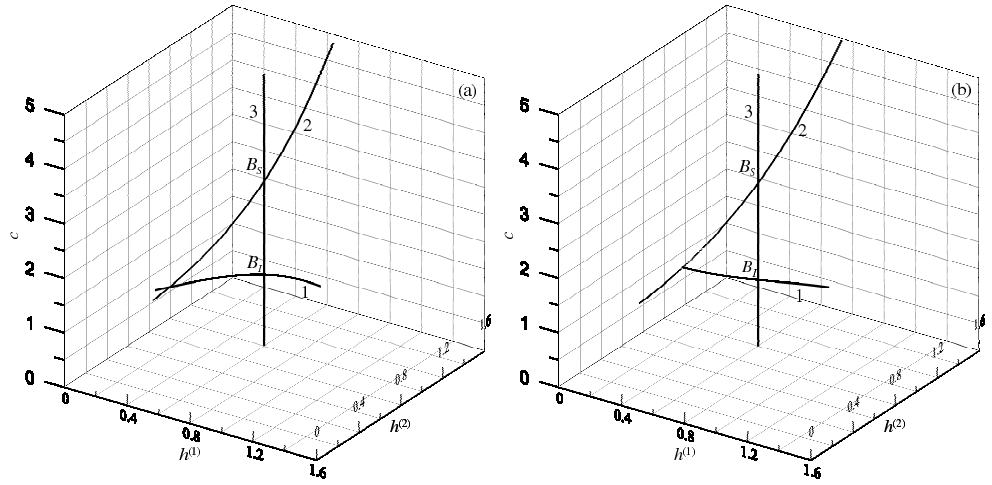

Figure 2.13: Fixed points of the steady flow in the case of (a) water-benzene system and (b) benzene-water system at $H = 0.6$. Curves 1, 2 and 3 denote the bifurcating fixed points of the first type, bifurcating fixed points of the second type and waveless flow, respectively.

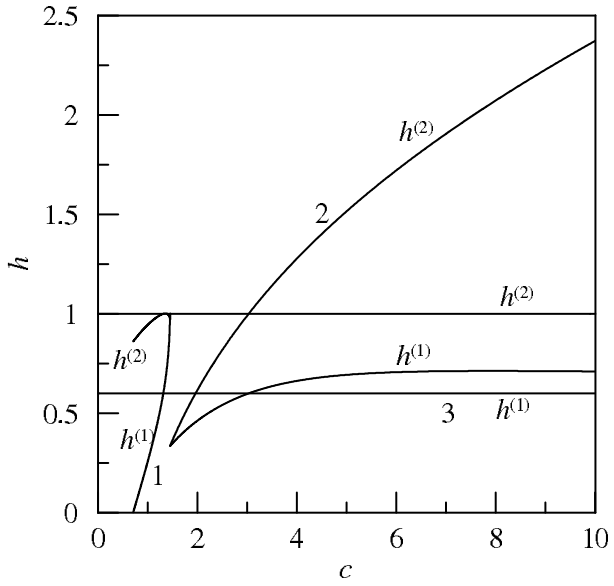

Figure 2.14: Fixed points of the steady flow in the case of water-benzene system at $H = 0.6$. Curves 1, 2 and 3 denote the bifurcating fixed points of the first type, bifurcating fixed points of the second type and waveless flow, respectively.

2.4.3 Solutions in neighbourhood of a fixed point

To investigate solutions of equations (2.29) in the neighbourhood of a fixed point $\left(h_f^{(1)}, h_f^{(2)}, q_f^{(1)}, q_f^{(2)}, c_f\right)$, we are looking for solution in the form

$$h^{(1)} = h_f^{(1)} + \hat{h}^{(1)}, \quad h^{(2)} = h_f^{(2)} + \hat{h}^{(2)}, \quad q^{(1)} = q_f^{(1)} + \hat{q}^{(1)}, \quad q^{(2)} = q_f^{(2)} + \hat{q}^{(2)}$$

where $q_f^{(1)} = ch_f^{(1)} + q_\infty^{(1)}$ and $q_f^{(2)} = ch_f^{(2)} + q_\infty^{(2)}$, and $\hat{h}^{(1)}$, $\hat{h}^{(2)}$, $\hat{q}^{(1)}$ and $\hat{q}^{(2)}$ are small perturbations.

Similar to (2.20), we linearise the following functions:

$$\begin{aligned}
&J^{(k)} = J_0^{(k)} + J_1^{(k)}\hat{h}^{(1)} + J_2^{(k)}\hat{h}^{(2)} + J_3^{(k)}\hat{q}^{(1)} + J_4^{(k)}\hat{q}^{(2)}, \quad k = 1, 2,\\
&\quad J_0^{(k)} = J^{(k)}\Big|_{h_f^{(1)}, h_f^{(2)}, q_f^{(1)}, q_f^{(2)}}, \quad J_1^{(k)} = \frac{\partial J^{(k)}}{\partial h^{(1)}}\Big|_{h_f^{(1)}, h_f^{(2)}, q_f^{(1)}, q_f^{(2)}}, \quad J_2^{(k)} = \frac{\partial J^{(k)}}{\partial h^{(2)}}\Big|_{h_f^{(1)}, h_f^{(2)}, q_f^{(1)}, q_f^{(2)}},\\
&\quad J_3^{(k)} = \frac{\partial J^{(k)}}{\partial q^{(1)}}\Big|_{h_f^{(1)}, h_f^{(2)}, q_f^{(1)}, q_f^{(2)}}, \quad J_4^{(k)} = \frac{\partial J^{(k)}}{\partial q^{(2)}}\Big|_{h_f^{(1)}, h_f^{(2)}, q_f^{(1)}, q_f^{(2)}},\\
&U_{kj} = U_{kj,0} + U_{kj,1}\hat{h}^{(1)} + U_{kj,2}\hat{h}^{(2)} + U_{kj,3}\hat{q}^{(1)} + U_{kj,4}\hat{q}^{(2)}, \quad (kj) = (11), (12),\\
&\quad U_{kj,0} = U_{kj}\Big|_{h_f^{(1)}, h_f^{(2)}, q_f^{(1)}, q_f^{(2)}}, \quad U_{kj,1} = \frac{\partial U_{kj}}{\partial h^{(1)}}\Big|_{h_f^{(1)}, h_f^{(2)}, q_f^{(1)}, q_f^{(2)}}, \quad U_{kj,2} = \frac{\partial U_{kj}}{\partial h^{(2)}}\Big|_{h_f^{(1)}, h_f^{(2)}, q_f^{(1)}, q_f^{(2)}},\\
&\quad U_{kj,3} = \frac{\partial U_{kj}}{\partial q^{(1)}}\Big|_{h_f^{(1)}, h_f^{(2)}, q_f^{(1)}, q_f^{(2)}}, \quad U_{kj,4} = \frac{\partial U_{kj}}{\partial q^{(2)}}\Big|_{h_f^{(1)}, h_f^{(2)}, q_f^{(1)}, q_f^{(2)}},
\end{aligned}$$

and then linearise the equations

$$\begin{aligned}
&-c^2\frac{d\hat{h}^{(1)}}{d\xi} + \frac{d}{d\xi}\left(J_1^{(1)}\hat{h}^{(1)} + J_2^{(1)}\hat{h}^{(2)} + J_3^{(1)}\hat{q}^{(1)} + J_4^{(1)}\hat{q}^{(2)}\right)\\
&\quad = \frac{h_f^{(1)}}{5\delta}\left(\frac{\sigma_0}{\rho_0}\frac{d^3\hat{h}^{(1)}}{d\xi^3} + \frac{1}{\rho_0}\frac{d^3\hat{h}^{(2)}}{d\xi^3} + 2\varphi\nu_0\left(U_{12,1}\hat{h}^{(1)} + U_{12,2}\hat{h}^{(2)} + U_{12,3}\hat{q}^{(1)} + U_{12,4}\hat{q}^{(2)}\right)\right)\\
&\quad + \frac{2\varphi\nu_0 U_{12,0} + 1}{5\delta}\hat{h}^{(1)},
\end{aligned}$$

$$
\begin{aligned}
&-c^2\frac{d\hat{h}^{(2)}}{d\xi}+\frac{d}{d\xi}\left(J_1^{(2)}\hat{h}^{(1)}+J_2^{(2)}\hat{h}^{(2)}+J_3^{(2)}\hat{q}^{(1)}+J_4^{(2)}\hat{q}^{(2)}\right)\\
&\quad=\frac{1}{5\delta}\left[\frac{\sigma_0 h_f^{(1)}}{\rho_0}\frac{d^3\hat{h}^{(1)}}{d\xi^3}+\left(h_f^{(2)}+\left(\frac{1}{\rho_0}-1\right)h_f^{(1)}\right)\frac{d^3\hat{h}^{(2)}}{d\xi^3}\right]\\
&\quad+\frac{\varphi}{5\delta}\Bigg[2\nu_0 h_f^{(1)}\left(1-\rho_0\right)\left(U_{12,1}\hat{h}^{(1)}+U_{12,2}\hat{h}^{(2)}+U_{12,3}\hat{q}^{(1)}+U_{12,4}\hat{q}^{(2)}\right)\\
&\quad-\rho_0\nu_0\left(U_{11,1}\hat{h}^{(1)}+U_{11,2}\hat{h}^{(2)}+U_{11,3}\hat{q}^{(1)}+U_{11,4}\hat{q}^{(2)}\right)\Bigg]+\frac{2\varphi\nu_0 U_{12,0}\left(1-\rho_0\right)}{5\delta}\hat{h}^{(1)}+\frac{\hat{h}^{(2)}}{5\delta},\\
&\hat{q}^{(1)}=c\hat{h}^{(1)},\quad \hat{q}^{(2)}=c\hat{h}^{(2)}.
\end{aligned}
$$

Using the last two equations, we eliminate the terms $\hat{q}^{(1)}$ and $\hat{q}^{(2)}$, and then rewrite the equations in the form:

$$
\begin{aligned}
&\frac{\sigma_0 h_f^{(1)}}{5\delta\rho_0}\frac{d^3\hat{h}^{(1)}}{d\xi^3}+\left[c^2-J_1^{(1)}-cJ_3^{(1)}\right]\frac{d\hat{h}^{(1)}}{d\xi}\\
&\quad+\frac{1}{5\delta}\left[2\varphi\nu_0 h_f^{(1)}\left(U_{12,1}+cU_{12,3}\right)+2\varphi\nu_0 U_{12,0}+1\right]\hat{h}^{(1)}\\
&\quad+\frac{h_f^{(1)}}{5\delta\rho_0}\frac{d^3\hat{h}^{(2)}}{d\xi^3}-\left[J_2^{(1)}+cJ_4^{(1)}\right]\frac{d\hat{h}^{(2)}}{d\xi}+\frac{2\varphi\nu_0 h_f^{(1)}}{5\delta}\left(U_{12,2}+cU_{12,4}\right)\hat{h}^{(2)}=0,\\
&\frac{\sigma_0 h_f^{(1)}}{5\delta\rho_0}\frac{d^3\hat{h}^{(1)}}{d\xi^3}-\left[J_1^{(2)}+cJ_3^{(2)}\right]\frac{d\hat{h}^{(1)}}{d\xi}\\
&\quad+\frac{\varphi}{5\delta}\left[2\nu_0 h_f^{(1)}\left(1-\rho_0\right)\left(U_{12,1}+cU_{12,3}\right)-\rho_0\nu_0\left(U_{11,1}+cU_{11,3}\right)+2\nu_0 U_{12,0}\left(1-\rho_0\right)\right]\hat{h}^{(1)}\\
&\quad+\frac{1}{5\delta}\left(h_f^{(2)}+\left(\frac{1}{\rho_0}-1\right)h_f^{(1)}\right)\frac{d^3\hat{h}^{(2)}}{d\xi^3}+\left[c^2-J_2^{(2)}-cJ_4^{(2)}\right]\frac{d\hat{h}^{(2)}}{d\xi}\\
&\quad+\frac{1}{5\delta}\left[2\varphi\nu_0 h_f^{(1)}\left(1-\rho_0\right)\left(U_{12,2}+cU_{12,4}\right)-\varphi\rho_0\nu_0\left(U_{11,2}+cU_{11,4}\right)+1\right]\hat{h}^{(2)}=0.
\end{aligned}
\tag{2.31}
$$

For a linear independent solution

$$
\hat{h}^{(1)}=\breve{h}^{(1)}e^{\lambda\xi},\quad \hat{h}^{(2)}=\breve{h}^{(2)}e^{\lambda\xi},
\tag{2.32}
$$

where λ is a complex number to be found, we can rewrite the linear system for $\breve{h}^{(1)}$ and

$\breve{h}^{(2)}$ in the form

$$\begin{aligned}
\left(b_{11,3}\lambda^3 + b_{11,1}\lambda + b_{11,0}\right)\breve{h}^{(1)} + \left(b_{12,3}\lambda^3 + b_{12,1}\lambda + b_{12,0}\right)\breve{h}^{(2)} = 0, \\
\left(b_{21,3}\lambda^3 + b_{21,1}\lambda + b_{21,0}\right)\breve{h}^{(1)} + \left(b_{22,3}\lambda^3 + b_{22,1}\lambda + b_{22,0}\right)\breve{h}^{(2)} = 0,
\end{aligned} \tag{2.33}$$

where

$$\begin{aligned}
b_{11,3} &= \frac{\sigma_0 h_f^{(1)}}{5\delta\rho_0}, \\
b_{11,1} &= c^2 - J_1^{(1)} - cJ_3^{(1)}, \\
b_{11,0} &= \frac{1}{5\delta}\left[2\varphi\nu_0 h_f^{(1)}\left(U_{12,1} + cU_{12,3}\right) + 2\varphi\nu_0 U_{12,0} + 1\right], \\
b_{12,3} &= \frac{h_f^{(1)}}{5\delta\rho_0}, \\
b_{12,1} &= -\left[J_2^{(1)} + cJ_4^{(1)}\right], \\
b_{12,0} &= \frac{2\varphi\nu_0 h_f^{(1)}}{5\delta}\left(U_{12,2} + cU_{12,4}\right), \\
b_{21,3} &= \frac{\sigma_0 h_f^{(1)}}{5\delta\rho_0}, \\
b_{21,1} &= -\left(J_1^{(2)} + cJ_3^{(2)}\right), \\
b_{21,0} &= \frac{\varphi}{5\delta}\left[2\nu_0 h_f^{(1)}\left(1-\rho_0\right)\left(U_{12,1} + cU_{12,3}\right) - \rho_0\nu_0\left(U_{11,1} + cU_{11,3}\right) + 2\nu_0 U_{12,0}\left(1-\rho_0\right)\right], \\
b_{22,3} &= \frac{1}{5\delta}\left(h_f^{(2)} + \left(\frac{1}{\rho_0} - 1\right)h_f^{(1)}\right), \\
b_{22,1} &= c^2 - J_2^{(2)} - cJ_4^{(2)}, \\
b_{22,0} &= \frac{1}{5\delta}\left[2\varphi\nu_0 h_f^{(1)}\left(1-\rho_0\right)\left(U_{12,2} + cU_{12,4}\right) - \varphi\rho_0\nu_0\left(U_{11,2} + cU_{11,4}\right) + 1\right].
\end{aligned}$$

Nontrivial solution exists if the determinant of the linear algebraic system (2.33) is equal

to zero:

$$\det \begin{vmatrix} b_{11,3}\lambda^3 + b_{11,1}\lambda + b_{11,0} & b_{12,3}\lambda^3 + b_{12,1}\lambda + b_{12,0} \\ b_{21,3}\lambda^3 + b_{21,1}\lambda + b_{21,0} & b_{22,3}\lambda^3 + b_{22,1}\lambda + b_{22,0} \end{vmatrix} = 0,$$

that can be rewritten in the explicit form

$$\begin{aligned} b_6\lambda^6 + b_4\lambda^4 + b_3\lambda^3 + b_2\lambda^2 + b_1\lambda + b_0 = 0, \\ b_6 = b_{11,3}b_{22,3} - b_{21,3}b_{12,3}, \\ b_4 = b_{11,1}b_{22,3} + b_{11,3}b_{22,1} - b_{21,1}b_{12,3} - b_{21,3}b_{12,1}, \\ b_3 = b_{11,0}b_{22,3} + b_{11,3}b_{22,0} - b_{21,0}b_{12,3} - b_{21,3}b_{12,0}, \\ b_2 = b_{11,1}b_{22,1} - b_{21,1}b_{12,1}, \\ b_1 = b_{11,0}b_{22,1} + b_{11,1}b_{22,0} - b_{12,1}b_{21,0} - b_{12,0}b_{21,1}, \\ b_0 = b_{11,0}b_{22,0} - b_{21,0}b_{12,0}. \end{aligned}$$

Six linear independent solutions of (2.32) give us a fundamental system of (2.31).

Examples of calculations are shown in Fig. 2.15 in the case of water-benzene system at $H = 0.6$ and $\delta = 0.1$ for the steady flow. The amplification factors λ_r of small perturbations in the neighbourhood of the fixed points are demonstrated by solid curves corresponding to real λ and dashed curves corresponding to real parts of complex conjugate λ. The asymptotic behaviour of very long waves depends on the values of λ either real or complex. In the case λ is real, there is the exponential linear independent solution at the neighbourhood of the fixed point. If λ is a complex conjugate then, there is exponentially-oscillating linear independent solution in the neighbourhood of the fixed point.

Table 2.3 shows the values of λ at different values of c. Let's analyse the results

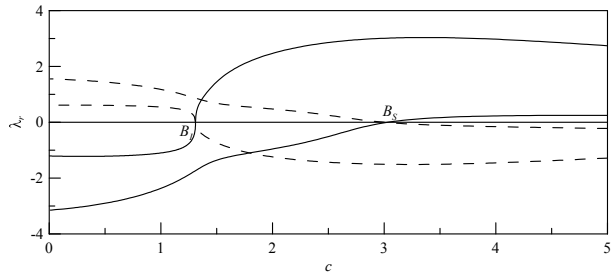

Figure 2.15: Amplification factors λ_r of small perturbations in the neighbourhood of the fixed point corresponding to the waveless flow in the case of water-benzene system at $H = 0.6$ and $\delta = 0.1$. Solid curves correspond to real values of λ, and dashed curves correspond to real parts of complex conjugate values of λ.

shown in Table 2.3. There are one positive, one negative real values of λ and two complex conjugate values of λ with positive and negative real parts at $c = 2.24$, see Table 2.3a and $c = 2.42$, see Table 2.3b. It means that a very long wave tends to the waveless flow as $\xi \to \pm\infty$ with exponentially decreasing oscillations.

On the other hand, there are two real positive values of λ and two complex conjugate values of λ with negative real part at $c = 5.46$, see Table 2.3c, and $c = 4.06$, see Table 2.3d. It means that a very long wave should exponentially tends to the waveless flow as $\xi \to -\infty$, and tends to the waveless flow as $\xi \to \infty$ with exponentially decreasing oscillations. Solution with such asymptotic behaviour at $\xi \to \pm\infty$, if it exists, is a solitary wave in the physical space, or a homoclinic trajectory in the phase space $\left(h^{(1)}, \left(h^{(1)}\right)', \left(h^{(1)}\right)'', h^{(2)}, \left(h^{(2)}\right)', \left(h^{(2)}\right)''\right)$. Similar to the case of the one-layer film, we can expect that there exist periodic orbits (or periodic waves in the physical space) which are close to a homoclinic trajectory. Homoclinic and heteroclinic trajectories are not studied in this thesis but we can use values of λ to analyse properties of very long periodic solutions. It is worthy to note that existence of the bifurcating fixed points of the first and second types indicate on possibility of corresponding homoclinic trajectories and heteroclinic trajectories connecting different fixed points.

Velocity c	complex λ	real λ
(a) 2.24	$-2.21 \pm 4.43i$	4.42
	$0.41 \pm 0.97i$	-0.83
(b) 2.42	$-2.27 \pm 4.65i$	4.53
	$0.33 \pm 0.99i$	-0.67
(c) 5.46	$-2.31 \pm 8.21i$	4.72
	$-0.15 \pm 3.19i$	0.22
(d) 4.06	$-1.56 \pm 5.66i$	3.19
	$-0.15 \pm 1.86i$	0.24

Table 2.3: Complex conjugate and real values of λ at $\delta = 0.1$ and $H = 0.3$ (a,b,c), and $\delta = 0.1$ and $H = 0.7$ (d).

Chapter 3

Periodic Steady-Travelling Waves

In this chapter, we study bifurcating families of steady-travelling space-periodic waves in two-layer liquid films down a vertical wall. It is worthy to note that how small deviation affects bifurcation schemes of steady-travelling waves is not studied in this thesis.

3.1 Eigenvalue problem

We consider solutions of (2.17) in the form $h^{(1)}(\eta)$, $h^{(2)}(\eta)$, $q^{(1)}(\eta)$, $q^{(2)}(\eta)$ where $\eta = \alpha_\kappa(x_\kappa - ct_\kappa)$, α_κ is the given wavenumber, which allows us to study periodic waves, and c is the wave velocity to be found. Then, the differential equations become

$$
\begin{aligned}
&-c\frac{dh^{(1)}}{d\eta} + \frac{dq^{(1)}}{d\eta} = 0, \\
&-c\frac{dq^{(1)}}{d\eta} + \frac{dJ^{(1)}}{d\eta} = \frac{h^{(1)}}{5\delta\alpha_\kappa}\left(\frac{\alpha_\kappa^3\sigma_0}{\rho_0}\frac{d^3h^{(1)}}{d\eta^3} + \frac{\alpha_\kappa^3}{\rho_0}\frac{d^3h^{(2)}}{d\eta^3} + 2\varphi\nu_0U_{12} + 1\right), \\
&-c\frac{dh^{(2)}}{d\eta} + \frac{dq^{(2)}}{d\eta} = 0, \\
&-c\frac{dq^{(2)}}{d\eta} + \frac{dJ^{(2)}}{d\eta} = \frac{\alpha_\kappa^2}{5\delta}\left[\frac{\sigma_0h^{(1)}}{\rho_0}\frac{d^3h^{(1)}}{d\eta^3} + \left(h^{(2)} + \left(\frac{1}{\rho_0} - 1\right)h^{(1)}\right)\frac{d^3h^{(2)}}{d\eta^3}\right] \\
&\quad + \frac{\varphi}{5\delta\alpha_\kappa}\left[2\nu_0U_{12}h^{(1)}\left(1-\rho_0\right) - \rho_0\nu_0U_{11}\right] + \frac{h^{(2)}}{5\delta\alpha_\kappa}.
\end{aligned}
\tag{3.1}
$$

Integrating the continuity equations leads to

$$q^{(1)} = ch^{(1)} + A^{(1)}, \quad q^{(2)} = ch^{(2)} + A^{(2)}, \tag{3.2}$$

where $A^{(1)}$ and $A^{(2)}$ are the constants.

We consider 2π-periodic waves. To find constants $A^{(1)}$ and $A^{(2)}$, we calculate the averages of (3.2) over the period $[0, 2\pi]$ that gives us the formulas for $A^{(1)}$ and $A^{(2)}$:

$$A^{(1)} = q_0^{(1)} - ch_0^{(1)}, \quad A^{(2)} = q_0^{(2)} - ch_0^{(2)},$$

where the average thickness of the first layer $h_0^{(1)}$, the average film thickness $h_0^{(2)}$, the average flow rates in the first layer $q_0^{(1)}$ and the film $q_0^{(2)}$

$$h_0^{(1)} = \frac{1}{2\pi}\int_0^{2\pi} h^{(1)} d\eta, \quad q_0^{(1)} = \frac{1}{2\pi}\int_0^{2\pi} q^{(1)} d\eta, \quad h_0^{(2)} = \frac{1}{2\pi}\int_0^{2\pi} h^{(2)} d\eta, \quad q_0^{(2)} = \frac{1}{2\pi}\int_0^{2\pi} q^{(2)} d\eta$$

have been introduced.

Having eliminated $A^{(1)}$ and $A^{(2)}$, from (3.2), we obtain the flow rates

$$q^{(1)} = c\left(h^{(1)} - h_0^{(1)}\right) + q_0^{(1)}, \quad q^{(2)} = c\left(h^{(2)} - h_0^{(2)}\right) + q_0^{(2)}.$$

Finally, eliminating the flow rates $q^{(1)}$ and $q^{(2)}$ from the momentum equations in (3.1) gives us the following equations for $h^{(1)}$ and $h^{(2)}$:

$$\begin{aligned}
-c^2\frac{dh^{(1)}}{d\eta} + \frac{dJ^{(1)}}{d\eta} &= h^{(1)}\left[\frac{1}{5\delta\alpha_\kappa}\left(\frac{\alpha_\kappa^3\sigma_0}{\rho_0}\frac{d^3h^{(1)}}{d\eta^3} + \frac{\alpha_\kappa^3}{\rho_0}\frac{d^3h^{(2)}}{d\eta^3} + 2\varphi\nu_0 U_{12} + 1\right)\right], \quad (3.3)\\
-c^2\frac{dh^{(2)}}{d\eta} + \frac{dJ^{(2)}}{d\eta} &= \frac{\alpha_\kappa^2}{5\delta}\left[\frac{\sigma_0 h^{(1)}}{\rho_0}\frac{d^3h^{(1)}}{d\eta^3} + \left(h^{(2)} + \left(\frac{1}{\rho_0} - 1\right)h^{(1)}\right)\frac{d^3h^{(2)}}{d\eta^3}\right]\\
&+\frac{\varphi}{5\delta\alpha_\kappa}\left[2\nu_0 U_{12}h^{(1)}\left(1-\rho_0\right) - \rho_0\nu_0 U_{11}\right] + \frac{h^{(2)}}{5\delta\alpha_\kappa},
\end{aligned}$$

where the coefficients are calculating by using (2.16) and (2.18).

The equations (3.3) are accompanied with the following periodic boundary conditions

$$h^{(1)}\big|_0 = h^{(1)}\big|_{2\pi}, \quad \left.\frac{dh^{(1)}}{d\eta}\right|_0 = \left.\frac{dh^{(1)}}{d\eta}\right|_{2\pi}, \quad \left.\frac{d^2h^{(1)}}{d\eta^2}\right|_0 = \left.\frac{d^2h^{(1)}}{d\eta^2}\right|_{2\pi}, \tag{3.4}$$
$$h^{(2)}\big|_0 = h^{(2)}\big|_{2\pi}, \quad \left.\frac{dh^{(2)}}{d\eta}\right|_0 = \left.\frac{dh^{(2)}}{d\eta}\right|_{2\pi}, \quad \left.\frac{d^2h^{(2)}}{d\eta^2}\right|_0 = \left.\frac{d^2h^{(2)}}{d\eta^2}\right|_{2\pi},$$

and conditions of constancy of the average thicknesses

$$h_0^{(1)} = \frac{1}{2\pi}\int\limits_0^{2\pi} h^{(1)}d\eta = H, \quad h_0^{(2)} = \frac{1}{2\pi}\int\limits_0^{2\pi} h^{(2)}d\eta = 1. \tag{3.5}$$

These relations follow from the continuity equation in (2.17) integrated over the period 2π.

The problem (3.3), (3.4) and (3.5) includes the system of differential equations of sixth order for functions $h^{(1)}(\eta)$ and $h^{(2)}(\eta)$, and eigenvalues $c, q_0^{(1)}$ and $q_0^{(2)}$ depending on the similarity parameters $\delta, \rho_0, \nu_0, \sigma_0$ and H, and the wavenumber $s \equiv \alpha_\kappa/\alpha_{\kappa,n}$. The system (3.3), (3.4) and (3.5) is accompanied by the additional relation expressing the invariance of solutions with regard to a shift along η-axis.

We look for solution in the form of the finite Fourier series

$$h^{(1)}(\eta) = \sum_{n=1}^{2N} a_n^{\left(h^{(1)}\right)} e^{i(N-n)\eta}, \quad a_n^{\left(h^{(1)}\right)} = \overline{a_{2N-n}^{\left(h^{(1)}\right)}}, \ n = 1, \ldots, N, \quad a_{2N}^{\left(h^{(1)}\right)} = 0, \tag{3.6}$$
$$h^{(2)}(\eta) = \sum_{n=1}^{2N} a_n^{\left(h^{(2)}\right)} e^{i(N-n)\eta}, \quad a_n^{\left(h^{(2)}\right)} = \overline{a_{2N-n}^{\left(h^{(2)}\right)}}, \ n = 1, \ldots, N, \quad a_{2N}^{\left(h^{(2)}\right)} = 0.$$

Substituting this solution in the system (3.3), conditions (3.5) and constancy of the first harmonic phase for $h^{(2)}$, we get nonlinear algebraic system for the Fourier coefficients and eigenvalues $c, q_0^{(1)}$ and $q_0^{(2)}$.

Nonlinear algebraic system for the coefficients of Fourier series (3.6) are shown in

Appendix B where the phase shift of the first harmonic of $h^{(2)}(\eta)$ is also calculated. We assume that this shift is a constant in accordance with the invariance of the solution.

3.2 Results

In the theory of film flows, steady-travelling waves, or regular waves are sorted into families which are continuously parameterized by the normalized wavenumber s at given values of other similarity parameters, in this specific case, δ, ρ_0, σ_0 and H. To identify the wave families we use the notation $\gamma^n_{\pm m,j}$, see [55, 56, 57]. In this notation, the lower index j means that waves of the family have one large hump ($j = 1, m = 1, 2, ...$) or one deep trough ($j = 1, m = -1, -2, ...$) or two large humps ($j = 2, m = 1, 2, ...$) or two deep troughs ($j = 2, m = -1, -2, ...$). The lower index $m = \pm 1, \pm 2, ...$ is a family number such that the velocities of very long-waves increase as the index m is passing $-1, -2, ...$ and the velocity decreases as $m = 1, 2, ...$ The upper index $n = 1, 2, ...$ shows the harmonics in the bifurcation point of the family. This index depends on the similarity parameters for all families except the families $\gamma^1_{-1,1}$ and $\gamma^2_{-1,2}$.

Fig. 3.1 shows an example of the bifurcation scheme of the families of nonlinear waves. Family $\gamma^1_{-1,1}$ bifurcates from the waveless flow at the normalized wavenumber $s = 1$ as the first harmonic, see Fig. 3.2c.

As the wavenumber decreases, the shape and surface amplitude of waves of the first family change, see Fig. 3.2b, and then the wave takes on a solitary-like shape with a long interval of constant thickness of the first layer and the film, see Fig. 3.2a. The surface shape shown in Fig. 3.2a is typical for long waves of the so-called first family [52] in an one-layer film. We also note that the amplitude of the interface wave is small in comparison with the surface wave amplitude.

Family $\gamma^2_{-2,1}$, see Fig. 3.1, bifurcates from the first family $\gamma^1_{-1,1}$. At the bifurcation point, the wave is determined by the second harmonic, see Fig. 3.3c.

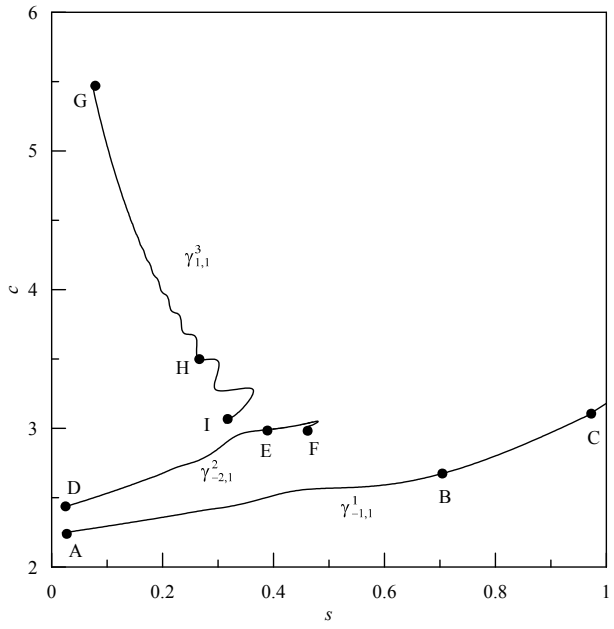

Figure 3.1: Bifurcation scheme of the wave families at $\delta = 0.1$ and $H = 0.3$.

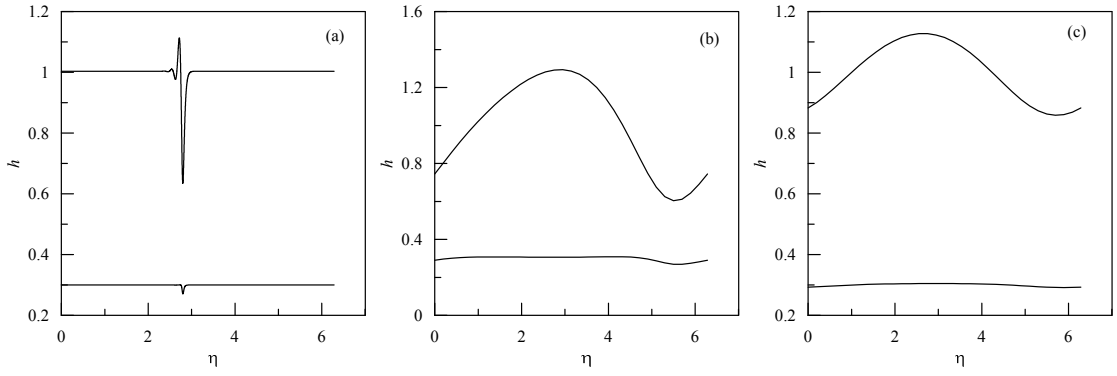

Figure 3.2: Examples of waves belonging to the family $\gamma^1_{-1,1}$ at $s = 0.019$ (a), $s = 0.7$ (b) and $s = 0.9632$ (c). Panels (a), (b) and (c) correspond to the points A, B and C, respectively, in Fig. 3.1.

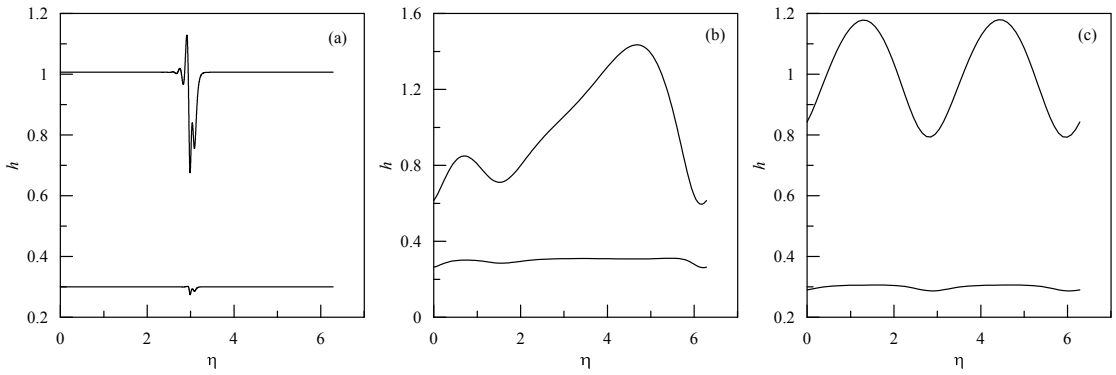

Figure 3.3: Examples of waves belonging to the family $\gamma^2_{-2,1}$ at $s = 0.018$ (a), $s = 0.4$ (b) and $s = 0.4616$ (c). Panels (a), (b) and (c) correspond to the points D, E and F, respectively, in Fig. 3.1.

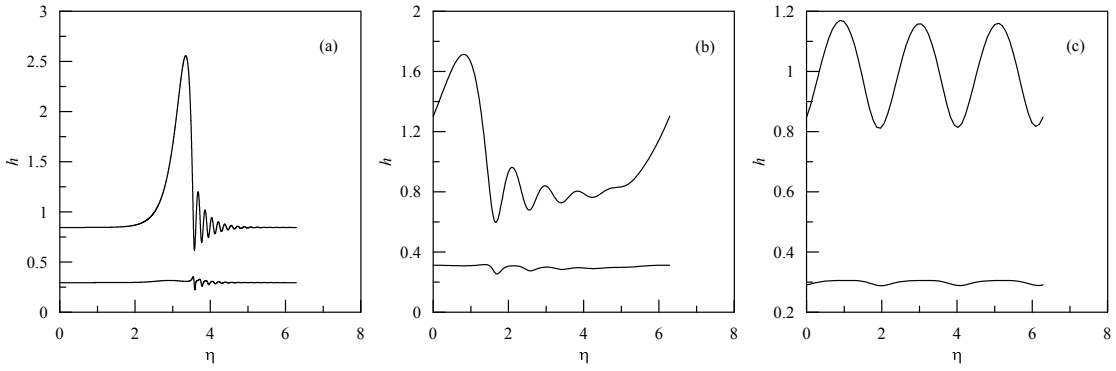

Figure 3.4: Examples of waves belonging to the family $\gamma^3_{+1,1}$ at $s = 0.074$ (a), $s = 0.25$ (b) and $s = 0.3125$ (c). Panels (a), (b) and (c) correspond to the points G, H and I, respectively, in Fig. 3.1.

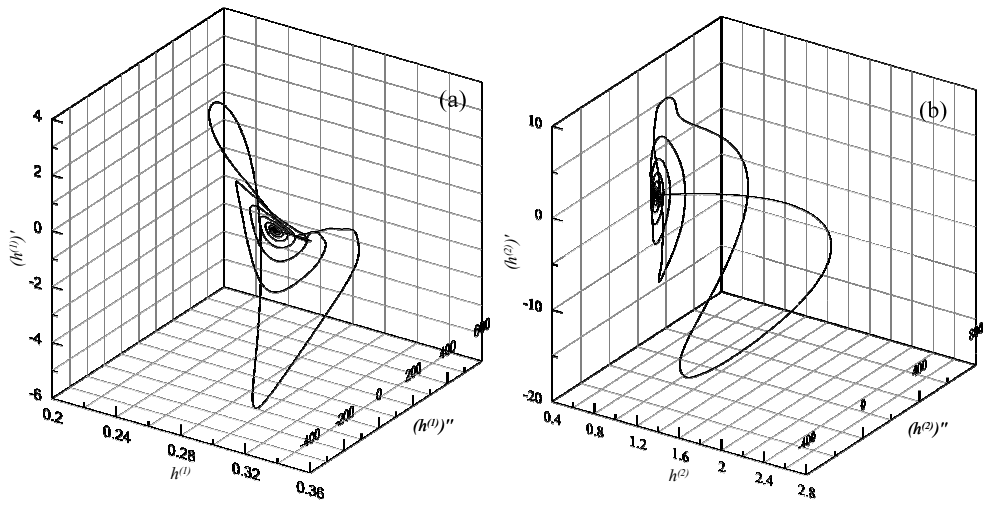

Figure 3.5: Projections of 6-dimensional phase trajectory of the family $\gamma^3_{+1,1}$ in 3-dimensional subspace $\left(h^{(1)}, \left(h^{(1)}\right)', \left(h^{(1)}\right)''\right)$ (a) and $\left(h^{(2)}, \left(h^{(2)}\right)', \left(h^{(2)}\right)''\right)$ (b) at $s = 0.074$, correspond to the panel (a) in Fig. 3.4

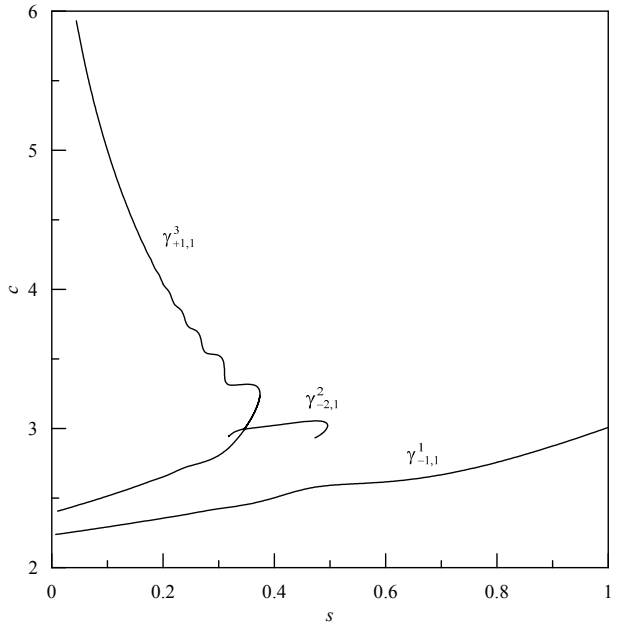

Figure 3.6: Bifurcation scheme of the wave families at $\delta = 0.1$ and $H = 0.6$.

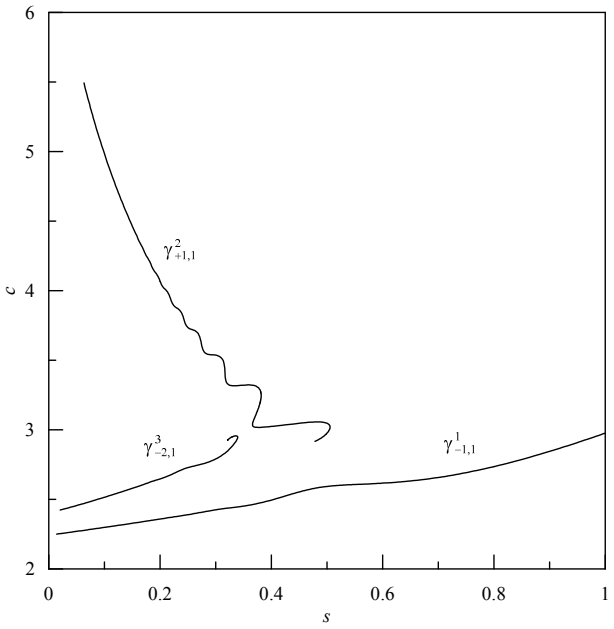

Figure 3.7: Bifurcation scheme of the wave families at $\delta = 0.1$ and $H = 0.7$.

This regular wave corresponds to a limit cycle in the 6-dimensional phase space $\left(h^{(1)}, \left(h^{(1)}\right)', \left(h^{(1)}\right)'', h^{(2)}, \left(h^{(2)}\right)', \left(h^{(2)}\right)''\right)$, and Fig. 3.3c shows that this family bifurcates from the first family as a period-doubling limit cycle since the wavenumber at the bifurcation point is about 0.5 and thus the wave period is about 4π in comparison with the period 2π of the wave bifurcating from the waveless flow. As the wavenumber s decreases, the shape of wave from this family transforms to a solitary-like form, see Figs. 3.3a and b. Comparing Figs. 3.2a and 3.3a, we see additional oscillation in the trough of the wave in Fig. 3.3a.

Period-tripling bifurcation, see Fig. 3.4c, where the wave whose period is closed to 6π is shown, creates the wave family $\gamma^3_{+1,1}$, see Fig. 3.1, whose shape at small values of the wavenumber has a large hump (Fig. 3.4a) in contrast with the long waves of the families $\gamma^1_{-1,1}$ and $\gamma^2_{-2,1}$. This hump is also observed in shape of intermediate waves of the family (Fig. 3.4b). We can also analyse the projections in 3-dimensional subspaces $\left(h^{(1)}, \left(h^{(1)}\right)', \left(h^{(1)}\right)''\right)$ and $\left(h^{(2)}, \left(h^{(2)}\right)', \left(h^{(2)}\right)''\right)$ of the trajectory corresponding to the

long wave belonging to the family $\gamma^3_{+1,1}$, see Fig. 3.5. This projection is also similar to the corresponding solution of the so-called second family in the one-layer film, see [9]. Using the results of Section 2.4.3, see Table 2.3c, there are two real values $\lambda^{(1)} > 0$ and $\lambda^{(2)} > 0$, and two complex conjugate roots $\lambda^{(3)}$ and $\lambda^{(4)}$ such that $\lambda_r^{(3)} < 0$ and $\lambda_r^{(4)} < 0$ when $c = 5.46$. We can see in Figs. 3.4a and 3.5 that the periodic solution corresponds to solution at $s \to 0$ with exponential behaviour at $\xi \to -\infty$ and exponentially-oscillating behaviour at $\xi \to +\infty$.

In the shown results at $H = 0.3$, the amplitude of the interface waves is respectively small in comparison with the wave amplitudes on the free surface. It is consistent with the fact that these waves bifurcates from the waveless flow similar to the waves in the one-layer film, see Fig. 1 in [64]. To understand the role of the parameter H, we demonstrate the bifurcation scheme at $H = 0.6$ and $H = 0.7$ in Fig. 3.6 and Fig. 3.7, respectively. Comparison with the case $H = 0.3$ (Fig. 3.1) shows that increasing H leads to swapping their bifurcation points by the families $\gamma_{-2,1}$ and $\gamma_{+1,1}$, and this effect is inherent for the wave families in film flows when a similarity parameter varies. Detailed description of the swapping with variation of the film parameter δ can be found in [65].

In Fig. 3.8, projections in 3D subspaces $\left(h^{(1)}, \left(h^{(1)}\right)', \left(h^{(1)}\right)''\right)$ and $\left(h^{(2)}, \left(h^{(2)}\right)', \left(h^{(2)}\right)''\right)$ of the 6-dimensional phase trajectory of the wave belonging to the family $\gamma^1_{-1,1}$ are shown. It is seen that the projection shown in Fig. 3.8b is a curve that is similar to the phase trajectory in 3D space of a long periodic first family wave in the one-layer film [9]. In the latter case, a phase trajectory of a long wave belongs to a neighbourhood of the solitary wave trajectory of the first family $\gamma^1_{-1,1}$: the trajectory leaves a neighbourhood of the fixed point $(1, 0, 0)$ along the unstable two-dimensional manifold and returns to the same point along the stable one-dimensional manifold as η varies from $-\infty$ to $+\infty$. The wave shown in Fig. 3.2a has the long part of almost constant thickness of the film surface, $h^{(2)} \approx 1$, and the interface, $h^{(1)} \approx H$, and we can use the results of Section 2.4.3. For

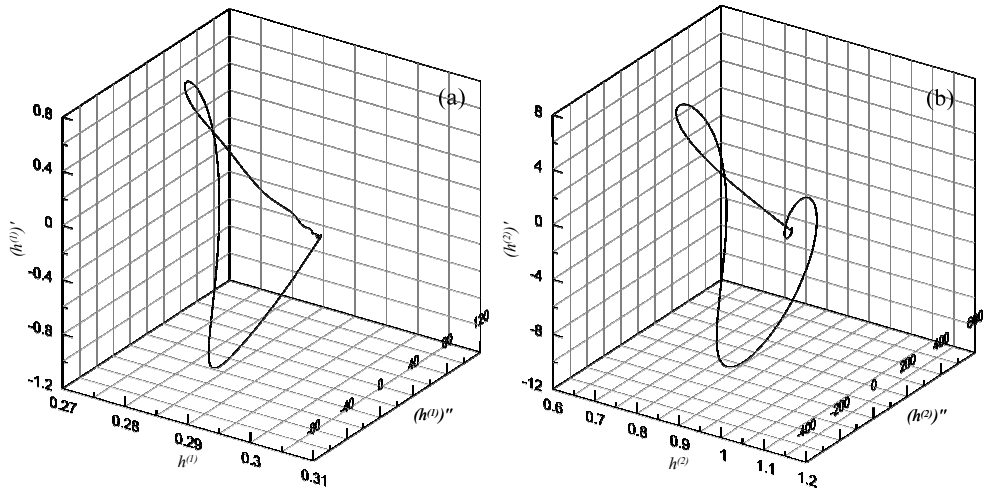

Figure 3.8: Projections of 6-dimensional phase trajectory of the family $\gamma^1_{-1,1}$ in 3-dimensional subspace $\left(h^{(1)}, \left(h^{(1)}\right)', \left(h^{(1)}\right)''\right)$ (a) and $\left(h^{(2)}, \left(h^{(2)}\right)', \left(h^{(2)}\right)''\right)$ (b) , at $s = 0.019$, correspond to Fig. 3.2a.

its velocity, $c = 2.24$, see Fig. 3.1 and Table 2.3a, there are two real values $\lambda^{(1)} > 0$ and $\lambda^{(2)} < 0$, and two complex conjugate roots $\lambda^{(3)}$ and $\lambda^{(4)}$ such that $\lambda^{(3)}_r < 0$ and $\lambda^{(4)}_r > 0$. It means that the asymptotic behaviour of solution includes exponential and exponentially-oscillating decreasing in the neighbourhood of the nonlinear part of the wave. It is similar in Fig. 3.3a for the velocity $c = 2.42$, see Table 2.3b. Fig. 3.8b indicates that the extension of dimension of the phase space from 3 to 6 weakly affects the projection in the subspace $\left(h^{(2)}, \left(h^{(2)}\right)', \left(h^{(2)}\right)''\right)$ despite there are additional values of λ. On the other hand, the projection shown Fig. 3.8a demonstrates the role of other stable and unstable manifolds in the neighbourhood of the fixed point $(H, 0, 0, 1, 0, 0)$ in the 6-dimensional space.

Examples of waves belonging to different families at $H = 0.7$ are shown in Fig. 3.9. It is seen that in all cases the interface wave almost imitates the surface wave, and their amplitudes are close. The projections of the phase trajectories in 3D-subspaces confirm that the amplitudes of the pairs $h^{(1)}$ and $h^{(2)}$, $\left(h^{(1)}\right)'$ and $\left(h^{(2)}\right)'$, and $\left(h^{(1)}\right)''$ and $\left(h^{(2)}\right)''$ have the same order, see Fig. 3.10. For the velocity $c = 4.06$ in Fig. 3.9, there are two

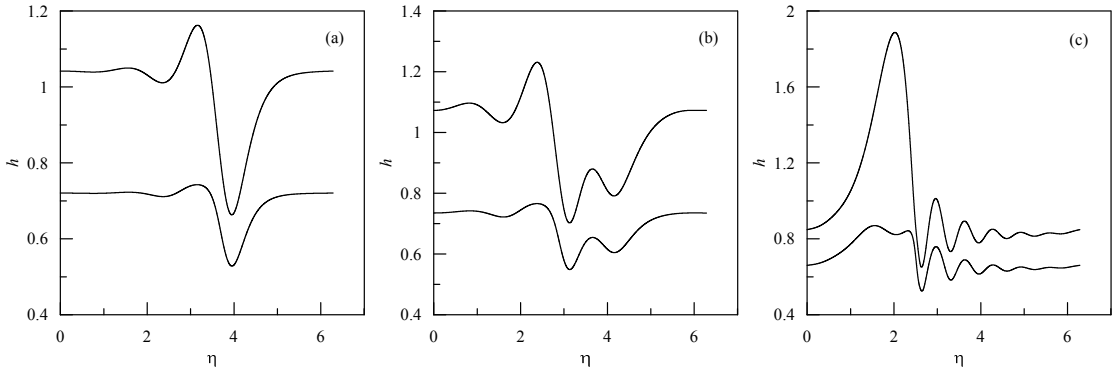

Figure 3.9: Examples of waves belonging to the families $\gamma^1_{-1,1}$ (a), $\gamma^3_{-2,1}$ (b) and $\gamma^2_{+1,1}$ (c) at $s = 0.2$, $\delta = 0.1$ and $H = 0.7$.

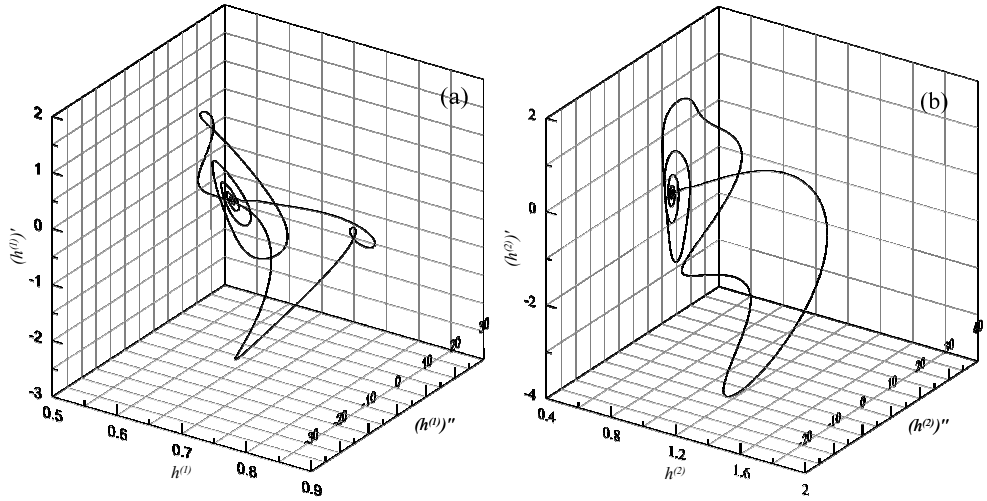

Figure 3.10: Projections of 6-dimensional phase trajectory of the family $\gamma^2_{+1,1}$ in 3-dimensional subspace $\left(h^{(1)}, \left(h^{(1)}\right)', \left(h^{(1)}\right)''\right)$ (a) and $\left(h^{(2)}, \left(h^{(2)}\right)', \left(h^{(2)}\right)''\right)$ (b) at $s = 0.2$, correspond to the panel (c) in Fig. 3.9

real roots $\lambda^{(1)} > 0$ and $\lambda^{(2)} > 0$, and two complex conjugate roots $\lambda^{(3)}$ and $\lambda^{(4)}$ such that $\lambda_r^{(3)} < 0$ and $\lambda_r^{(4)} < 0$, see Table 2.3d.

The bifurcation schemes show that there are wavy solution(s) in parallel with the waveless flow for all wavenumbers from the unstable interval $s \in (0, 1)$, and the number of these solutions varied from 1 to 4. The analogy to the one-layer film allows us to predict a countable set of wave families as the wavenumber s tends to zero [55, 56, 57].

To be observed experimentally, wave regimes have to develop from arbitrary initial conditions, and it has to be stable to small perturbations. In the next section we show that such regimes, so-called dominating waves, exist in two-layer falling films.

Chapter 4

Dominating Waves

In this chapter, we study unsteady space-periodic solutions to find attractive wave regimes.

4.1 Space-periodic solutions

In the case of space-periodic solutions of (2.17), (2.16) and (2.18) it is convenient to use the following replacement

$$\tau = \alpha_\kappa t_\kappa, \quad \xi = \alpha_\kappa x_\kappa, \quad \alpha_\kappa = \frac{2\pi}{L_\kappa}, \tag{4.1}$$

where L_κ is wavelength. Then, the system (2.17) becomes

$$\begin{aligned}
&\frac{\partial h^{(1)}}{\partial \tau} + \frac{\partial q^{(1)}}{\partial \xi} = 0, \\
&\frac{\partial q^{(1)}}{\partial \tau} + \frac{\partial J^{(1)}}{\partial \xi} = \frac{h^{(1)}}{5\delta\alpha_\kappa}\left(\frac{\alpha_\kappa^3\sigma_0}{\rho_0}\frac{\partial^3 h^{(1)}}{\partial \xi^3} + \frac{\alpha_\kappa^3}{\rho_0}\frac{\partial^3 h^{(2)}}{\partial \xi^3} + 2\varphi\nu_0 U_{12} + 1\right), \\
&\frac{\partial h^{(2)}}{\partial \tau} + \frac{\partial q^{(2)}}{\partial \xi} = 0, \\
&\frac{\partial q^{(2)}}{\partial \tau} + \frac{\partial J^{(2)}}{\partial \xi} = \frac{\alpha_\kappa^2}{5\delta}\left[\frac{\sigma_0 h^{(1)}}{\rho_0}\frac{\partial^3 h^{(1)}}{\partial \xi^3} + \left(h^{(2)} + \left(\frac{1}{\rho_0} - 1\right)h^{(1)}\right)\frac{\partial^3 h^{(2)}}{\partial \xi^3}\right] \\
&\quad + \frac{\varphi}{5\delta\alpha_\kappa}\left[2\nu_0 U_{12} h^{(1)}\left(1-\rho_0\right) - \rho_0\nu_0 U_{11}\right] + \frac{h^{(2)}}{5\delta\alpha_\kappa},
\end{aligned} \tag{4.2}$$

where the coefficients $U_{12}, U_{11}, U_{22}, U_{20}$ and $J^{(1)}, J^{(2)}$ are defined in (2.16) and (2.18).

To solve the system (4.2) numerically, it is convenient to exclude divisions in the right-hand sides. So, new variables are introduced as:

$$r^{(1)} \equiv \frac{1}{h^{(1)}}, \quad r^{(2)} \equiv \frac{1}{h^{(2)} - h^{(1)}}, \quad r^{(3)} \equiv \frac{1}{(3 - 4\rho_0\nu_0)\, h^{(1)} + 4\rho_0\nu_0 h^{(2)}},$$

and these variables satisfy the following differential equations:

$$\begin{aligned}
&\frac{\partial r^{(1)}}{\partial \tau} = -\frac{1}{\left(h^{(1)}\right)^2}\frac{\partial h^{(1)}}{\partial \tau} = \left(r^{(1)}\right)^2 \frac{\partial q^{(1)}}{\partial \xi}, \\
&\frac{\partial r^{(2)}}{\partial \tau} = -\frac{1}{\left(h^{(2)} - h^{(1)}\right)^2}\frac{\partial \left(h^{(2)} - h^{(1)}\right)}{\partial \tau} = \left(r^{(2)}\right)^2 \left(\frac{\partial q^{(2)}}{\partial \xi} - \frac{\partial q^{(1)}}{\partial \xi}\right), \\
&\frac{\partial r^{(3)}}{\partial \tau} = -\frac{1}{\left[(3 - 4\rho_0\nu_0)\, h^{(1)} + 4\rho_0\nu_0 h^{(2)}\right]^2}\left[(3 - 4\rho_0\nu_0)\frac{\partial h^{(1)}}{\partial \tau} + 4\rho_0\nu_0\frac{\partial h^{(2)}}{\partial \tau}\right], \\
&\quad = \left(r^{(3)}\right)^2 \left[(3 - 4\rho_0\nu_0)\frac{\partial q^{(1)}}{\partial \xi} + 4\rho_0\nu_0\frac{\partial q^{(2)}}{\partial \xi}\right].
\end{aligned}$$

and we obtain the evolution equations in the form

$$\begin{aligned}
&\frac{\partial h^{(1)}}{\partial \tau} + \frac{\partial q^{(1)}}{\partial \xi} = 0, \\
&\frac{\partial q^{(1)}}{\partial \tau} + \frac{\partial J^{(1)}}{\partial \xi} = h^{(1)}\left[\frac{1}{5\delta\alpha_\kappa}\left(\frac{\alpha_\kappa^3\sigma_0}{\rho_0}\frac{\partial^3 h^{(1)}}{\partial \xi^3} + \frac{\alpha_\kappa^3}{\rho_0}\frac{\partial^3 h^{(2)}}{\partial \xi^3} + 2\varphi\nu_0 U_{12} + 1\right)\right], \\
&\frac{\partial h^{(2)}}{\partial \tau} + \frac{\partial q^{(2)}}{\partial \xi} = 0, \\
&\frac{\partial q^{(2)}}{\partial \tau} + \frac{\partial J^{(2)}}{\partial \xi} = \frac{\alpha_\kappa^2}{5\delta}\left[\frac{\sigma_0 h^{(1)}}{\rho_0}\frac{\partial^3 h^{(1)}}{\partial \xi^3} + \left(h^{(2)} + \left(\frac{1}{\rho_0} - 1\right) h^{(1)}\right)\frac{\partial^3 h^{(2)}}{\partial \xi^3}\right] \\
&\quad + \frac{\varphi}{5\delta\alpha_\kappa}\left[2\nu_0 U_{12} h^{(1)}\left(1 - \rho_0\right) - \rho_0\nu_0 U_{11}\right] + \frac{h^{(2)}}{5\delta\alpha_\kappa}, \\
&\frac{\partial r^{(1)}}{\partial \tau} = \left(r^{(1)}\right)^2 \frac{\partial q^{(1)}}{\partial \xi}, \\
&\frac{\partial r^{(2)}}{\partial \tau} = \left(r^{(2)}\right)^2 \left(\frac{\partial q^{(2)}}{\partial \xi} - \frac{\partial q^{(1)}}{\partial \xi}\right), \\
&\frac{\partial r^{(3)}}{\partial \tau} = \left(r^{(3)}\right)^2 \left[(3 - 4\rho_0\nu_0)\frac{\partial q^{(1)}}{\partial \xi} + 4\rho_0\nu_0\frac{\partial q^{(2)}}{\partial \xi}\right],
\end{aligned}$$

where

$$
\begin{aligned}
U_{12} &= 3r^{(1)}r^{(3)}\left\{3q^{(2)}r^{(2)} - \left[3r^{(2)} + 2\left(r^{(1)}\right)^2\left(\left(3-\rho_0\nu_0\right)h^{(1)} + \rho_0\nu_0 h^{(2)}\right)\right]q^{(1)}\right\} \qquad (4.3)\\
U_{11} &= 2q^{(1)}\left(r^{(1)}\right)^2 - \frac{2h^{(1)}U_{12}}{3},\\
U_{22} &= -\frac{\rho_0\nu_0}{2}\left(U_{11} + 2U_{12}h^{(1)}\right)r^{(2)},\\
U_{20} &= \left(q^{(2)} - q^{(1)}\right)r^{(2)} + \frac{1}{3}\left[2\left(h^{(2)}\right)^2 + 2h^{(1)}h^{(2)} - \left(h^{(1)}\right)^2\right]U_{22},\\
J^{(1)} &= \left(h^{(1)}\right)^3\left[\frac{U_{11}^2}{3} + \frac{U_{11}U_{12}}{2}h^{(1)} + \frac{U_{12}^2}{5}\left(h^{(1)}\right)^2\right],\\
J^{(2)} &= J^{(1)} + U_{20}^2\left(h^{(2)} - h^{(1)}\right) - 2U_{20}U_{22}h^{(2)}\left[\left(h^{(2)}\right)^2 - \left(h^{(1)}\right)^2\right] +\\
&\quad \frac{2}{3}\left[2U_{22}^2\left(h^{(2)}\right)^2 + U_{20}U_{22}\right]\left[\left(h^{(2)}\right)^3 - \left(h^{(1)}\right)^3\right] -\\
&\quad U_{22}^2h^{(2)}\left[\left(h^{(2)}\right)^4 - \left(h^{(1)}\right)^4\right] + \frac{U_{22}^2}{5}\left[\left(h^{(2)}\right)^5 - \left(h^{(1)}\right)^5\right].
\end{aligned}
$$

It is also convenient to use a travelling coordinate $\eta = \xi - c_s\tau$, where c_s is a given velocity, instead of ξ. Then, the evolution equations become

$$
\begin{aligned}
&\frac{\partial h^{(1)}}{\partial\tau} - c_s\frac{\partial h^{(1)}}{\partial\eta} + \frac{\partial q^{(1)}}{\partial\eta} = 0, \qquad (4.4)\\
&\frac{\partial q^{(1)}}{\partial\tau} - c_s\frac{\partial q^{(1)}}{\partial\eta} + \frac{\partial J^{(1)}}{\partial\eta} = h^{(1)}\left[\frac{1}{5\delta\alpha_\kappa}\left(\frac{\alpha_\kappa^3\sigma_0}{\rho_0}\frac{\partial^3h^{(1)}}{\partial\eta^3} + \frac{\alpha_\kappa^3}{\rho_0}\frac{\partial^3h^{(2)}}{\partial\eta^3} + 2\varphi\nu_0U_{12} + 1\right)\right],\\
&\frac{\partial h^{(2)}}{\partial\tau} - c_s\frac{\partial h^{(2)}}{\partial\eta} + \frac{\partial q^{(2)}}{\partial\eta} = 0,\\
&\frac{\partial q^{(2)}}{\partial\tau} - c_s\frac{\partial q^{(2)}}{\partial\eta} + \frac{\partial J^{(2)}}{\partial\eta} = \frac{\alpha_\kappa^2}{5\delta}\left[\frac{\sigma_0h^{(1)}}{\rho_0}\frac{\partial^3h^{(1)}}{\partial\eta^3} + \left(h^{(2)} + \left(\frac{1}{\rho_0} - 1\right)h^{(1)}\right)\frac{\partial^3h^{(2)}}{\partial\eta^3}\right]\\
&\quad + \frac{\varphi}{5\delta\alpha_\kappa}\left[2\nu_0U_{12}h^{(1)}\left(1-\rho_0\right) - \rho_0\nu_0U_{11}\right] + \frac{h^{(2)}}{5\delta\alpha_\kappa},\\
&\frac{\partial r^{(1)}}{\partial\tau} - c_s\frac{\partial r^{(1)}}{\partial\eta} = \left(r^{(1)}\right)^2\frac{\partial q^{(1)}}{\partial\eta},\\
&\frac{\partial r^{(2)}}{\partial\tau} - c_s\frac{\partial r^{(2)}}{\partial\eta} = \left(r^{(2)}\right)^2\left(\frac{\partial q^{(2)}}{\partial\eta} - \frac{\partial q^{(1)}}{\partial\eta}\right),\\
&\frac{\partial r^{(3)}}{\partial\tau} - c_s\frac{\partial r^{(3)}}{\partial\eta} = \left(r^{(3)}\right)^2\left[\left(3 - 4\rho_0\nu_0\right)\frac{\partial q^{(1)}}{\partial\eta} + 4\rho_0\nu_0\frac{\partial q^{(2)}}{\partial\eta}\right],
\end{aligned}
$$

where the coefficients $U_{12}, U_{11}, U_{22}, U_{20}$ and $J^{(1)}, J^{(2)}$ are defined in (4.3).

Solutions of (4.4) are looked in the form of finite Fourier series:

$$
\begin{aligned}
h^{(1)}(\eta,\tau) &= \sum_{n=1}^{2N} a_n^{\left(h^{(1)}\right)}(\tau) e^{i(N-n)(\eta-\eta_0)}, \quad a_n^{\left(h^{(1)}\right)} = \overline{a_{2N-n}^{\left(h^{(1)}\right)}},\ n=1,\dots,N, \quad a_{2N}^{\left(h^{(1)}\right)} = 0,\\
q^{(1)}(\eta,\tau) &= \sum_{n=1}^{2N} a_n^{\left(q^{(1)}\right)}(\tau) e^{i(N-n)(\eta-\eta_0)}, \quad a_n^{\left(q^{(1)}\right)} = \overline{a_{2N-n}^{\left(q^{(1)}\right)}},\ n=1,\dots,N, \quad a_{2N}^{\left(q^{(1)}\right)} = 0,\\
h^{(2)}(\eta,\tau) &= \sum_{n=1}^{2N} a_n^{\left(h^{(2)}\right)}(\tau) e^{i(N-n)(\eta-\eta_0)}, \quad a_n^{\left(h^{(2)}\right)} = \overline{a_{2N-n}^{\left(h^{(2)}\right)}},\ n=1,\dots,N, \quad a_{2N}^{\left(h^{(2)}\right)} = 0,\\
q^{(2)}(\eta,\tau) &= \sum_{n=1}^{2N} a_n^{\left(q^{(2)}\right)}(\tau) e^{i(N-n)(\eta-\eta_0)}, \quad a_n^{\left(q^{(2)}\right)} = \overline{a_{2N-n}^{\left(q^{(2)}\right)}},\ n=1,\dots,N, \quad a_{2N}^{\left(q^{(2)}\right)} = 0,\\
r^{(1)}(\eta,\tau) &= \sum_{n=1}^{2N} a_n^{\left(r^{(1)}\right)}(\tau) e^{i(N-n)(\eta-\eta_0)}, \quad a_n^{\left(r^{(1)}\right)} = \overline{a_{2N-n}^{\left(r^{(1)}\right)}},\ n=1,\dots,N, \quad a_{2N}^{\left(r^{(1)}\right)} = 0,\\
r^{(2)}(\eta,\tau) &= \sum_{n=1}^{2N} a_n^{\left(r^{(2)}\right)}(\tau) e^{i(N-n)(\eta-\eta_0)}, \quad a_n^{\left(r^{(2)}\right)} = \overline{a_{2N-n}^{\left(r^{(2)}\right)}},\ n=1,\dots,N, \quad a_{2N}^{\left(r^{(2)}\right)} = 0,\\
r^{(3)}(\eta,\tau) &= \sum_{n=1}^{2N} a_n^{\left(r^{(3)}\right)}(\tau) e^{i(N-n)(\eta-\eta_0)}, \quad a_n^{\left(r^{(3)}\right)} = \overline{a_{2N-n}^{\left(r^{(3)}\right)}},\ n=1,\dots,N, \quad a_{2N}^{\left(r^{(3)}\right)} = 0.
\end{aligned}
$$

To apply the fast Fourier transform, we consider $N = 2^{p_\eta}$ where p_η is an integer.

Substituting the Fourier series into (4.4) and collecting the coefficients at the same harmonics lead to the formulation of the dynamical system for $a_n^{\left(h^{(1)}\right)}$, $a_n^{\left(q^{(1)}\right)}$, $a_n^{\left(h^{(2)}\right)}$, $a_n^{\left(q^{(2)}\right)}$, $a_n^{\left(r^{(1)}\right)}$, $a_n^{\left(r^{(2)}\right)}$ and $a_n^{\left(r^{(3)}\right)}$:

$$
\begin{aligned}
\frac{da_n^{\left(h^{(1)}\right)}}{d\tau} &= F_n^{\left(h^{(1)}\right)}\left(a_m^{\left(h^{(1)}\right)}, a_m^{\left(q^{(1)}\right)}, a_m^{\left(h^{(2)}\right)}, a_m^{\left(q^{(2)}\right)}, a_m^{\left(r^{(1)}\right)}, a_m^{\left(r^{(2)}\right)}, a_m^{\left(r^{(3)}\right)}\right), \qquad (4.5)\\
\frac{da_n^{\left(q^{(1)}\right)}}{d\tau} &= F_n^{\left(q^{(1)}\right)}\left(a_m^{\left(h^{(1)}\right)}, a_m^{\left(q^{(1)}\right)}, a_m^{\left(h^{(2)}\right)}, a_m^{\left(q^{(2)}\right)}, a_m^{\left(r^{(1)}\right)}, a_m^{\left(r^{(2)}\right)}, a_m^{\left(r^{(3)}\right)}\right),\\
\frac{da_n^{\left(h^{(2)}\right)}}{d\tau} &= F_n^{\left(h^{(2)}\right)}\left(a_m^{\left(h^{(1)}\right)}, a_m^{\left(q^{(1)}\right)}, a_m^{\left(h^{(2)}\right)}, a_m^{\left(q^{(2)}\right)}, a_m^{\left(r^{(1)}\right)}, a_m^{\left(r^{(2)}\right)}, a_m^{\left(r^{(3)}\right)}\right),\\
\frac{da_n^{\left(q^{(2)}\right)}}{d\tau} &= F_n^{\left(q^{(2)}\right)}\left(a_m^{\left(h^{(1)}\right)}, a_m^{\left(q^{(1)}\right)}, a_m^{\left(h^{(2)}\right)}, a_m^{\left(q^{(2)}\right)}, a_m^{\left(r^{(1)}\right)}, a_m^{\left(r^{(2)}\right)}, a_m^{\left(r^{(3)}\right)}\right),
\end{aligned}
$$

$$\frac{da_n^{\left(r^{(1)}\right)}}{d\tau} = F_n^{\left(r^{(1)}\right)}\left(a_m^{\left(h^{(1)}\right)}, a_m^{\left(q^{(1)}\right)}, a_m^{\left(h^{(2)}\right)}, a_m^{\left(q^{(2)}\right)}, a_m^{\left(r^{(1)}\right)}, a_m^{\left(r^{(2)}\right)}, a_m^{\left(r^{(3)}\right)}\right),$$
$$\frac{da_n^{\left(r^{(2)}\right)}}{d\tau} = F_n^{\left(r^{(2)}\right)}\left(a_m^{\left(h^{(1)}\right)}, a_m^{\left(q^{(1)}\right)}, a_m^{\left(h^{(2)}\right)}, a_m^{\left(q^{(2)}\right)}, a_m^{\left(r^{(1)}\right)}, a_m^{\left(r^{(2)}\right)}, a_m^{\left(r^{(3)}\right)}\right),$$
$$\frac{da_n^{\left(r^{(3)}\right)}}{d\tau} = F_n^{\left(r^{(3)}\right)}\left(a_m^{\left(h^{(1)}\right)}, a_m^{\left(q^{(1)}\right)}, a_m^{\left(h^{(2)}\right)}, a_m^{\left(q^{(2)}\right)}, a_m^{\left(r^{(1)}\right)}, a_m^{\left(r^{(2)}\right)}, a_m^{\left(r^{(3)}\right)}\right), \quad n = 1, \ldots, 2N.$$

The dynamical system includes the similarity parameters δ, ρ_0, ν_0, σ_0 and the wavenumber α_κ. There is also a free parameter c_s which does not affect a solution except its velocity.

Thus, the modelling wave motions in two-layer film are described by the system (4.4) for the functions $h^{(1)}$, $q^{(1)}$, $h^{(2)}$, $q^{(2)}$, $r^{(1)}$, $r^{(2)}$ and $r^{(3)}$ depending on η and τ in the physical space, or by the dynamical system (4.5) in the phase space.

In [64] and [63] the term 'dominating wave' was introduced for the one-layer film flow as the steady-travelling periodic wave developing in transient computations. In particular, a steady-travelling wave developed in transient computation is characterized by approaching velocities of the harmonics to each other, see Appendix C.

A dominating wave depends on values of the similarity parameters but it does not depend on initial conditions. The film thickness of a dominating wave is maximum among the thicknesses of all steady-travelling waves existing at the same values of the similarity parameters [64, 63]. Depending on the wave numbers, the set of dominating waves involves waves of different families. Waves of the first family $\gamma_{-1,1}$ are dominating at $s \in (s_a, 1)$ where $s_a \approx 0.5$. In the domain of longer waves, the dominating waves belong to one of slow one-humped families $\gamma_{-j,1}$, $j = 2, 3, \ldots$ or the fast one-humped family $\gamma_{+1,1}$. It is important to note that the parameters of the dominating waves are discontinuous functions since these waves belong to different families. In [63], [53] and [55], it has been shown that the concept of the dominating waves allows a researcher to select

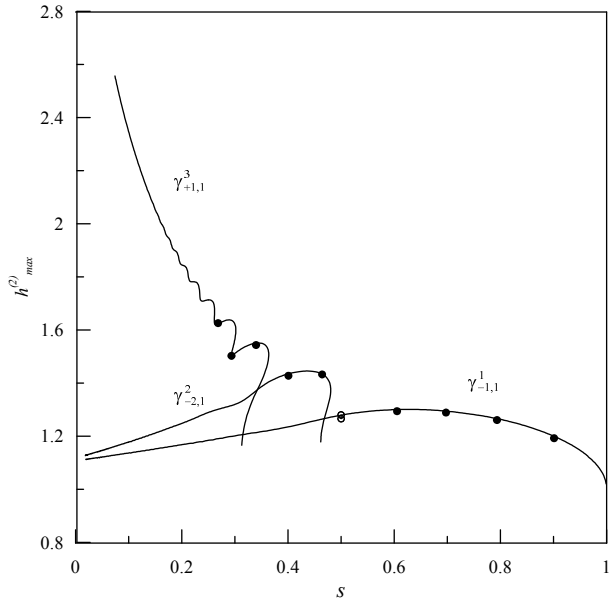

Figure 4.1: Maximum film thicknesses of bifurcating families $\gamma^1_{-1,1}$, $\gamma^2_{-2,1}$, $\gamma^3_{+1,1}$ at $\delta = 0.1$ and $H = 0.3$. The full and open circles correspond to results of transient computations.

theoretical solutions corresponding to waves observed in experiments. In parallel with the dominating waves, oscillating wave regimes [64, 63, 55, 57] were also revealed in neighbourhoods of the bifurcation points. Such regimes are characterized by time-harmonic or stochastic oscillations of wave parameters around some average values which are close to the parameters of one of steady-travelling waves.

Below we show that the evolution system (2.17) also possesses its dominating waves and describe typical evolution scenarios in two-layer films.

4.2 Results

In parallel with normalized wavenumber $s = \alpha_\kappa/\alpha_{\kappa,n}$, we use notation $s^{(i)} \equiv \alpha^{(i)}_{\kappa,n}/\alpha_{\kappa,n}$ where $\alpha^{(i)}_{\kappa,n}$ is the neutral wavenumber of the interface mode of instability.

Fig. 4.1 shows the example of bifurcations of three wave families in the plane $(s, h^{(2)}_{max})$, where $h^{(2)}_{max}$ is the maximum thickness of the film layer. This is the same bifurcation scheme as shown in Fig. 3.1 in plane (s, c). In this case the neutral wavenumbers are

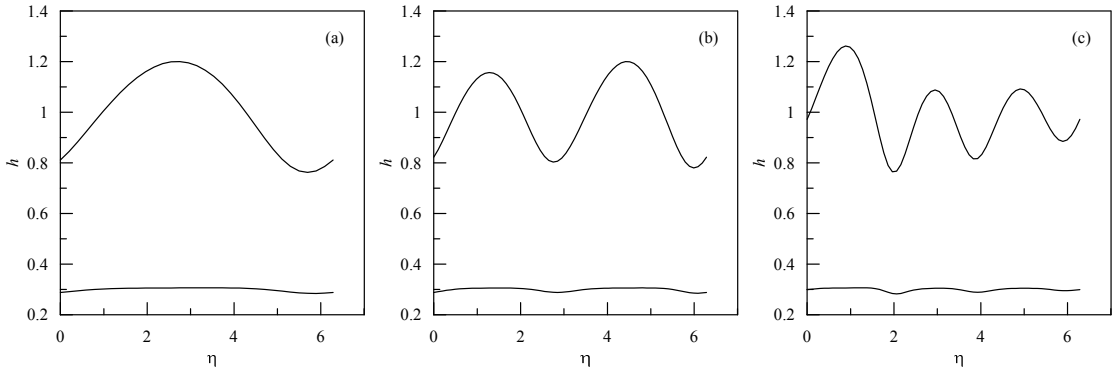

Figure 4.2: Examples of waves belonging to the family $\gamma^1_{-1,1}$ at $s = 0.9$ (a), family $\gamma^2_{-2,1}$ at $s = 0.462$ (b) and family $\gamma^3_{+1,1}$ at $s = 0.3203$ (c) for the case corresponding to Fig. 4.1.

$\alpha_{\kappa,n} = 1.41$ and $\alpha^{(i)}_{\kappa,n} = 0.2256$. Examples of waves belonging to the families are shown in Fig. 4.2 where the waves are taken at the wavenumbers from the neighbourhoods of the bifurcation points. We remind that the family $\gamma^1_{-1,1}$ bifurcates from the waveless flow as the first harmonic, the family $\gamma^2_{-2,1}$ bifurcates from the family $\gamma^1_{-1,1}$ as a period-doubling wave, and the family $\gamma^3_{+1,1}$ is created by period-tripling bifurcation. The same wave families are shown in Fig. 4.3 where $h^{(1)}_{max}$ is the maximum thickness of the first layer.

As shown in Fig. 4.2, the amplitude of the interface waves at $H = 0.3$ is relatively small in comparison with that of the surface waves. To understand the role of the parameter H, we have also computed the wave families at $H = 0.6$, see Figs. 4.4 and 4.5 which are the same bifurcation schemes of Fig. 3.6. In this case the neutral wavenumbers are $\alpha_{\kappa,n} = 1.24$ and $\alpha^{(i)}_{\kappa,n} = 0.248$. It is seen that changing the position of the waveless interface does not strongly affect the maximum film thickness $h^{(2)}_{max}$, see Figs. 4.1 and 4.4 although the amplitude of the interface $h^{(1)}_{max} - h^{(1)}_0$ has increased, see Figs. 4.3 and 4.5.

We consider unsteady wave dynamics in two cases of the first layer thickness H for water-benzene system. The results are summarised in Figs. 4.1 and 4.3 at $H = 0.3$, and in Figs. 4.4 and 4.5 at $H = 0.6$ where the circles denote solutions of the problem (2.17) at relatively large value of time τ. The full circles indicate that the maximum of the

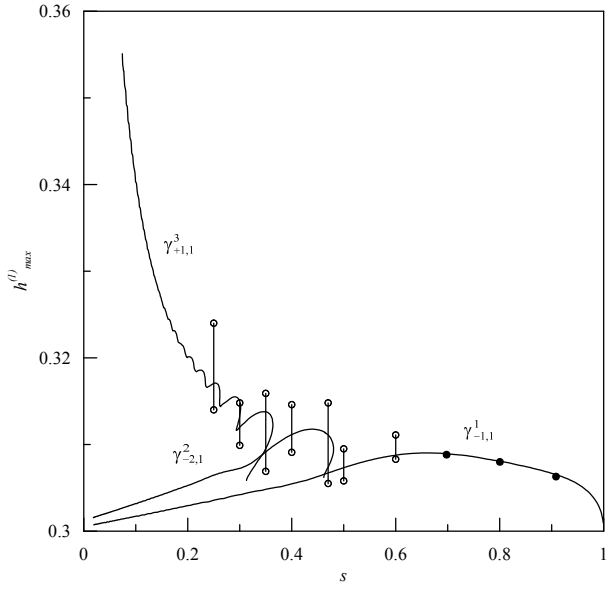

Figure 4.3: Maximum first layer thicknesses in the case shown in Fig. 4.1.

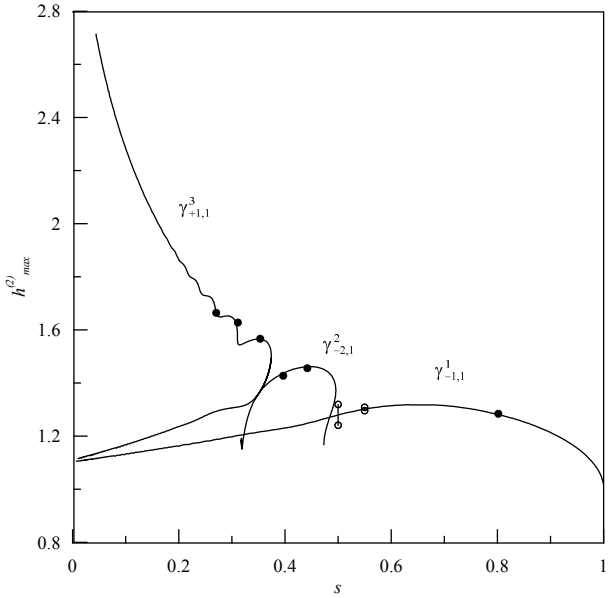

Figure 4.4: Maximum film thicknesses of bifurcating families $\gamma^1_{-1,1}$, $\gamma^2_{-2,1}$, $\gamma^3_{+1,1}$ at $\delta = 0.1$ and $H = 0.6$. Full and open circles show results of transient computations.

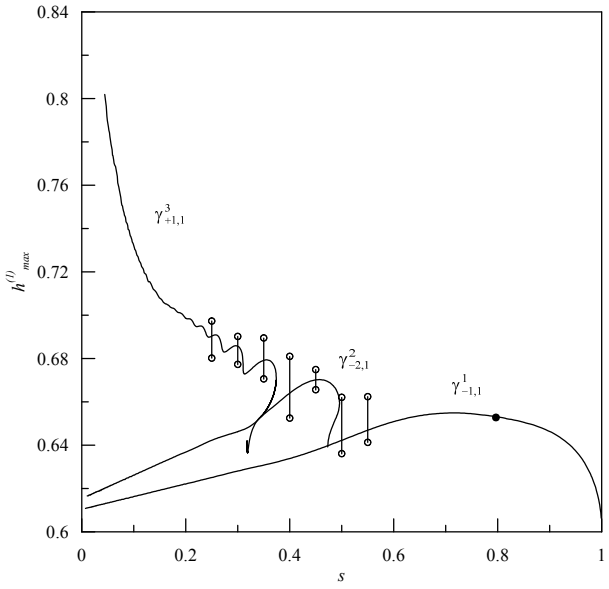

Figure 4.5: Maximum first layer thicknesses in the case shown in Fig. 4.4.

film thickness or the first layer thickness has developed to a constant, or its oscillating amplitude is very small. The open circles, connected with the vertical lines, settle the intervals of variation of $h^{(1)}_{max}$ and $h^{(2)}_{max}$ as $\tau \to \infty$ in oscillating regimes. The results for the film thickness summarized in Figs. 4.1 and 4.4 are similar to the one for the one-layer film when the oscillating regimes exist in neighbourhoods of the fold bifurcations of the families, see computations at $s = 0.5$ in Fig. 4.1 and at $s = 0.5$ and $s = 0.55$ in Fig. 4.4 corresponding to the fold bifurcation of family $\gamma^2_{-2,1}$ affecting attractors of waves belonging to family $\gamma^1_{-1,1}$. In other computed cases the attracting regimes are steady-travelling periodic waves. On the other hand, Figs. 4.3 and 4.5 demonstrate that all computations, except the cases when s is close to 1, have led to oscillating regimes of $h^{(1)}_{max}$. It means that the dynamical system of the evolution equations (2.17) has attractive tori in the phase space of the Fourier coefficients in most cases in contrast to the one-layer film where the attracting wave regimes are predominantly limit circles in the phase space of the Fourier coefficients.

To understand the structure of the attracting solutions, we have plotted Figs. 4.6

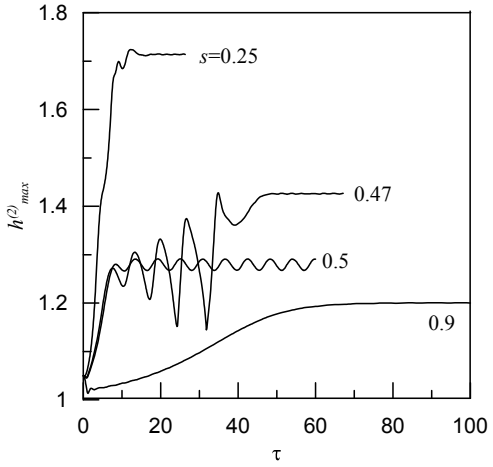

Figure 4.6: Dependency of the maximum film layer thickness on time for different values of s at $\delta = 0.1$ and $H = 0.3$.

and 4.7 corresponding to the results in Figs. 4.1 and 4.3. It is seen that the maximum film thickness tends to constants at $s = 0.25, 0.47$ and 0.9, and the maximum interface thickness tends to oscillations of constant amplitudes at $s = 0.25$ and 0.47, or the damped oscillation at $s = 0.9$. In the only case when $h^{(2)}_{max}(\tau)$ comes to the oscillating regime, $s = 0.5$, the maximum interface thickness has stochastic oscillations.

It is important to note that the wave shapes $h^{(2)}$ and $h^{(1)}$ of developed wave regimes are similar to the shapes of steady-travelling waves of maximum film thickness at the same values of the similarity parameters. Examples of such 'almost' steady-travelling waves developed in transient computations are shown in Fig. 4.8. These waves are slightly changing with time, see examples in Fig. 4.9 where it is seen that comparing with panel (a), there is additional oscillation on surface wave in panel (b). Examples of varying interface wave shapes at $s = 0.47$ are shown by Fig. 4.10.

The same wave dynamics are shown in the phase trajectories of the dynamical system, see Fig. 4.11, where the projections of phase trajectories onto planes of the first Fourier coefficients for the film surface in panel (a) and the interface in panel (b) are shown. Comparison of the panels also demonstrates that the wave shapes at the surface and

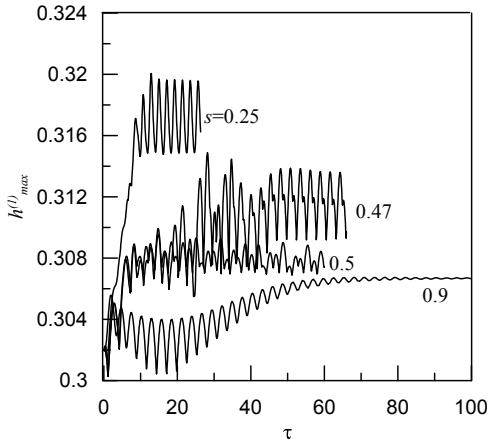

Figure 4.7: Dependency of the maximum first layer thickness in the cases shown in Fig. 4.6.

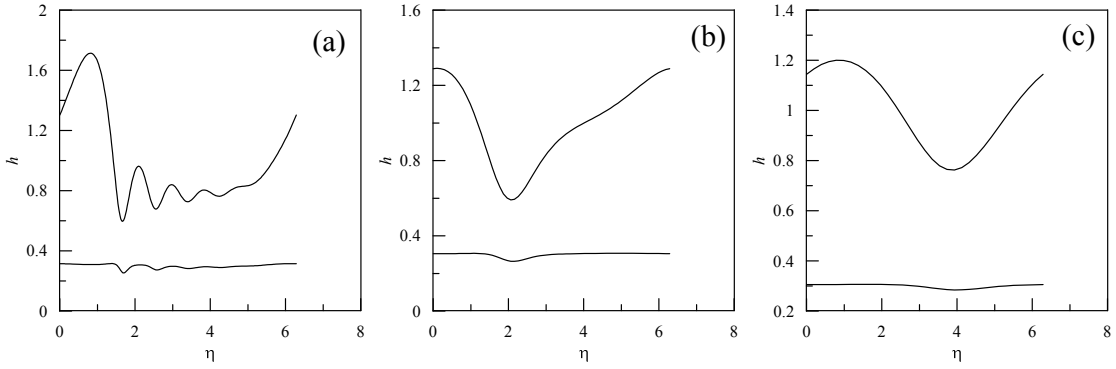

Figure 4.8: Examples of developed oscillating waves at $s = 0.25$ (a), $s = 0.5$ (b) and $s = 0.9$ (c) at $\delta = 0.1$ and $H = 0.3$.

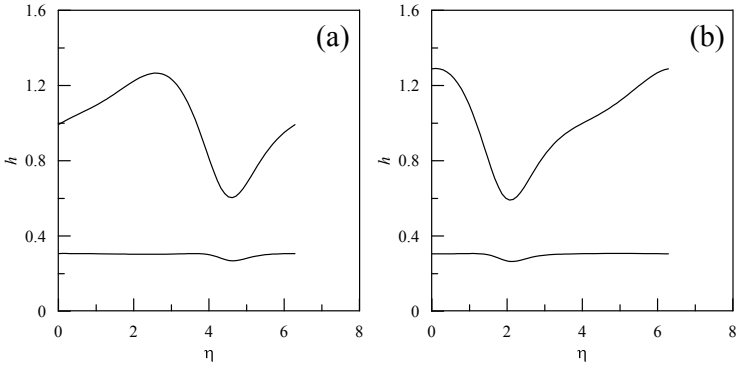

Figure 4.9: Examples of waves for $s = 0.5$ at $t = 10.5$ (a) and $t = 60$ (b) at $\delta = 0.1$ and $H = 0.3$.

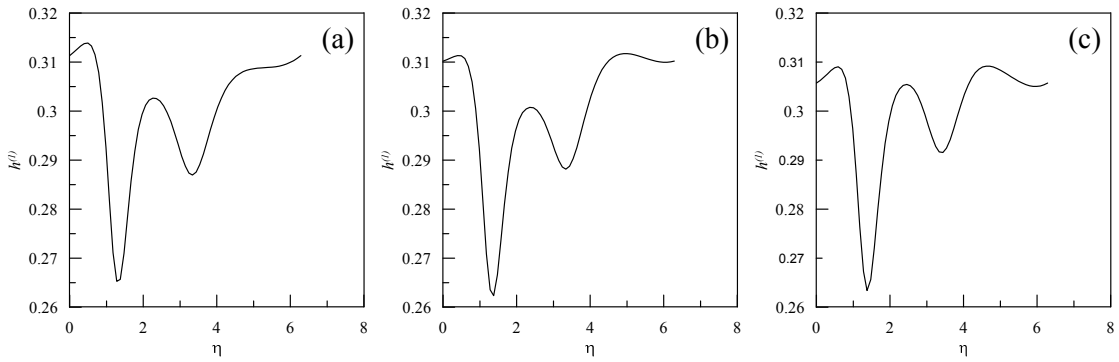

Figure 4.10: Examples of waves at interface for $s = 0.47$ at $t = 50.8$ (a), $t = 51.4$ (b) and $t = 52.4$ (c) at $\delta = 0.1$ and $H = 0.3$.

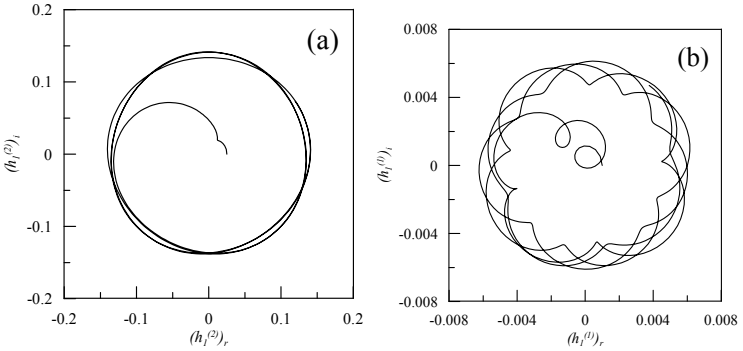

Figure 4.11: Projections of the phase trajectories at $\delta = 0.1$, $H = 0.3$ and $s = 0.5$ corresponding to Fig. 4.6 and 4.7 at planes of Fourier coefficients for the film layer (a) and the first layer (b).

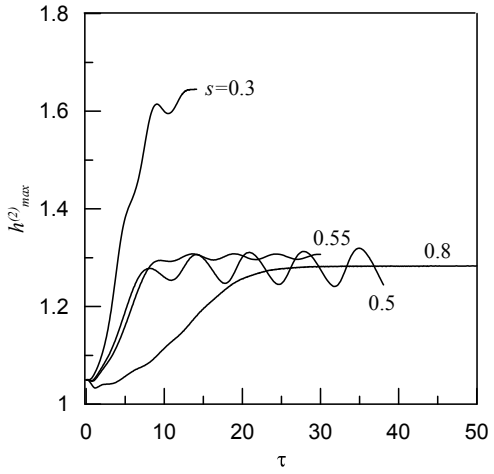

Figure 4.12: Dependency of the maximum film layer thickness on time for different values of s at $\delta = 0.1$ and $H = 0.6$.

interface are not coherent.

To analyse the case $H = 0.6$, we have plotted Figs. 4.12 and 4.13 corresponding to the results in Figs. 4.4 and 4.5. The maximum film thickness tends to constants at $s = 0.3$ and 0.8 on the computed time intervals while the maximum interface does not reach a constant at $s = 0.3$ and demonstrates the damped oscillation at $s = 0.8$. Moreover, the maximum film layer thicknesses are apt to harmonic oscillations of constant amplitudes even as the maximum first layer thicknesses have non-harmonic oscillations at $s = 0.5$ and 0.55. Examples of 'almost' steady-travelling waves at $s = 0.3, 0.5$ and 0.8 shown in Fig. 4.14. demonstrate the role of the waveless thickness H: its increasing leads to growth of the interfacial wave amplitude.

Fig. 4.15 showing an example of variation of the wave shape in time also demonstrates the interface amplitude of the same order as the surface amplitude has.

It is important to note that although most transient computations lead to two-periodic oscillating regimes, or tori in the phase space, there are attracting limit cycles for relatively short waves, see Fig.4.16.

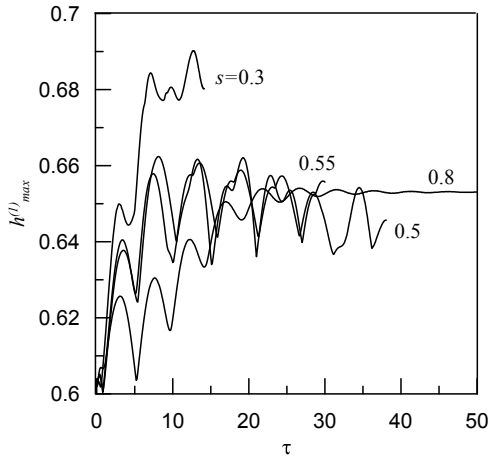

Figure 4.13: Dependency of the maximum first layer thickness in the cases shown in Fig. 4.12.

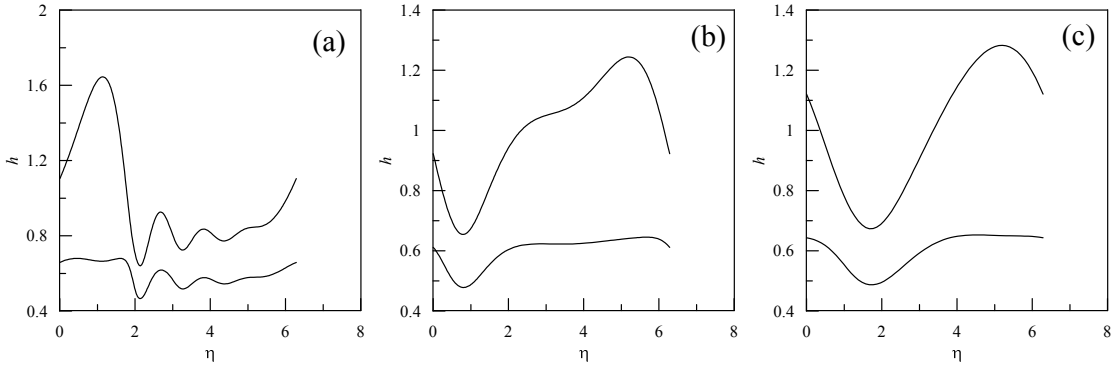

Figure 4.14: Examples of developed oscillating waves at $s = 0.3$ (a), $s = 0.5$ (b) and $s = 0.8$ (c) at $\delta = 0.1$ and $H = 0.6$.

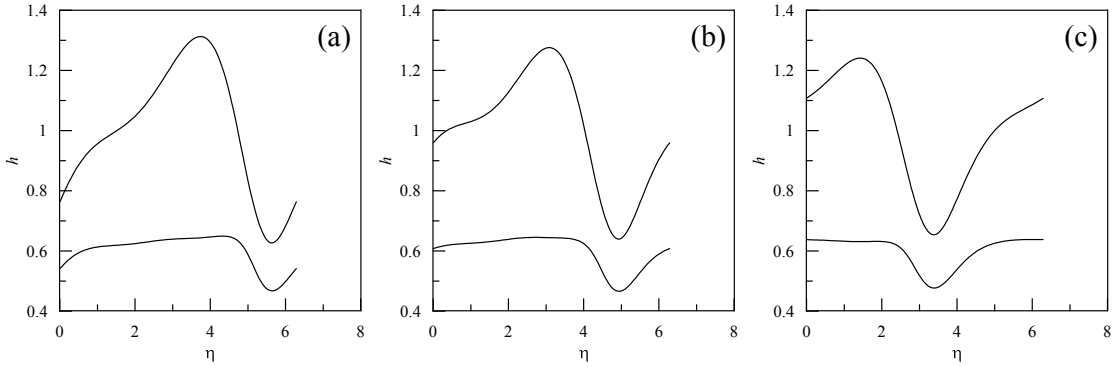

Figure 4.15: Examples of waves for $s = 0.5$ at $t = 27.9$ (a), $t = 30$ (b) and $t = 31.8$ (c) at $\delta = 0.1$ and $H = 0.6$.

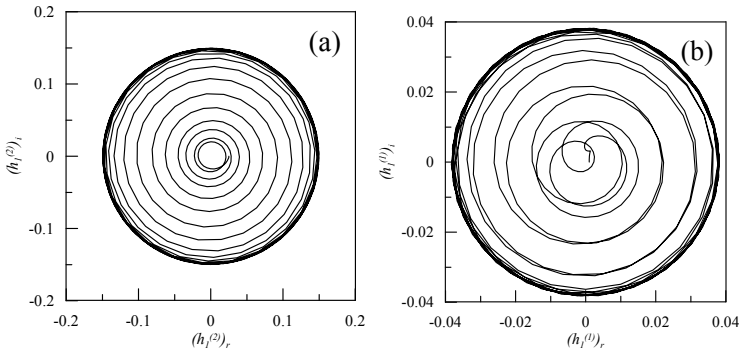

Figure 4.16: Projections of the phase trajectories at $s = 0.8$ corresponding to Figs. 4.12 and 4.13 at planes of the first Fourier coefficients for film layer (a) and first layer (b) at $\delta = 0.1$ and $H = 0.6$.

Chapter 5

Mass Transfer

In this chapter, mass transfer of weakly soluble gas in two-layer film flows is studied. Then, the diffusion problem in the regime of regular waves is stated and solved numerically.

5.1 Problem statement

5.1.1 Dimensional form

Let's $\tilde{C}_v$ is a volume concentration of a weakly soluble gas. We assume that the volume concentration at the free surface is a given value $\tilde{C}_{v,s}$, and there is no gas flux through the wall. If $D_v^{(1)}$ and $D_v^{(2)}$ are the diffusion coefficients for liquids in the first and second layers, respectively, then the boundary problem for the gas concentration is:

$$\frac{\partial \tilde{C}_v}{\partial \tilde{t}} + \tilde{u}\frac{\partial \tilde{C}_v}{\partial \tilde{x}} + \tilde{v}\frac{\partial \tilde{C}_v}{\partial \tilde{y}} = D_v^{(j)}\left(\frac{\partial^2 \tilde{C}_v}{\partial \tilde{x}^2} + \frac{\partial^2 \tilde{C}_v}{\partial \tilde{y}^2}\right), \tag{5.1}$$

$$\tilde{y} = 0: \quad q_{v,n} = 0,$$

$$\tilde{y} = \tilde{h}^{(1)}\left(\tilde{x}, \tilde{t}\right): \quad \left[\tilde{C}_v\right]_1^2 = 0, \quad [q_{v,n}]_1^2 = 0,$$

$$\tilde{y} = \tilde{h}^{(2)}\left(\tilde{x}, \tilde{t}\right): \quad \tilde{C}_v = \tilde{C}_{v,s},$$

$$\tilde{x} = \tilde{L}_l: \quad \tilde{C}_v = \tilde{C}_{v,l}\left(\tilde{y}, \tilde{t}\right),$$

$$\tilde{x} = \tilde{L}_r: \quad \tilde{C}_v = \tilde{C}_{v,r}\left(\tilde{y}, \tilde{t}\right),$$

where

$$\vec{\tilde{q}}_v = -D_v^{(j)} \mathrm{grad}\, \tilde{C}_v, \quad \vec{\tilde{n}} = \frac{\left(-\frac{\partial \tilde{h}}{\partial \tilde{x}}, 1\right)}{\sqrt{1 + \left(\frac{\partial \tilde{h}}{\partial \tilde{x}}\right)^2}} \tag{5.2}$$

$$\tilde{q}_{v,n} = \vec{\tilde{q}}_v \cdot \vec{\tilde{n}} = -D_v^{(j)} \frac{\frac{\partial \tilde{C}_v}{\partial \tilde{y}} - \frac{\partial \tilde{h}}{\partial \tilde{x}} \frac{\partial \tilde{C}_v}{\partial \tilde{x}}}{\sqrt{1 + \left(\frac{\partial \tilde{h}}{\partial \tilde{x}}\right)^2}}.$$

and as before the notation $[f]_1^2 \equiv f^{(2)} - f^{(1)}$ denotes the jump in quantity f from the value in the first liquid, $f^{(1)}$, to the value in the second, $f^{(2)}$.

Diffusion fluxes through the film surface, and the interface between layers over the interval $\left[\tilde{L}_l, \tilde{L}_r\right]$ are calculated as follows:

$$\tilde{Q}_{v,n} = \int_{\tilde{L}_l}^{\tilde{L}_r} q_{v,n} \sqrt{1 + \left(\frac{\partial \tilde{h}}{\partial \tilde{x}}\right)^2}\, d\tilde{x}, \tag{5.3}$$

where $\tilde{h} = \tilde{h}^{(1)}$ or $\tilde{h} = \tilde{h}^{(2)}$.

In the following analysis, we also use the average gas concentration in the first layer and the second layer

$$\tilde{C}_{v,av}^{(1)} = \frac{1}{\tilde{h}^{(1)}} \int_0^{\tilde{h}^{(1)}} \tilde{C}_v d\tilde{y}, \quad \tilde{C}_{v,av}^{(2)} = \frac{1}{\tilde{h}^{(2)} - \tilde{h}^{(1)}} \int_{\tilde{h}^{(1)}}^{\tilde{h}^{(2)}} \tilde{C}_v d\tilde{y}. \tag{5.4}$$

5.1.2 Dimensionless form

Using the replacement the dimensionless variables (2.3) and new variables

$$C_v = \frac{\tilde{C}_v}{C_{v,c}}, \quad q_{v,n} = \mathrm{ScRe} \frac{\tilde{q}_{v,n}}{C_{v,c} U_c} \quad Q_{v,n} = \mathrm{ScRe} \frac{\tilde{Q}_{v,n}}{C_{v,c} U_c H_c},$$

where $\mathrm{Sc} \equiv \nu^{(2)}/D_v^{(2)}$ is the Schmidt number, the problem (5.1), (5.2), (5.3) and (5.4) is rewritten in the dimensionless form

$$\frac{\partial C_v}{\partial t} + u\frac{\partial C_v}{\partial x} + v\frac{\partial C_v}{\partial y} = \frac{D_0^{(j)}}{\mathrm{ScRe}}\left(\frac{\partial^2 C_v}{\partial x^2} + \frac{\partial^2 C_v}{\partial y^2}\right),$$

$$y = 0: \quad \frac{\partial C_v}{\partial y} = 0,$$

$$y = h^{(1)}(x,t): \quad [C_v]_1^2 = 0, \quad [q_{v,n}]_1^2 = 0,$$

$$y = h^{(2)}(x,t): \quad C_v = C_{v,s},$$

$$x = L_l: \quad C_v = C_{v,l}(y,t),$$

$$x = L_r: \quad C_v = C_{v,r}(y,t),$$

where $C_{v,s} = \tilde{C}_{v,s}/C_{v,c}$, $D_0^{(1)} = D_v^{(1)}/D_v^{(2)}$, $D_0^{(2)} = 1$ and

$$q_{v,n} = -D_0^{(j)} \frac{\frac{\partial C_v}{\partial y} - \frac{\partial h^{(j)}}{\partial x}\frac{\partial C_v}{\partial x}}{\sqrt{1 + \left(\frac{\partial h^{(j)}}{\partial x}\right)^2}}.$$

Integral mass fluxes through the interface and the surface are written respectively in the following form:

$$Q_{v,n}^{(1)} = -D_0^{(1)} \int_{L_l}^{L_r} \left(\frac{\partial C_v}{\partial y} - \frac{\partial h^{(1)}}{\partial x}\frac{\partial C_v}{\partial x}\right)\Big|_{y=h^{(1)}-0} dx,$$

$$Q_{v,n}^{(2)} = -D_0^{(2)} \int_{L_l}^{L_r} \left(\frac{\partial C_v}{\partial y} - \frac{\partial h^{(2)}}{\partial x}\frac{\partial C_v}{\partial x}\right)\Big|_{y=h^{(2)}-0} dx$$

and the average concentrations in the layers become

$$C_{v,av}^{(1)} = \frac{1}{h^{(1)}} \int_0^{h^{(1)}} C_v dy, \quad C_{v,av}^{(2)} = \frac{1}{h^{(2)} - h^{(1)}} \int_{h^{(1)}}^{h^{(2)}} C_v dy.$$

5.1.3 Approximate problem

Using the stretching variables (2.10) and introducing $L_{\kappa,l} \equiv \kappa L_l$ and $L_{\kappa,r} \equiv \kappa L_r$, we rewrite the problem as follows

$$\begin{aligned}
&\frac{\partial C_v}{\partial t_\kappa} + u\frac{\partial C_v}{\partial x_\kappa} + v_\kappa \frac{\partial C_v}{\partial y} = \frac{D_0^{(j)}}{\kappa \mathrm{ScRe}}\left(\kappa^2 \frac{\partial^2 C_v}{\partial x_\kappa^2} + \frac{\partial^2 C_v}{\partial y^2}\right),\\
&y = 0: \quad \frac{\partial C_v}{\partial y} = 0,\\
&y = h^{(1)}(x_\kappa, t_\kappa): \quad [C_v]_1^2 = 0, \quad [q_{v,n}]_1^2 = 0,\\
&y = h^{(2)}(x_\kappa, t_\kappa): \quad C_v = C_{v,s},\\
&x_\kappa = L_{\kappa,l}: \quad C_v = C_{v,l}(y, t_\kappa),\\
&x_\kappa = L_{\kappa,r}: \quad C_v = C_{v,r}(y, t_\kappa),
\end{aligned}$$

where

$$q_{v,n} = -D_0^{(j)} \frac{\frac{\partial C_v}{\partial y} - \kappa^2 \frac{\partial h^{(j)}}{\partial x_\kappa}\frac{\partial C_v}{\partial x_\kappa}}{\sqrt{1 + \left(\kappa \frac{\partial h^{(j)}}{\partial x_\kappa}\right)^2}}.$$

Then, the integral mass fluxes through the interface and the surface are

$$\begin{aligned}
Q_{v,n}^{(1)} &= -\frac{D_0^{(1)}}{\kappa} \int\limits_{L_{\kappa,l}}^{L_{\kappa,r}} \left(\frac{\partial C_v}{\partial y} - \kappa^2 \frac{\partial h^{(1)}}{\partial x_\kappa}\frac{\partial C_v}{\partial x_\kappa}\right)\Big|_{y=h^{(1)}-0} dx_\kappa,\\
Q_{v,n}^{(2)} &= -\frac{D_0^{(2)}}{\kappa} \int\limits_{L_{\kappa,l}}^{L_{\kappa,r}} \left(\frac{\partial C_v}{\partial y} - \kappa^2 \frac{\partial h^{(2)}}{\partial x_\kappa}\frac{\partial C_v}{\partial x_\kappa}\right)\Big|_{y=h^{(2)}-0} dx_\kappa.
\end{aligned}$$

Omitting the terms $O(\kappa^2)$ and using (2.12) we obtain the following problem

$$\begin{aligned}
&\frac{\partial C_v}{\partial t_\kappa} + u\frac{\partial C_v}{\partial x_\kappa} + v_\kappa\frac{\partial C_v}{\partial y} = \frac{\varphi D_0^{(j)}}{5\delta \mathrm{Sc}}\frac{\partial^2 C_v}{\partial y^2},\\
&y = 0: \quad \frac{\partial C_v}{\partial y} = 0,\\
&y = h^{(1)}(x_\kappa, t_\kappa): \quad [C_v]_1^2 = 0, \quad [q_{v,n}]_1^2 = 0,\\
&y = h^{(2)}(x_\kappa, t_\kappa): \quad C_v = C_{v,s},\\
&x_\kappa = L_{\kappa,l}: \quad C_v = C_{v,l}(y, t_\kappa),
\end{aligned}$$

where

$$q_{v,n} = -D_0^{(j)}\frac{\partial C_v}{\partial y}.$$

Integral mass fluxes through the interface and the surface are rewritten, respectively:

$$\begin{aligned}
Q_{v,n}^{(1)} &= -\frac{D_0^{(1)}}{\kappa}\int\limits_{L_{\kappa,l}}^{L_{\kappa,r}} \frac{\partial C_v}{\partial y}\Big|_{y=h^{(1)}-0} dx_\kappa,\\
Q_{v,n}^{(2)} &= -\frac{D_0^{(2)}}{\kappa}\int\limits_{L_{\kappa,l}}^{L_{\kappa,r}} \frac{\partial C_v}{\partial y}\Big|_{y=h^{(2)}-0} dx_\kappa.
\end{aligned}$$

Finally, average concentrations in the layers are:

$$C_{v,av}^{(1)} = \frac{1}{h^{(1)}}\int\limits_0^{h^{(1)}} C_v dy, \quad C_{v,av}^{(2)} = \frac{1}{h^{(2)} - h^{(1)}}\int\limits_{h^{(1)}}^{h^{(2)}} C_v dy.$$

5.1.4 Velocity profile

The diffusion equation is solved in the case of the velocity profile (2.14)

$$
\begin{aligned}
y \in \left[0, h^{(1)}\right]: \quad & u^{(1)} = U_{11} y + U_{12} y^2, \\
y \in \left[h^{(1)}, h^{(2)}\right]: \quad & u^{(2)} = U_{20} + U_{22}\left(y^2 - 2h^{(2)} y\right).
\end{aligned}
$$

Using the continuity equation in the first layer we obtain

$$
\begin{aligned}
\frac{\partial v_\kappa^{(1)}}{\partial y} &= -\frac{\partial u^{(1)}}{\partial x_\kappa} = -\frac{\partial U_{11}}{\partial x_\kappa} y - \frac{\partial U_{12}}{\partial x_\kappa} y^2, \\
v_\kappa^{(1)} &= -\frac{\partial U_{11}}{\partial x_\kappa}\frac{y^2}{2} - \frac{\partial U_{12}}{\partial x_\kappa}\frac{y^3}{3}.
\end{aligned}
$$

Similarly, in the second layer we have:

$$
\begin{aligned}
\frac{\partial v_\kappa^{(2)}}{\partial y} &= -\frac{\partial U_{20}}{\partial x_\kappa} + \left(U_{22}\frac{\partial h^{(2)}}{\partial x_\kappa} + h^{(2)}\frac{\partial U_{22}}{\partial x_\kappa}\right) 2y - \frac{\partial U_{22}}{\partial x_\kappa} y^2, \\
v_\kappa^{(2)} &= -\frac{\partial U_{11}}{\partial x_\kappa}\frac{\left(h^{(1)}\right)^2}{2} - \frac{\partial U_{12}}{\partial x_\kappa}\frac{\left(h^{(1)}\right)^3}{3} \\
&\quad -\frac{\partial U_{20}}{\partial x_\kappa}\left(y - h^{(1)}\right) + \left(U_{22}\frac{\partial h^{(2)}}{\partial x_\kappa} + h^{(2)}\frac{\partial U_{22}}{\partial x_\kappa}\right)\left(y^2 - \left(h^{(1)}\right)^2\right) - \frac{\partial U_{22}}{\partial x_\kappa}\frac{y^3 - \left(h^{(1)}\right)^3}{3}.
\end{aligned}
$$

Thus, the velocity components are

$$
\begin{aligned}
u^{(1)} &= U_{11} y + U_{12} y^2, \\
u^{(2)} &= U_{20} + U_{22}\left(y^2 - 2h^{(2)} y\right), \\
v_\kappa^{(1)} &= -\frac{\partial U_{11}}{\partial x_\kappa}\frac{y^2}{2} - \frac{\partial U_{12}}{\partial x_\kappa}\frac{y^3}{3}, \\
v_\kappa^{(2)} &= -\frac{\partial U_{11}}{\partial x_\kappa}\frac{\left(h^{(1)}\right)^2}{2} - \frac{\partial U_{12}}{\partial x_\kappa}\frac{\left(h^{(1)}\right)^3}{3} \\
&\quad -\frac{\partial U_{20}}{\partial x_\kappa}\left(y - h^{(1)}\right) + \left(U_{22}\frac{\partial h^{(2)}}{\partial x_\kappa} + h^{(2)}\frac{\partial U_{22}}{\partial x_\kappa}\right)\left(y^2 - \left(h^{(1)}\right)^2\right) - \frac{\partial U_{22}}{\partial x_\kappa}\frac{y^3 - \left(h^{(1)}\right)^3}{3},
\end{aligned}
$$

where coefficients U_{11}, U_{12}, U_{20} and U_{22} depending on $h^{(1)}\left(x_\kappa, t_\kappa\right)$, $h^{(2)}\left(x_\kappa, t_\kappa\right)$, $q^{(1)}\left(x_\kappa, t_\kappa\right)$ and $q^{(2)}\left(x_\kappa, t_\kappa\right)$, and their derivatives are calculated as follows

$$
\begin{aligned}
&w = 4\rho_0\nu_0 h^{(1)}(h^{(2)} - h^{(1)}) + 3(h^{(1)})^2,\\
&U_{12} = \frac{3}{w}\left(\frac{3q^{(2)}}{h^{(2)} - h^{(1)}} - \frac{3q^{(1)}}{h^{(2)} - h^{(1)}} - 2\frac{\rho_0\nu_0(h^{(2)} - h^{(1)}) + 3h^{(1)}}{(h^{(1)})^2}q^{(1)}\right),\\
&U_{11} = \frac{2q^{(1)}}{(h^{(1)})^2} - \frac{2h^{(1)}}{3}U_{12},\\
&U_{20} = \frac{q^{(2)} - q^{(1)}}{h^{(2)} - h^{(1)}} + \frac{\rho_0\nu_0 U_{11} + 2\rho_0\nu_0 U_{12}h^{(1)}}{6\left(h^{(2)} - h^{(1)}\right)}\left(-2(h^{(2)})^2 - 2h^{(2)}h^{(1)} + (h^{(1)})^2\right),\\
&U_{22} = -\frac{\rho_0\nu_0 U_{11} + 2\rho_0\nu_0 U_{12}h^{(1)}}{2(h^{(2)} - h^{(1)})},\\
&\frac{\partial U_{11}}{\partial x_\kappa} = \frac{\partial U_{11}}{\partial h^{(1)}}\frac{\partial h^{(1)}}{\partial x_\kappa} + \frac{\partial U_{11}}{\partial h^{(2)}}\frac{\partial h^{(2)}}{\partial x_\kappa} + \frac{\partial U_{11}}{\partial q^{(1)}}\frac{\partial q^{(1)}}{\partial x_\kappa} + \frac{\partial U_{11}}{\partial q^{(2)}}\frac{\partial q^{(2)}}{\partial x_\kappa},\\
&\frac{\partial U_{12}}{\partial x_\kappa} = \frac{\partial U_{12}}{\partial h^{(1)}}\frac{\partial h^{(1)}}{\partial x_\kappa} + \frac{\partial U_{12}}{\partial h^{(2)}}\frac{\partial h^{(2)}}{\partial x_\kappa} + \frac{\partial U_{12}}{\partial q^{(1)}}\frac{\partial q^{(1)}}{\partial x_\kappa} + \frac{\partial U_{12}}{\partial q^{(2)}}\frac{\partial q^{(2)}}{\partial x_\kappa},\\
&\frac{\partial U_{20}}{\partial x_\kappa} = \frac{\partial U_{20}}{\partial h^{(1)}}\frac{\partial h^{(1)}}{\partial x_\kappa} + \frac{\partial U_{20}}{\partial h^{(2)}}\frac{\partial h^{(2)}}{\partial x_\kappa} + \frac{\partial U_{20}}{\partial q^{(1)}}\frac{\partial q^{(1)}}{\partial x_\kappa} + \frac{\partial U_{20}}{\partial q^{(2)}}\frac{\partial q^{(2)}}{\partial x_\kappa},\\
&\frac{\partial U_{22}}{\partial x_\kappa} = \frac{\partial U_{22}}{\partial h^{(1)}}\frac{\partial h^{(1)}}{\partial x_\kappa} + \frac{\partial U_{22}}{\partial h^{(2)}}\frac{\partial h^{(2)}}{\partial x_\kappa} + \frac{\partial U_{22}}{\partial q^{(1)}}\frac{\partial q^{(1)}}{\partial x_\kappa} + \frac{\partial U_{22}}{\partial q^{(2)}}\frac{\partial q^{(2)}}{\partial x_\kappa}.
\end{aligned}
$$

5.2 Diffusion in regime of regular waves

Variables ξ and τ

Let's consider the diffusion in regime of regular waves. First, we use the variables (4.1)

$$\tau = \alpha_\kappa t_\kappa, \quad \xi = \alpha_\kappa x_\kappa, \quad \alpha_\kappa = \frac{2\pi}{L_\kappa},$$

and also introduce the velocity

$$V_\kappa = \frac{v_\kappa}{\alpha_\kappa}.$$

If $L_{\xi,l} \equiv \alpha_\kappa L_{\kappa,l}$ and $L_{\xi,r} \equiv \alpha_\kappa L_{\kappa,r}$, then the problem is rewritten as follows:

$$\begin{aligned}
&\frac{\partial C_v}{\partial \tau} + u\frac{\partial C_v}{\partial \xi} + V_\kappa \frac{\partial C_v}{\partial y} = \frac{\varphi D_0^{(j)}}{5\delta\alpha_\kappa \mathrm{Sc}}\frac{\partial^2 C_v}{\partial y^2},\\
&y = 0: \quad \frac{\partial C_v}{\partial y} = 0,\\
&y = h^{(1)}(\xi,\tau): \quad [C_v]_1^2 = 0, \quad [q_{v,n}]_1^2 = 0,\\
&y = h^{(2)}(\xi,\tau): \quad C_v = C_{v,s},\\
&\xi = L_{\xi,l}: \quad C_v = C_{v,l}(y,\tau),
\end{aligned}$$

where

$$q_{v,n} = -D_0^{(j)}\frac{\partial C_v}{\partial y}.$$

Integral mass fluxes through the interface and the surface are written as

$$\begin{aligned}
Q_{v,n}^{(1)} &= -\frac{D_0^{(1)}}{\alpha_\kappa \kappa}\int\limits_{L_{\xi,l}}^{L_{\xi,r}} \left.\frac{\partial C_v}{\partial y}\right|_{y=h^{(1)}-0} d\xi,\\
Q_{v,n}^{(2)} &= -\frac{D_0^{(2)}}{\alpha_\kappa \kappa}\int\limits_{L_{\xi,l}}^{L_{\xi,r}} \left.\frac{\partial C_v}{\partial y}\right|_{y=h^{(2)}-0} d\xi.
\end{aligned}$$

Formulas for the average concentrations in the first and second layers are not changed.

The diffusion equation is solved in the case of the velocity profiles for the longitudinal components $u^{(1)}$ and $u^{(2)}$ from (2.14) and the cross-section velocities

$$\begin{aligned}
V_\kappa^{(1)} &= -\frac{\partial U_{11}}{\partial \xi}\frac{y^2}{2} - \frac{\partial U_{12}}{\partial \xi}\frac{y^3}{3},\\
V_\kappa^{(2)} &= -\frac{\partial U_{11}}{\partial \xi}\frac{\left(h^{(1)}\right)^2}{2} - \frac{\partial U_{12}}{\partial \xi}\frac{\left(h^{(1)}\right)^3}{3}\\
&\quad -\frac{\partial U_{20}}{\partial \xi}\left(y - h^{(1)}\right) + \left(U_{22}\frac{\partial h^{(2)}}{\partial \xi} + h^{(2)}\frac{\partial U_{22}}{\partial \xi}\right)\left(y^2 - \left(h^{(1)}\right)^2\right) - \frac{\partial U_{22}}{\partial \xi}\frac{y^3 - \left(h^{(1)}\right)^3}{3},
\end{aligned}$$

where the coefficients U_{11}, U_{12}, U_{20} and U_{22} depend on $h^{(1)}(\xi,\tau)$, $h^{(2)}(\xi,\tau)$, $q^{(1)}(\xi,\tau)$ and $q^{(2)}(\xi,\tau)$ and their derivatives are calculated as follows, see (2.14),

$$
\begin{aligned}
&w = 4\rho_0\nu_0 h^{(1)}(h^{(2)}-h^{(1)}) + 3(h^{(1)})^2,\\
&U_{12} = \frac{3}{w}\left(\frac{3q^{(2)}}{h^{(2)}-h^{(1)}} - \frac{3q^{(1)}}{h^{(2)}-h^{(1)}} - 2\frac{\rho_0\nu_0(h^{(2)}-h^{(1)})+3h^{(1)}}{(h^{(1)})^2}q^{(1)}\right),\\
&U_{11} = \frac{2q^{(1)}}{(h^{(1)})^2} - \frac{2h^{(1)}}{3}U_{12},\\
&U_{20} = \frac{q^{(2)}-q^{(1)}}{h^{(2)}-h^{(1)}} + \frac{\rho_0\nu_0 U_{11} + 2\rho_0\nu_0 U_{12}h^{(1)}}{6\left(h^{(2)}-h^{(1)}\right)}\left(-2(h^{(2)})^2 - 2h^{(2)}h^{(1)} + (h^{(1)})^2\right),\\
&U_{22} = -\frac{\rho_0\nu_0 U_{11} + 2\rho_0\nu_0 U_{12}h^{(1)}}{2(h^{(2)}-h^{(1)})},\\
&\frac{\partial U_{11}}{\partial\xi} = \frac{\partial U_{11}}{\partial h^{(1)}}\frac{\partial h^{(1)}}{\partial\xi} + \frac{\partial U_{11}}{\partial h^{(2)}}\frac{\partial h^{(2)}}{\partial\xi} + \frac{\partial U_{11}}{\partial q^{(1)}}\frac{\partial q^{(1)}}{\partial\xi} + \frac{\partial U_{11}}{\partial q^{(2)}}\frac{\partial q^{(2)}}{\partial\xi},\\
&\frac{\partial U_{12}}{\partial\xi} = \frac{\partial U_{12}}{\partial h^{(1)}}\frac{\partial h^{(1)}}{\partial\xi} + \frac{\partial U_{12}}{\partial h^{(2)}}\frac{\partial h^{(2)}}{\partial\xi} + \frac{\partial U_{12}}{\partial q^{(1)}}\frac{\partial q^{(1)}}{\partial\xi} + \frac{\partial U_{12}}{\partial q^{(2)}}\frac{\partial q^{(2)}}{\partial\xi},\\
&\frac{\partial U_{20}}{\partial\xi} = \frac{\partial U_{20}}{\partial h^{(1)}}\frac{\partial h^{(1)}}{\partial\xi} + \frac{\partial U_{20}}{\partial h^{(2)}}\frac{\partial h^{(2)}}{\partial\xi} + \frac{\partial U_{20}}{\partial q^{(1)}}\frac{\partial q^{(1)}}{\partial\xi} + \frac{\partial U_{20}}{\partial q^{(2)}}\frac{\partial q^{(2)}}{\partial\xi},\\
&\frac{\partial U_{22}}{\partial\xi} = \frac{\partial U_{22}}{\partial h^{(1)}}\frac{\partial h^{(1)}}{\partial\xi} + \frac{\partial U_{22}}{\partial h^{(2)}}\frac{\partial h^{(2)}}{\partial\xi} + \frac{\partial U_{22}}{\partial q^{(1)}}\frac{\partial q^{(1)}}{\partial\xi} + \frac{\partial U_{22}}{\partial q^{(2)}}\frac{\partial q^{(2)}}{\partial\xi}.
\end{aligned}
$$

Variable ζ

Then, we introduce the normalised coordinate

$$\zeta = \frac{y}{h^{(2)}(\xi,\tau)},$$

and replace the derivatives in accordance to the following formulas:

$$
\begin{aligned}
&\frac{\partial}{\partial\tau} = \frac{\partial}{\partial\tau} - \frac{\zeta}{h^{(2)}}\frac{\partial h^{(2)}}{\partial\tau}\frac{\partial}{\partial\zeta},\\
&\frac{\partial}{\partial\xi} = \frac{\partial}{\partial\xi} - \frac{\zeta}{h^{(2)}}\frac{\partial h^{(2)}}{\partial\xi}\frac{\partial}{\partial\zeta},\\
&\frac{\partial}{\partial y} = \frac{1}{h^{(2)}}\frac{\partial}{\partial\zeta}.
\end{aligned}
$$

If $h(\xi,\tau) \equiv \dfrac{h^{(1)}}{h^{(2)}}$, then the problem is rewritten as

$$\frac{\partial C_v}{\partial \tau} + u\frac{\partial C_v}{\partial \xi} + \frac{1}{h^{(2)}}\left[V_\kappa - \zeta\left(\frac{\partial h^{(2)}}{\partial \tau} + u\frac{\partial h^{(2)}}{\partial \xi}\right)\right]\frac{\partial C_v}{\partial \zeta} = \frac{\varphi D_0^{(j)}}{5\delta\alpha_\kappa \mathrm{Sc}\left(h^{(2)}\right)^2}\frac{\partial^2 C_v}{\partial \zeta^2},$$

$$\zeta = 0: \quad \frac{\partial C_v}{\partial \zeta} = 0,$$

$$\zeta = h: \quad [C_v]_1^2 = 0, \quad [q_{v,n}]_1^2 = 0,$$

$$\zeta = 1: \quad C_v = C_{v,s},$$

$$\xi = L_{\xi,l}: \quad C_v = C_{v,l}(\zeta,\tau),$$

where

$$q_{v,n} = -\frac{D_0^{(j)}}{h^{(2)}}\frac{\partial C_v}{\partial \zeta}.$$

The integral mass fluxes through the interface and the surface are rewritten as

$$Q_{v,n}^{(1)} = -\frac{D_0^{(1)}}{\alpha_\kappa \kappa}\int\limits_{L_{\xi,l}}^{L_{\xi,r}} \frac{1}{h^{(2)}}\left.\frac{\partial C_v}{\partial \zeta}\right|_{\zeta=h-0} d\xi,$$

$$Q_{v,n}^{(2)} = -\frac{D_0^{(2)}}{\alpha_\kappa \kappa}\int\limits_{L_{\xi,l}}^{L_{\xi,r}} \frac{1}{h^{(2)}}\left.\frac{\partial C_v}{\partial \zeta}\right|_{\zeta=1-0} d\xi,$$

and the average concentrations in the first and second layers are

$$C_{v,av}^{(1)} = \frac{1}{h}\int\limits_0^h C_v d\zeta,$$

$$C_{v,av}^{(2)} = \frac{1}{1-h}\int\limits_h^1 C_v d\zeta.$$

The diffusion equation is solved in the case of the velocity profile:

$$
\begin{aligned}
&u^{(1)} = U_{11}h^{(2)}\zeta + U_{12}\left(h^{(2)}\right)^2\zeta^2,\\
&u^{(2)} = U_{20} + U_{22}\left(h^{(2)}\right)^2\left(\zeta^2 - 2\zeta\right),\\
&V_\kappa^{(1)} = -\frac{\partial U_{11}}{\partial \xi}\left(h^{(2)}\right)^2\frac{\zeta^2}{2} - \frac{\partial U_{12}}{\partial \xi}\left(h^{(2)}\right)^3\frac{\zeta^3}{3},\\
&V_\kappa^{(2)} = -\frac{\partial U_{11}}{\partial \xi}\frac{\left(h^{(1)}\right)^2}{2} - \frac{\partial U_{12}}{\partial \xi}\frac{\left(h^{(1)}\right)^3}{3}\\
&\quad -\frac{\partial U_{20}}{\partial \xi}h^{(2)}\left(\zeta - h\right) + \left(U_{22}\frac{\partial h^{(2)}}{\partial \xi} + h^{(2)}\frac{\partial U_{22}}{\partial \xi}\right)\left(h^{(2)}\right)^2\left(\zeta^2 - h^2\right)\\
&\quad -\frac{\partial U_{22}}{\partial \xi}\left(h^{(2)}\right)^3\frac{\zeta^3 - h^3}{3},
\end{aligned}
$$

where the coefficients U_{11}, U_{12}, U_{20} and U_{22} depend on $h^{(1)}(\xi,\tau)$, $h^{(2)}(\xi,\tau)$, $q^{(1)}(\xi,\tau)$ and $q^{(2)}(\xi,\tau)$ are calculated as follows

$$
\begin{aligned}
&w = 4\rho_0\nu_0 h^{(1)}(h^{(2)} - h^{(1)}) + 3(h^{(1)})^2,\\
&U_{11} = \frac{2q^{(1)}}{(h^{(1)})^2} - \frac{2h^{(1)}}{3}U_{12},\\
&U_{12} = \frac{3}{w}\left(\frac{3q^{(2)}}{h^{(2)} - h^{(1)}} - \frac{3q^{(1)}}{h^{(2)} - h^{(1)}} - 2\frac{\rho_0\nu_0(h^{(2)} - h^{(1)}) + 3h^{(1)}}{(h^{(1)})^2}q^{(1)}\right),\\
&U_{20} = \frac{q^{(2)} - q^{(1)}}{h^{(2)} - h^{(1)}} + \frac{\rho_0\nu_0 U_{11} + 2\rho_0\nu_0 U_{12}h^{(1)}}{6\left(h^{(2)} - h^{(1)}\right)}\left(-2(h^{(2)})^2 - 2h^{(2)}h^{(1)} + (h^{(1)})^2\right),\\
&U_{22} = -\frac{\rho_0\nu_0 U_{11} + 2\rho_0\nu_0 U_{12}h^{(1)}}{2(h^{(2)} - h^{(1)})},\\
&\frac{\partial U_{11}}{\partial \xi} = \frac{\partial U_{11}}{\partial h^{(1)}}\frac{\partial h^{(1)}}{\partial \xi} + \frac{\partial U_{11}}{\partial h^{(2)}}\frac{\partial h^{(2)}}{\partial \xi} + \frac{\partial U_{11}}{\partial q^{(1)}}\frac{\partial q^{(1)}}{\partial \xi} + \frac{\partial U_{11}}{\partial q^{(2)}}\frac{\partial q^{(2)}}{\partial \xi},\\
&\frac{\partial U_{12}}{\partial \xi} = \frac{\partial U_{12}}{\partial h^{(1)}}\frac{\partial h^{(1)}}{\partial \xi} + \frac{\partial U_{12}}{\partial h^{(2)}}\frac{\partial h^{(2)}}{\partial \xi} + \frac{\partial U_{12}}{\partial q^{(1)}}\frac{\partial q^{(1)}}{\partial \xi} + \frac{\partial U_{12}}{\partial q^{(2)}}\frac{\partial q^{(2)}}{\partial \xi},\\
&\frac{\partial U_{20}}{\partial \xi} = \frac{\partial U_{20}}{\partial h^{(1)}}\frac{\partial h^{(1)}}{\partial \xi} + \frac{\partial U_{20}}{\partial h^{(2)}}\frac{\partial h^{(2)}}{\partial \xi} + \frac{\partial U_{20}}{\partial q^{(1)}}\frac{\partial q^{(1)}}{\partial \xi} + \frac{\partial U_{20}}{\partial q^{(2)}}\frac{\partial q^{(2)}}{\partial \xi},\\
&\frac{\partial U_{22}}{\partial \xi} = \frac{\partial U_{22}}{\partial h^{(1)}}\frac{\partial h^{(1)}}{\partial \xi} + \frac{\partial U_{22}}{\partial h^{(2)}}\frac{\partial h^{(2)}}{\partial \xi} + \frac{\partial U_{22}}{\partial q^{(1)}}\frac{\partial q^{(1)}}{\partial \xi} + \frac{\partial U_{22}}{\partial q^{(2)}}\frac{\partial q^{(2)}}{\partial \xi}.
\end{aligned}
$$

Variables ξ_v and τ_v

We again replace the variables

$$\tau_v = \frac{\tau}{\mathrm{Sc}}, \quad \xi_v = \frac{\xi}{\mathrm{Sc}}, \quad V_{\kappa,v} = \mathrm{Sc} \cdot V_\kappa,$$

to exclude the Schmidt number from the boundary-value problem for the gas concentration. If $L_{\xi_v,l} \equiv L_{\xi,l}/\mathrm{Sc}$ and $L_{\xi_v,r} \equiv L_{\xi,r}/\mathrm{Sc}$, then the problem is rewritten as follows:

$$\begin{aligned}
&\frac{\partial C_v}{\partial \tau_v} + u\frac{\partial C_v}{\partial \xi_v} + \frac{1}{h^{(2)}}\left[V_{\kappa,v} - \zeta\left(\frac{\partial h^{(2)}}{\partial \tau_v} + u\frac{\partial h^{(2)}}{\partial \xi_v}\right)\right]\frac{\partial C_v}{\partial \zeta} = \frac{\varphi D_0^{(j)}}{5\delta\alpha_\kappa\left(h^{(2)}\right)^2}\frac{\partial^2 C_v}{\partial \zeta^2},\\
&\zeta = 0: \quad \frac{\partial C_v}{\partial \zeta} = 0,\\
&\zeta = h: \quad [C_v]_1^2 = 0, \quad [q_{v,n}]_1^2 = 0,\\
&\zeta = 1: \quad C_v = C_{v,s},\\
&\xi_v = L_{\xi_v,l}: \quad C_v = C_{v,l}\left(\zeta, \tau_v\right),
\end{aligned}$$

where

$$q_{v,n} = -\frac{D_0^{(j)}}{h^{(2)}}\frac{\partial C_v}{\partial \zeta}.$$

The Schmidt number becomes a part of the expressions for the integral mass fluxes through the interface and the surface:

$$\begin{aligned}
Q_{v,n}^{(1)} &= -\frac{D_0^{(1)}\mathrm{Sc}}{\alpha_\kappa\kappa}\int\limits_{L_{\xi_v,l}}^{L_{\xi_v,r}}\frac{1}{h^{(2)}}\left.\frac{\partial C_v}{\partial \zeta}\right|_{\zeta=h-0} d\xi_v,\\
Q_{v,n}^{(2)} &= -\frac{D_0^{(2)}\mathrm{Sc}}{\alpha_\kappa\kappa}\int\limits_{L_{\xi_v,l}}^{L_{\xi_v,r}}\frac{1}{h^{(2)}}\left.\frac{\partial C_v}{\partial \zeta}\right|_{\zeta=1-0} d\xi_v.
\end{aligned}$$

Again, the formulas for the average concentrations in the first and second layers have

not been changed

$$C_{v,av}^{(1)} = \frac{1}{h}\int_0^h C_v d\zeta, \quad C_{v,av}^{(2)} = \frac{1}{1-h}\int_h^1 C_v d\zeta.$$

The diffusion equation is solved in the case of the velocity profile:

$$\begin{aligned}
u^{(1)} &= U_{11}h^{(2)}\zeta + U_{12}\left(h^{(2)}\right)^2\zeta^2,\\
u^{(2)} &= U_{20} + U_{22}\left(h^{(2)}\right)^2\left(\zeta^2 - 2\zeta\right),\\
V_{\kappa,v}^{(1)} &= \frac{1}{\mathrm{Sc}}\left(-\frac{\partial U_{11}}{\partial\xi}\left(h^{(2)}\right)^2\frac{\zeta^2}{2} - \frac{\partial U_{12}}{\partial\xi}\left(h^{(2)}\right)^3\frac{\zeta^3}{3}\right),\\
V_{\kappa,v}^{(2)} &= \frac{1}{\mathrm{Sc}}\Bigg[-\frac{\partial U_{11}}{\partial\xi}\frac{\left(h^{(1)}\right)^2}{2} - \frac{\partial U_{12}}{\partial\xi}\frac{\left(h^{(1)}\right)^3}{3}\\
&\quad -\frac{\partial U_{20}}{\partial\xi}h^{(2)}\left(\zeta - h\right) + \left(U_{22}\frac{\partial h^{(2)}}{\partial\xi} + h^{(2)}\frac{\partial U_{22}}{\partial\xi}\right)\left(h^{(2)}\right)^2\left(\zeta^2 - h^2\right)\\
&\quad -\frac{\partial U_{22}}{\partial\xi}\left(h^{(2)}\right)^3\frac{\zeta^3 - h^3}{3}\Bigg],
\end{aligned}$$

where the coefficients U_{11}, U_{12}, U_{20} and U_{22} depending on $h^{(1)}\left(\xi_v,\tau_v\right)$, $h^{(2)}\left(\xi_v,\tau_v\right)$, $q^{(1)}\left(\xi_v,\tau_v\right)$ and $q^{(2)}\left(\xi_v,\tau_v\right)$ are calculated as follows

$$\begin{aligned}
w &= 4\rho_0\nu_0 h^{(1)}(h^{(2)} - h^{(1)}) + 3(h^{(1)})^2,\\
U_{11} &= \frac{2q^{(1)}}{(h^{(1)})^2} - \frac{2h^{(1)}}{3}U_{12},\\
U_{12} &= \frac{3}{w}\left(\frac{3q^{(2)}}{h^{(2)} - h^{(1)}} - \frac{3q^{(1)}}{h^{(2)} - h^{(1)}} - 2\frac{\rho_0\nu_0(h^{(2)} - h^{(1)}) + 3h^{(1)}}{(h^{(1)})^2}q^{(1)}\right),\\
U_{20} &= \frac{q^{(2)} - q^{(1)}}{h^{(2)} - h^{(1)}} + \frac{\rho_0\nu_0 U_{11} + 2\rho_0\nu_0 U_{12}h^{(1)}}{6\left(h^{(2)} - h^{(1)}\right)}\left(-2(h^{(2)})^2 - 2h^{(2)}h^{(1)} + (h^{(1)})^2\right),\\
U_{22} &= -\frac{\rho_0\nu_0 U_{11} + 2\rho_0\nu_0 U_{12}h^{(1)}}{2(h^{(2)} - h^{(1)})},
\end{aligned}$$

$$\frac{\partial U_{11}}{\partial \xi_v} = \frac{\partial U_{11}}{\partial h^{(1)}}\frac{\partial h^{(1)}}{\partial \xi_v} + \frac{\partial U_{11}}{\partial h^{(2)}}\frac{\partial h^{(2)}}{\partial \xi_v} + \frac{\partial U_{11}}{\partial q^{(1)}}\frac{\partial q^{(1)}}{\partial \xi_v} + \frac{\partial U_{11}}{\partial q^{(2)}}\frac{\partial q^{(2)}}{\partial \xi_v},$$
$$\frac{\partial U_{12}}{\partial \xi_v} = \frac{\partial U_{12}}{\partial h^{(1)}}\frac{\partial h^{(1)}}{\partial \xi_v} + \frac{\partial U_{12}}{\partial h^{(2)}}\frac{\partial h^{(2)}}{\partial \xi_v} + \frac{\partial U_{12}}{\partial q^{(1)}}\frac{\partial q^{(1)}}{\partial \xi_v} + \frac{\partial U_{12}}{\partial q^{(2)}}\frac{\partial q^{(2)}}{\partial \xi_v},$$
$$\frac{\partial U_{20}}{\partial \xi_v} = \frac{\partial U_{20}}{\partial h^{(1)}}\frac{\partial h^{(1)}}{\partial \xi_v} + \frac{\partial U_{20}}{\partial h^{(2)}}\frac{\partial h^{(2)}}{\partial \xi_v} + \frac{\partial U_{20}}{\partial q^{(1)}}\frac{\partial q^{(1)}}{\partial \xi_v} + \frac{\partial U_{20}}{\partial q^{(2)}}\frac{\partial q^{(2)}}{\partial \xi_v},$$
$$\frac{\partial U_{22}}{\partial \xi_v} = \frac{\partial U_{22}}{\partial h^{(1)}}\frac{\partial h^{(1)}}{\partial \xi_v} + \frac{\partial U_{22}}{\partial h^{(2)}}\frac{\partial h^{(2)}}{\partial \xi_v} + \frac{\partial U_{22}}{\partial q^{(1)}}\frac{\partial q^{(1)}}{\partial \xi_v} + \frac{\partial U_{22}}{\partial q^{(2)}}\frac{\partial q^{(2)}}{\partial \xi_v}.$$

Regular wave

We consider the diffusion in the case of film flow with regular waves. A regular wave is characterized by its velocity c and the functions

$$h^{(1)}(\eta), \quad h^{(2)}(\eta), \quad q^{(1)}(\eta), \quad q^{(2)}(\eta), \quad \eta = \xi - c\tau = \mathrm{Sc}\,(\xi_v - c\tau_v),$$

introduced and discussed in Chapter 3. We substitute the solution in the problem statement

$$\frac{\partial C_v}{\partial \tau_v} + u\frac{\partial C_v}{\partial \xi_v} + \frac{1}{h^{(2)}}\left[V_{\kappa,v} - \zeta \mathrm{Sc}\,(u-c)\frac{dh^{(2)}}{d\eta}\right]\frac{\partial C_v}{\partial \zeta} = \frac{\varphi D_0^{(j)}}{5\delta\alpha_\kappa\left(h^{(2)}\right)^2}\frac{\partial^2 C_v}{\partial \zeta^2}, \quad (5.5)$$
$$\zeta = 0: \quad \frac{\partial C_v}{\partial \zeta} = 0,$$
$$\zeta = h: \quad [C_v]_1^2 = 0, \quad [q_{v,n}]_1^2 = 0,$$
$$\zeta = 1: \quad C_v = C_{v,s},$$
$$\xi_v = L_{\xi_v,l}: \quad C_v = C_{v,l}(\zeta, \tau_v),$$

where

$$q_{v,n} = -\frac{D_0^{(j)}}{h^{(2)}}\frac{\partial C_v}{\partial \zeta}.$$

Integral mass fluxes through the interface and the surface

$$Q_{v,n}^{(1)} = -\frac{D_0^{(1)}\mathrm{Sc}}{\alpha_\kappa \kappa} \int\limits_{L_{\xi_v,l}}^{L_{\xi_v,r}} \frac{1}{h^{(2)}} \left.\frac{\partial C_v}{\partial \zeta}\right|_{\zeta=h-0} d\xi_v,$$

$$Q_{v,n}^{(2)} = -\frac{D_0^{(2)}\mathrm{Sc}}{\alpha_\kappa \kappa} \int\limits_{L_{\xi_v,l}}^{L_{\xi_v,r}} \frac{1}{h^{(2)}} \left.\frac{\partial C_v}{\partial \zeta}\right|_{\zeta=1-0} d\xi_v,$$

and the average concentrations in the first and second layers are not changed:

$$C_{v,av}^{(1)} = \frac{1}{h}\int\limits_0^h C_v d\zeta, \quad C_{v,av}^{(2)} = \frac{1}{1-h}\int\limits_h^1 C_v d\zeta.$$

The diffusion equation is solved in the case of the velocity profile:

$$\begin{aligned}
u^{(1)} &= U_{11} h^{(2)} \zeta + U_{12} \left(h^{(2)}\right)^2 \zeta^2, \\
u^{(2)} &= U_{20} + U_{22} \left(h^{(2)}\right)^2 \left(\zeta^2 - 2\zeta\right), \\
V_{\kappa,v}^{(1)} &= -\frac{dU_{11}}{d\eta} \left(h^{(2)}\right)^2 \frac{\zeta^2}{2} - \frac{dU_{12}}{d\eta} \left(h^{(2)}\right)^3 \frac{\zeta^3}{3}, \\
V_{\kappa,v}^{(2)} &= -\frac{dU_{11}}{d\eta} \frac{\left(h^{(1)}\right)^2}{2} - \frac{dU_{12}}{d\eta} \frac{\left(h^{(1)}\right)^3}{3} \\
&\quad -\frac{dU_{20}}{d\eta} h^{(2)} \left(\zeta - h\right) + \left(U_{22}\frac{dh^{(2)}}{d\eta} + h^{(2)}\frac{dU_{22}}{d\eta}\right) \left(h^{(2)}\right)^2 \left(\zeta^2 - h^2\right) \\
&\quad -\frac{dU_{22}}{d\eta} \left(h^{(2)}\right)^3 \frac{\zeta^3 - h^3}{3},
\end{aligned}$$

where the coefficients U_{11}, U_{12}, U_{20} and U_{22} and their derivatives depend on $h^{(1)}(\eta)$, $h^{(2)}(\eta)$, $q^{(1)}(\eta)$ and $q^{(2)}(\eta)$ as follows

$$w = 4\rho_0\nu_0 h^{(1)}(h^{(2)} - h^{(1)}) + 3(h^{(1)})^2,$$

$$
\begin{aligned}
U_{11} &= \frac{2q^{(1)}}{(h^{(1)})^2} - \frac{2h^{(1)}}{3}U_{12},\\
U_{12} &= \frac{3}{w}\left(\frac{3q^{(2)}}{h^{(2)}-h^{(1)}} - \frac{3q^{(1)}}{h^{(2)}-h^{(1)}} - 2\frac{\rho_0\nu_0(h^{(2)}-h^{(1)})+3h^{(1)}}{(h^{(1)})^2}q^{(1)}\right),\\
U_{20} &= \frac{q^{(2)}-q^{(1)}}{h^{(2)}-h^{(1)}} + \frac{\rho_0\nu_0U_{11}+2\rho_0\nu_0U_{12}h^{(1)}}{6\left(h^{(2)}-h^{(1)}\right)}\left(-2(h^{(2)})^2-2h^{(2)}h^{(1)}+(h^{(1)})^2\right),\\
U_{22} &= -\frac{\rho_0\nu_0U_{11}+2\rho_0\nu_0U_{12}h^{(1)}}{2(h^{(2)}-h^{(1)})},\\
\frac{dU_{11}}{d\eta} &= \frac{\partial U_{11}}{\partial h^{(1)}}\frac{dh^{(1)}}{d\eta} + \frac{\partial U_{11}}{\partial h^{(2)}}\frac{dh^{(2)}}{d\eta} + \frac{\partial U_{11}}{\partial q^{(1)}}\frac{dq^{(1)}}{d\eta} + \frac{\partial U_{11}}{\partial q^{(2)}}\frac{dq^{(2)}}{d\eta},\\
\frac{dU_{12}}{d\eta} &= \frac{\partial U_{12}}{\partial h^{(1)}}\frac{dh^{(1)}}{d\eta} + \frac{\partial U_{12}}{\partial h^{(2)}}\frac{dh^{(2)}}{d\eta} + \frac{\partial U_{12}}{\partial q^{(1)}}\frac{dq^{(1)}}{d\eta} + \frac{\partial U_{12}}{\partial q^{(2)}}\frac{dq^{(2)}}{d\eta},\\
\frac{dU_{20}}{d\eta} &= \frac{\partial U_{20}}{\partial h^{(1)}}\frac{dh^{(1)}}{d\eta} + \frac{\partial U_{20}}{\partial h^{(2)}}\frac{dh^{(2)}}{d\eta} + \frac{\partial U_{20}}{\partial q^{(1)}}\frac{dq^{(1)}}{d\eta} + \frac{\partial U_{20}}{\partial q^{(2)}}\frac{dq^{(2)}}{d\eta},\\
\frac{dU_{22}}{d\eta} &= \frac{\partial U_{22}}{\partial h^{(1)}}\frac{dh^{(1)}}{d\eta} + \frac{\partial U_{22}}{\partial h^{(2)}}\frac{dh^{(2)}}{d\eta} + \frac{\partial U_{22}}{\partial q^{(1)}}\frac{dq^{(1)}}{d\eta} + \frac{\partial U_{22}}{\partial q^{(2)}}\frac{dq^{(2)}}{d\eta}.
\end{aligned}
$$

5.3 Numerical method

The finite-difference method is used to solve the diffusion equation numerically.

Grid and grid function To solve the problem (5.5), we choose the following grid and the grid function:

$$
\begin{aligned}
&\xi_{v,n} = L_{\xi_v,l} + \triangle\xi_v\cdot(n-1), \quad n=1,\dots,N, \qquad \triangle\xi_v = \frac{L_{\xi_v,r}-L_{\xi_v,l}}{N-1},\\
&\zeta_m = \triangle\zeta^{(1)}\cdot(m-1), \quad m=1,\dots,M^{(1)}, \qquad \triangle\zeta^{(1)} = \frac{h}{M^{(1)}-1},\\
&\zeta_m = h + \triangle\zeta^{(2)}\cdot\left(m-M^{(1)}\right), \quad m=M^{(1)}+1,\dots,M^{(2)}, \qquad \triangle\zeta^{(2)} = \frac{1-h}{M^{(2)}-M^{(1)}},\\
&C_{v,n,m} = C_v\left(\xi_{v,n},\zeta_m,\tau_v\right), \quad \check{C}_{v,n,m} = C_v\left(\xi_{v,n},\zeta_m,\tau_v+\frac{\triangle\tau_v}{2}\right),\\
&\qquad \hat{C}_{v,n,m} = C_v\left(\xi_{v,n},\zeta_m,\tau_v+\triangle\tau_v\right), \quad n=1,\dots,N, \quad m=1,\dots,M^{(2)}.
\end{aligned}
$$

To solve the diffusion equation, we use the following two-step scheme consisting of two half-steps for the convective and diffusion terms.

Convective term In this case, we use the explicit scheme including first order forward-time derivative and second order centred-space finite differences for the convective terms in each layer:

$$\frac{\check{C}_{v,n,m}-C_{v,n,m}}{\frac{\triangle\tau_v}{2}}+u^{(1)}\Big|_{\xi_{v,n},\zeta_m,\tau_v}\frac{\check{C}_{v,n,m}-\check{C}_{v,n-1,m}}{\triangle\xi_v}+V^{(1)}\Big|_{\xi_{v,n},\zeta_m,\tau_v}\frac{\check{C}_{v,n,m+1}-\check{C}_{v,n,m}}{\triangle\zeta^{(1)}}=$$
$$\left(\chi^{(1)}\frac{\partial^2 C_v}{\partial\zeta^2}\right)\Big|_{\xi_{v,n},\zeta_m,\tau_v},\quad n=2,\ldots,N,\quad m=1,\ldots,M^{(1)}-1, \tag{5.6}$$
$$\frac{\check{C}_{v,n,m}-C_{v,nm}}{\frac{\triangle\tau_v}{2}}+u^{(2)}\Big|_{\xi_{v,n},\zeta_m,\tau_v}\frac{\check{C}_{v,n,m}-\check{C}_{v,n-1,m}}{\triangle\xi_v}+V^{(2)}\Big|_{\xi_{v,n},\zeta_m,\tau_v}\frac{\check{C}_{v,n,m+1}-\check{C}_{v,n,m}}{\triangle\zeta^{(2)}}=$$
$$\left(\chi^{(2)}\frac{\partial^2 C_v}{\partial\zeta^2}\right)\Big|_{\xi_{v,n},\zeta_m,\tau_v},\quad n=2,\ldots,N,\quad m=M^{(1)}+1,\ldots,M^{(2)}-1.$$

Diffusion term In the half-step responsible for the diffusion term, we use the implicit scheme with first order forward-time derivative and the weighted approximation of the diffusion term with using centred-space finite differences at two moments of time $\tau_v+\frac{\triangle\tau_v}{2}$ and $\tau_v+\triangle\tau_v$.

$$\frac{\hat{C}_{v,n,m}-\check{C}_{v,n,m}}{\frac{\triangle\tau_v}{2}}+\left(u^{(1)}\frac{\partial C_v}{\partial\xi_v}+V^{(1)}\frac{\partial C_v}{\partial\zeta}\right)\Big|_{\xi_{v,n},\zeta_m,\tau_v+\frac{\triangle\tau_v}{2}}= \tag{5.7}$$
$$\lambda\chi^{(1)}\Big|_{\xi_{v,n},\tau_v+\triangle\tau_v}\frac{\hat{C}_{v,n,m+1}-2\hat{C}_{v,n,m}+\hat{C}_{v,n,m-1}}{\left(\triangle\zeta^{(1)}\right)^2}+$$
$$(1-\lambda)\,\chi^{(1)}\Big|_{\xi_{v,n},\tau_v+\frac{\triangle\tau_v}{2}}\frac{\check{C}_{v,n,m+1}-2\check{C}_{v,n,m}+\check{C}_{v,n,m-1}}{\left(\triangle\zeta^{(1)}\right)^2},$$
$$n=2,\ldots,N,\quad m=2,\ldots,M^{(1)}-1,$$

$$\frac{\hat{C}_{v,n,m}-\check{C}_{v,n,m}}{\frac{\triangle\tau_v}{2}}+\left(u^{(2)}\frac{\partial C_v}{\partial\xi_v}+V^{(2)}\frac{\partial C_v}{\partial\zeta}\right)\Big|_{\xi_{v,n},\zeta_m,\tau_v+\frac{\triangle\tau_v}{2}}=$$

$$\lambda\chi^{(2)}\Big|_{\xi_{v,n},\tau_v+\triangle\tau_v}\frac{\hat{C}_{v,n,m+1}-2\hat{C}_{v,n,m}+\hat{C}_{v,n,m-1}}{\left(\triangle\zeta^{(2)}\right)^2}+,$$

$$(1-\lambda)\,\chi^{(2)}\Big|_{\xi_{v,n},\tau_v+\frac{\triangle\tau_v}{2}}\frac{\check{C}_{v,n,m+1}-2\check{C}_{v,n,m}+\check{C}_{v,n,m-1}}{\left(\triangle\zeta^{(2)}\right)^2},$$

$$n=2,\ldots,N,\quad m=M^{(1)}+1,\ldots,M^{(2)}-1$$

where we take $\lambda=0.5$.

The schemes (5.6) and (5.7) are solved by standard methods, see Appendix D.

All results described in this section have been computed for water-benzene system at $\delta=0.1$, $D_0=0.553$ and $Sc=231.2$.

To analyse the results, the following characteristics are used:

$$q^{(1)}_{v,n}=-\frac{D_0}{h^{(2)}}\,\frac{\partial C_v}{\partial\zeta}\Big|_{\zeta=h-0},$$

$$Q^{(1)}_{v,n}=-\frac{D_0\mathrm{Sc}}{\alpha_\kappa\kappa}\int\limits_{L_{\xi_v,l}}^{L_{\xi_v,r}}\frac{1}{h^{(2)}}\,\frac{\partial C_v}{\partial\zeta}\Big|_{\zeta=h-0}d\xi_v,$$

$$C^{(1)}_{v,av}=\frac{1}{h}\int\limits_0^h C_v d\zeta,$$

$$q^{(2)}_{v,n}=-\frac{1}{h^{(2)}}\,\frac{\partial C_v}{\partial\zeta}\Big|_{\zeta=1-0},$$

$$Q^{(2)}_{v,n}=-\frac{\mathrm{Sc}}{\alpha_\kappa\kappa}\int\limits_{L_{\xi_v,l}}^{L_{\xi_v,r}}\frac{1}{h^{(2)}}\,\frac{\partial C_v}{\partial\zeta}\Big|_{\zeta=1-0}d\xi_v,$$

$$C^{(2)}_{v,av}=\frac{1}{1-h}\int\limits_h^1 C_v d\zeta.$$

5.4 Results

We start from discussing result of absorption of the boundary conditions $C_v^{(1)}\Big|_{x_\kappa=0} = C_v^{(2)}\Big|_{x_\kappa=0} = 0$. It is worthy to note that the soluble gas concentration is small and does not effect inertial properties of two phase flow. Fig. 5.1 is plotted for showing the functions characterised the absorption in the waveless flow $h^{(1)} = H$, $h^{(2)} = 1$, $q^{(2)} = 1$ and

$$q^{(1)} = \int_0^H U^{(1)} dy = \frac{H^2}{2\varphi\nu_0}\left[\frac{1}{\rho_0} + \left(\frac{2}{3} - \frac{1}{\rho_0}\right) H\right].$$

at $H = 0.3$.

The interface and wall concentrations, and the average concentrations in the layers are showed in panels (a) and (b), respectively. While the local flux at the surface is demonstrated in panel (c), the local flux at the interface is presented in panel (d). Fig. 5.2 shows the gas concentration in a few cross-sections globally and locally. It is seen as the diffusion boundary layer at the free surface is developed. In Fig. 5.2b, the profiles look smooth at the interface since the derivatives are relatively small.

Fig. 5.3 shows instant dependencies the film and concentration parameters on longitudinal coordinate x_κ at regime of the dominating wave of the first family $\gamma^1_{-1,1}$ at $H = 0.3$ and $s = 0.6$. It is worthy to note that the instant profiles were calculated till we have quasi steady flows when solution becomes periodic in outlet area and the figures shift if the different times are chosen. Particularly, the instant profiles of interface and surface are demonstrated in panel (a). Panel (b) illustrates the gas concentrations on the interface and wall which are increasing downstream. Panel (c) shows the average gas concentrations in both layers. It is seen that the amplitudes of the average concentration in the second layer are greater than in the first layer. The local flux at the surface and interface are given in panels (d) and (e), respectively. Whereas the oscillations of local flux on the

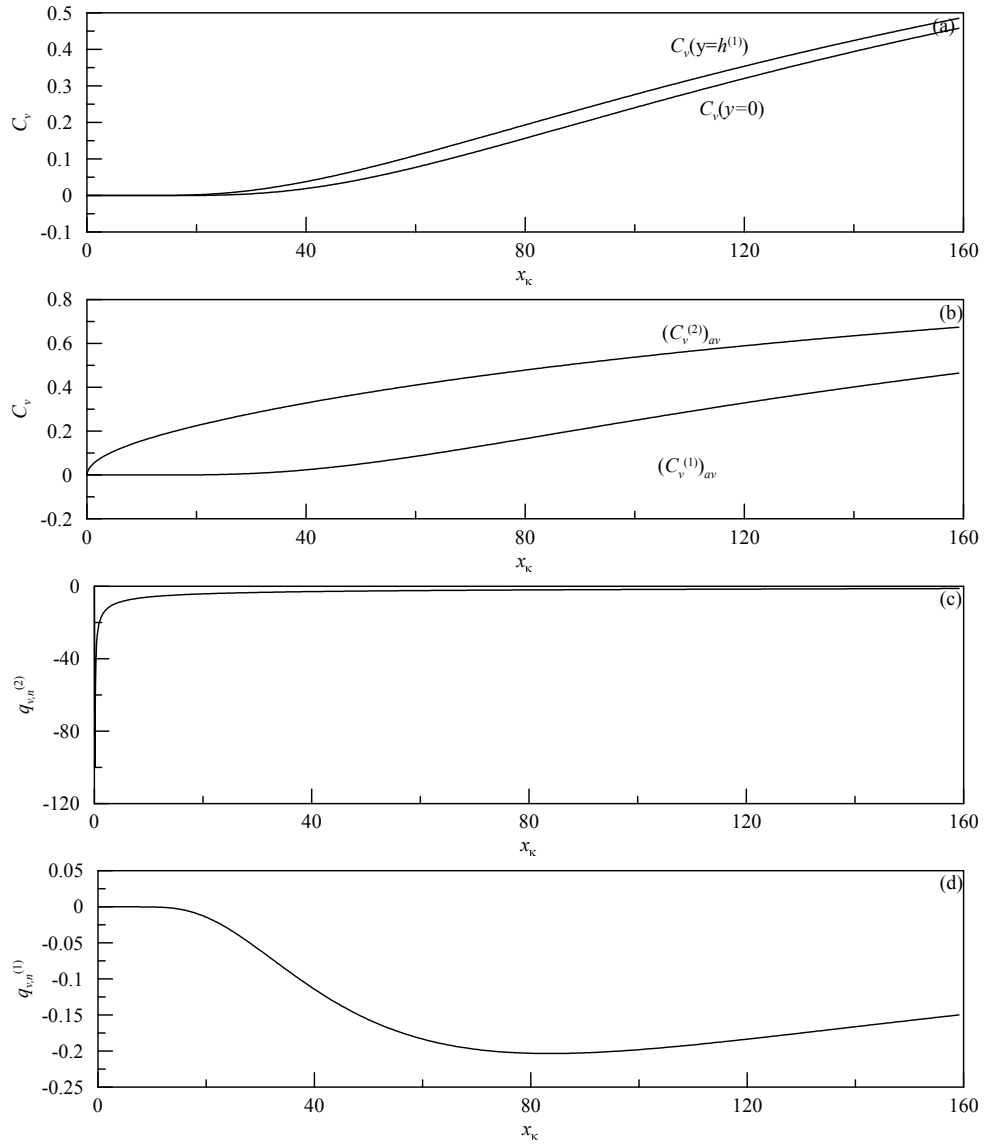

Figure 5.1: The interface and wall concentrations (a), the average concentrations in the layers (b), the local fluxes at the surface (c) and interface (d) for the waveless flow at $\delta = 0.1$ and $H = 0.3$ in water-benzene system.

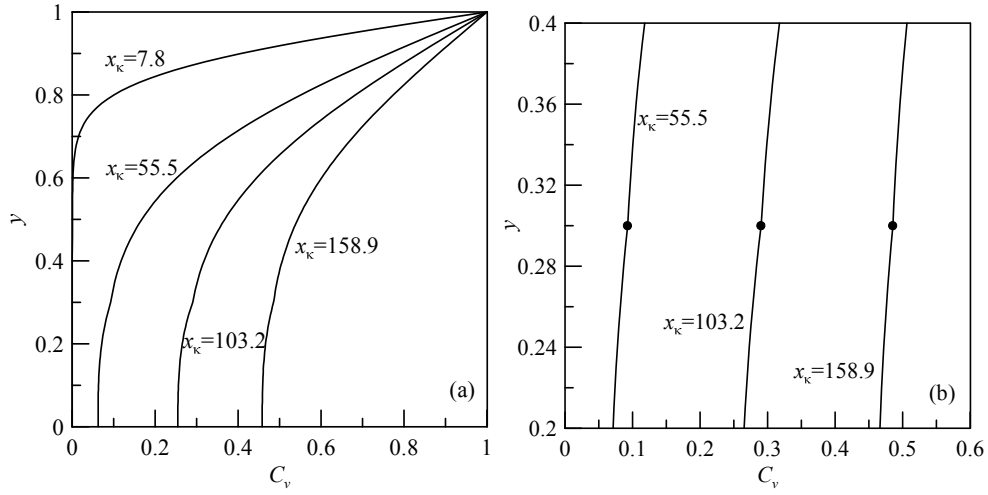

Figure 5.2: Global (a) and local (b) instant profiles of the gas concentration for the waveless flow at $H = 0.3$.

surface are decreasing , that of increases at the first stage and then starts to decrease slowly on interface.

Fig. 5.4a shows the local profiles of the surface and interface at the inlet area in the case shown in Fig. 5.3a. It is seen that the oscillation of the local flux at the interface is smaller than at the surface, see Fig. 5.4b. The gas concentration at the inlet area corresponding to the case in Fig. 5.4a is shown in Fig. 5.5. It can be said that when the layers have almost minimum thicknesses and close each other (at $x_\kappa = 42.6$), the concentration gradient is higher.

Fig. 5.6a shows the local profiles of the surface and interface at the outlet area corresponding to Fig. 5.3a. In the outlet area, the oscillations of the local flux at the interface is smaller than in the inlet area, see Figs. 5.4b and 5.6b.

Fig. 5.7 demonstrates the gas concentration at the outlet area. It is seen that the concentration at the outlet is higher than the inlet area, see Figs. 5.5 and 5.7. The concentration gradient, like in the previous case, is largest at minimum thicknesses of the layers.

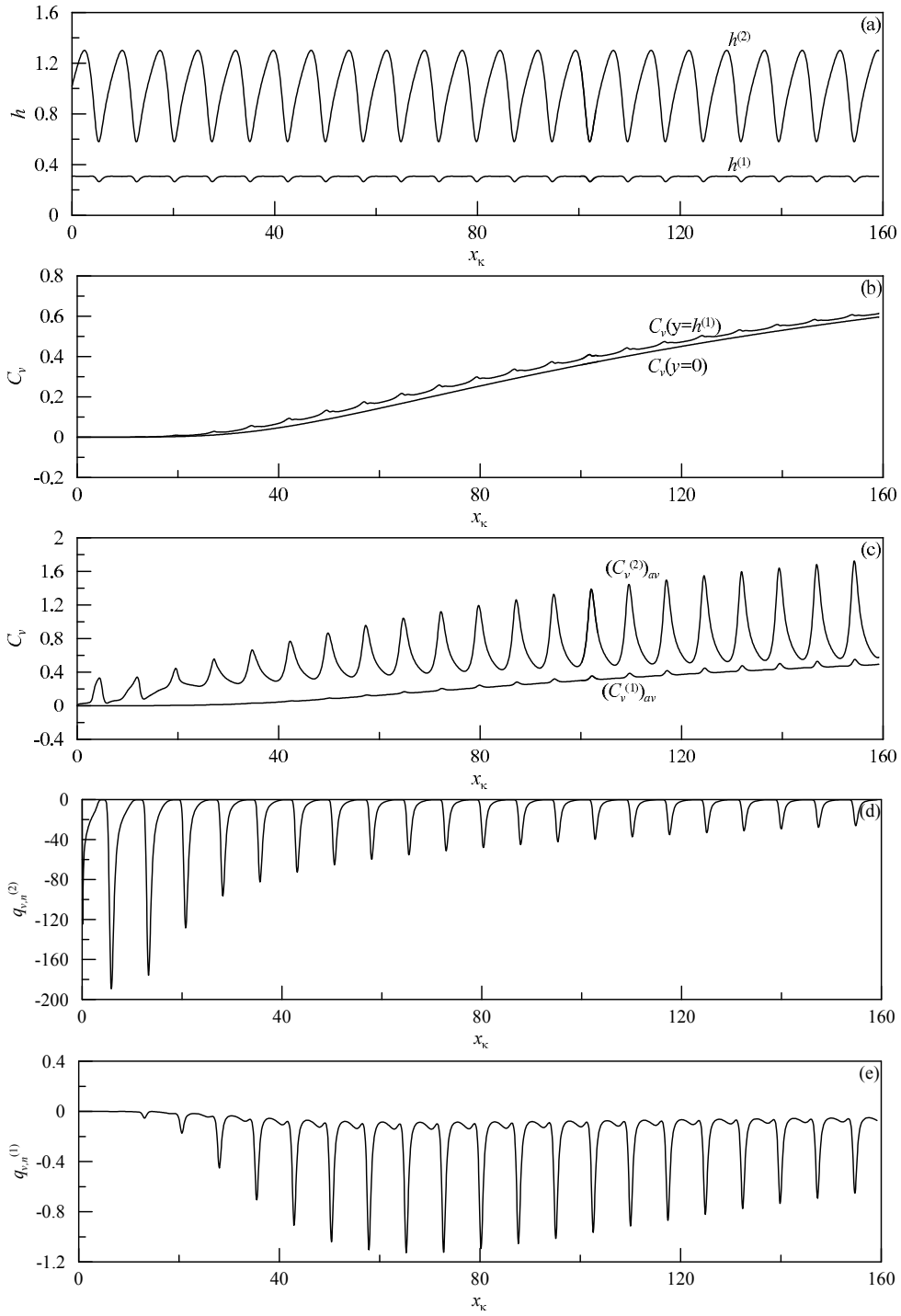

Figure 5.3: Instant profiles of the interface and surface (a), the interface and surface concentrations (b), the average concentrations in the layers (c), the local fluxes at the surface (d) and interface (e) at $\delta = 0.1$, $H = 0.3$ and $s = 0.6$ in water-benzene system.

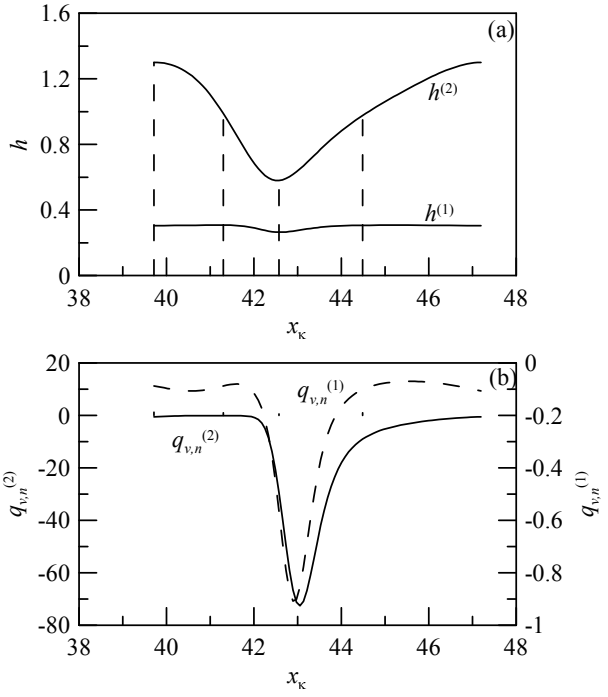

Figure 5.4: Instant profiles of the interface and surface (a) and the local fluxes (b) at the inlet area in the case shown in Fig. 5.3.

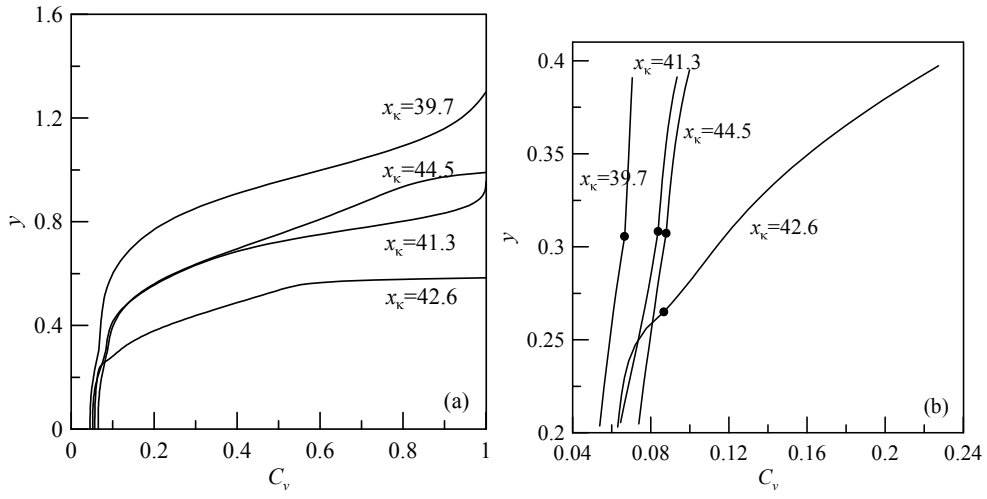

Figure 5.5: Global (a) and local (b) instant profiles of concentration at the inlet area in the case shown in Fig. 5.3.

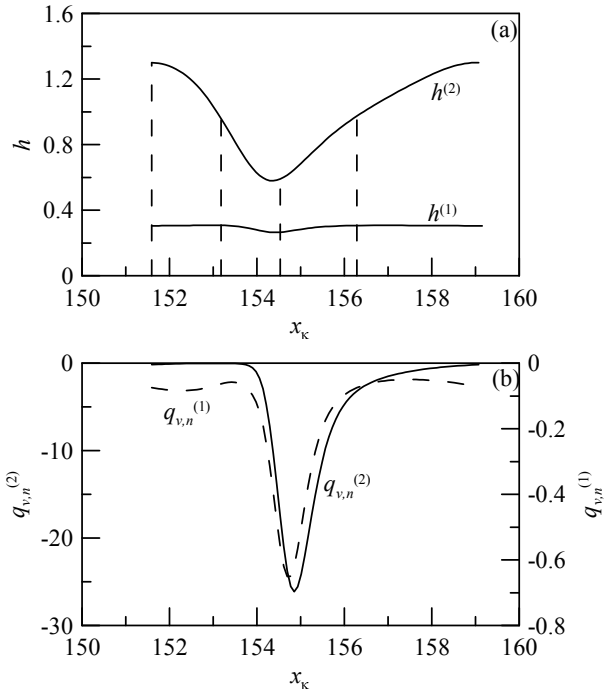

Figure 5.6: Instant profiles of the interface and surface (a) and the local fluxes (b) at the outlet area in the case shown in Fig. 5.3.

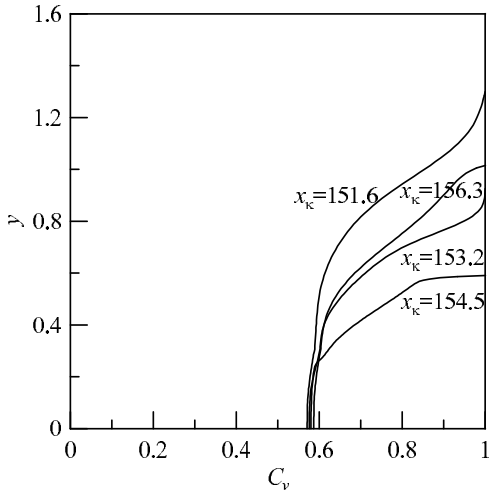

Figure 5.7: Instant profiles of concentration at the outlet area in the case shown in Fig. 5.3.

To analyse the absorption in the dominating wave regime belonging to the family $\gamma^3_{+1,1}$ at $H = 0.3$ and $s = 0.3$, we have plotted Fig. 5.8. Comparing all the panels in Fig. 5.3 with Fig. 5.8, we see ripples at the front of the wave in Fig. 5.8. In Fig. 5.8b, the differences of concentration on the interface and the surface is larger.

Considering the Fig. 5.6, there are additional small oscillations on interface and surface in Fig. 5.9 and the local fluxes at layers are greater. The gas concentration in a few sections at the inlet area is shown in Fig. 5.10.

Fig. 5.11 shows minimum and maximum values of $\lambda^{(2)} = Q^{(2)}_{v,n}/Q^{(2)}_{v,n,0}$ and $\lambda^{(1)} = Q^{(1)}_{v,n}/Q^{(1)}_{v,n,0}$ for absorption in regimes of the dominating waves at $H = 0.3$ where the values denoted by the subscript 0 are relevant to the waveless flow. We can see that wavy regimes drastically increase the absorption rate.

For demonstrating the effect of the average first layer thickness H, the absorption characteristics in the dominating wave of the family $\gamma^3_{+1,1}$ at $H = 0.6$ and $s = 0.2$ is shown in Fig. 5.12. The amplitude of humps at surface, see Fig. 5.12a, are bigger than the case $H = 0.3$ and $s = 0.3$, see Fig. 5.8a. It is seen that in all panels of Fig. 5.12, there are large oscillations of all parameters, for example, the gas concentrations, the average concentrations in both layers. It is not clearly seen but the values of C_v are positive in the corresponding panels. The local fluxes at the surface and the interface in Fig. 5.12d and e are also larger.

Fig. 5.13 shows maximum and minimum values of $\lambda^{(1)}$ and $\lambda^{(2)}$ at the surface and interface in some dominating waves at $H = 0.6$. This figure also demonstrates that the absorption rate increases in wavy films.

The absorption is also affected by the boundary conditions at $x_\kappa = 0$. Let's consider the case when $C^{(1)}_{v(\zeta)}\Big|_{x_\kappa=0} = 1, C^{(2)}_{v(\zeta)}\Big|_{x_\kappa=0} = 0$. Fig. 5.14 shows the case $H = 0.6$ and $s = 0.5$, when the dominating wave belongs to $\gamma^1_{-1,1}$. In Fig. 5.14a, while the surface profile is similar to Fig. 5.3a,the amplitude of the interface waves is relatively bigger. Unlike

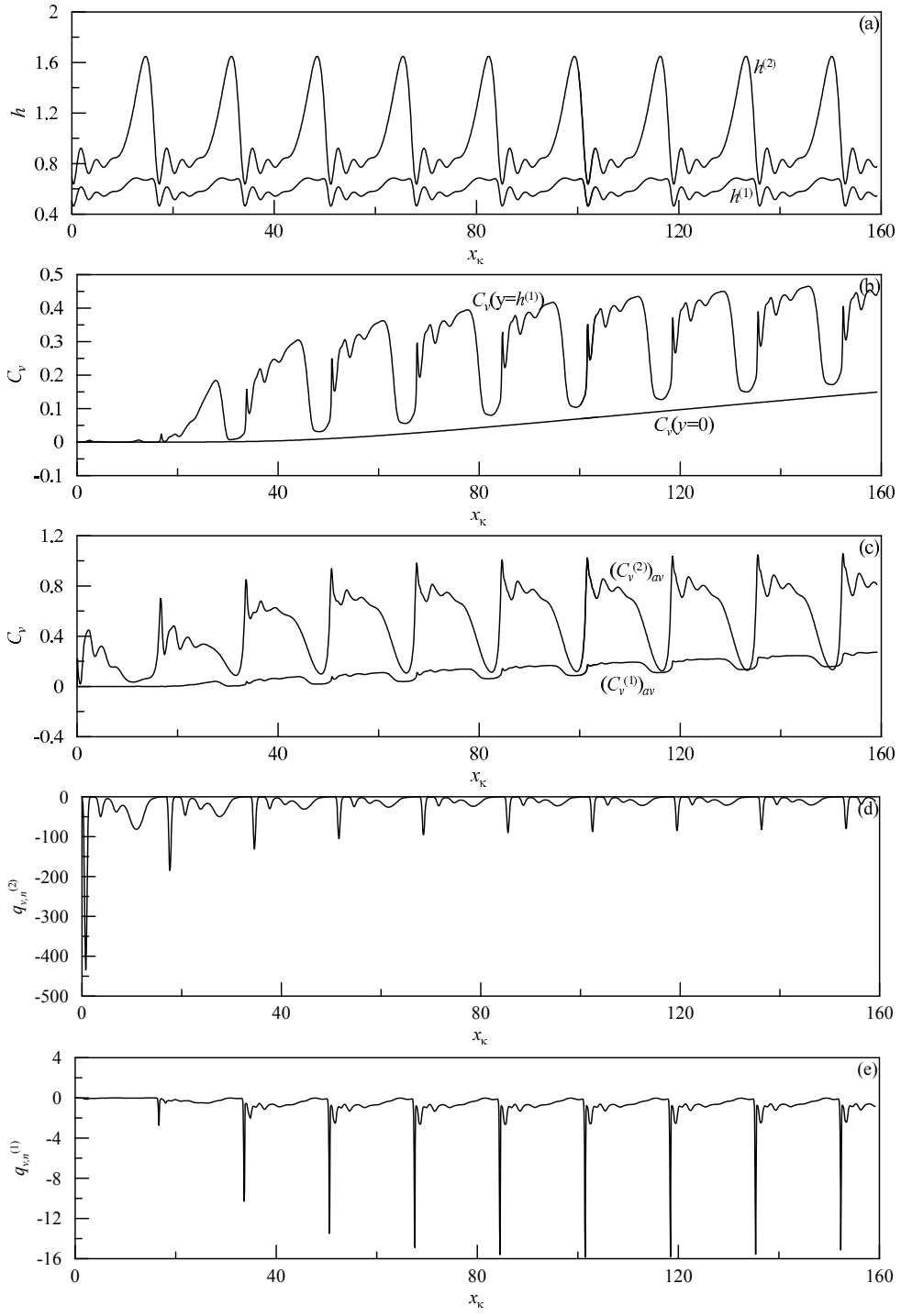

Figure 5.8: Instant profiles of the interface and surface (a), the interface and wall concentrations (b), the average concentrations in the layers (c), the local fluxes at the surface (d) and interface (e) at $\delta = 0.1$, $H = 0.3$ and $s = 0.3$ in water-benzene system.

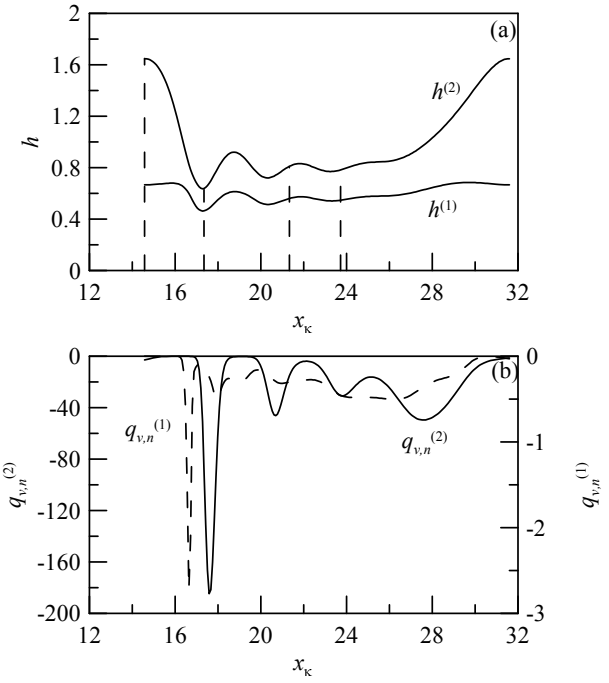

Figure 5.9: Instant profiles of the interface and surface (a) and the local fluxes (b) at the inlet area in the case shown in Fig. 5.8.

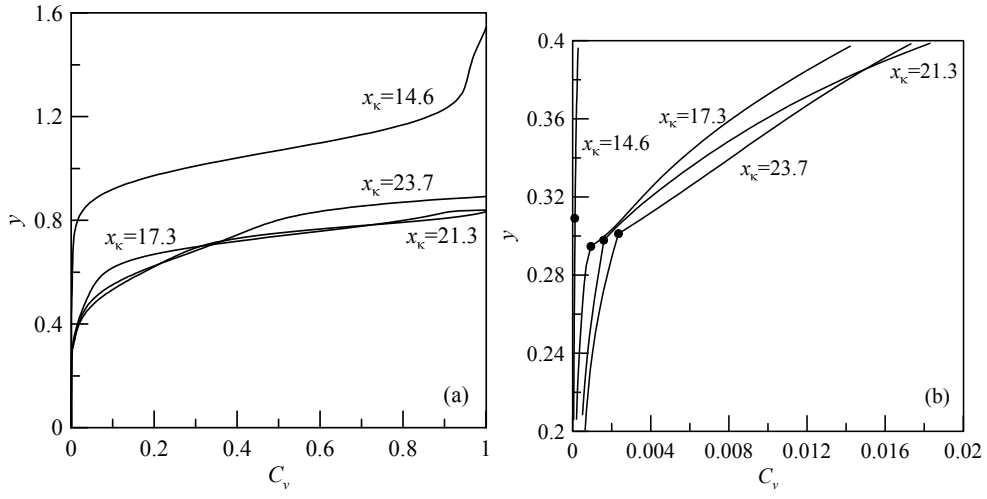

Figure 5.10: Global (a) and local (b) instant profiles of concentration at the inlet area in the case shown in Fig. 5.8.

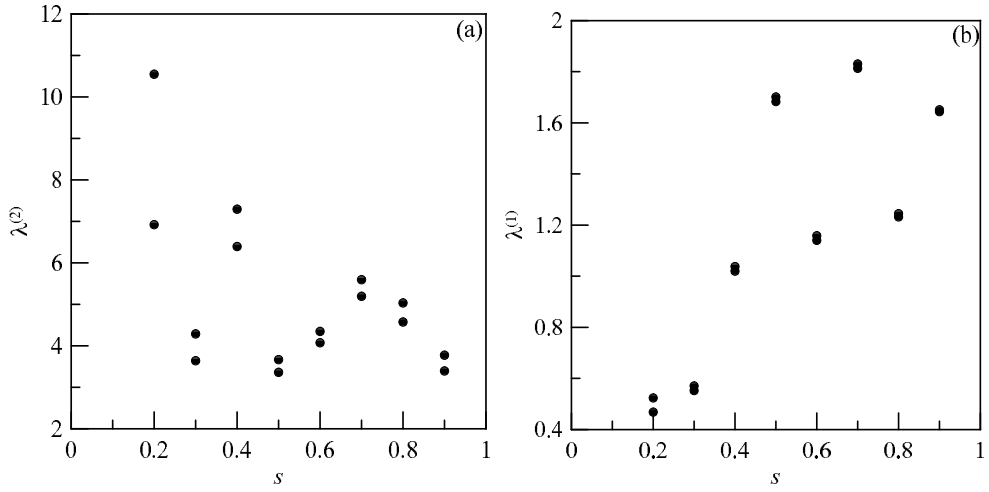

Figure 5.11: Minimum and maximum values of $\lambda^{(2)}$ (a) and $\lambda^{(1)}$ (b) at $H = 0.3$.

the previous cases, the wall concentration decreases slightly and interface concentrations increases with oscillations until the saturation begins, see Fig. 5.14b. It is seen that in Fig. 5.14c, the graphs of average concentrations in the layers overlap. The local fluxes at the surface and interface are smaller than the other cases, see Fig. 5.14d and Fig. 5.14e since there are gas in the first layer at $x_\kappa = 0$.

Different from the other cases, see Fig. 5.4b and 5.9b, the local fluxes of layers at the inlet area does not imitate each other, see Fig. 5.15b.

The concentration of gas at the inlet area decreases first and then increases dramatically for different values of x_κ shown in Fig. 5.16.

It is worthy to say that the absorption rate is essentially increased in wavy regimes in comparison with the waveless flow.

The main mechanism as shown above is local increasing gradients of concentration across each layer, and this is similar to the case of one-layer film. In this study, the case of a film rupture is not studied, and thus we do not discuss how it could affect the mass transfer.

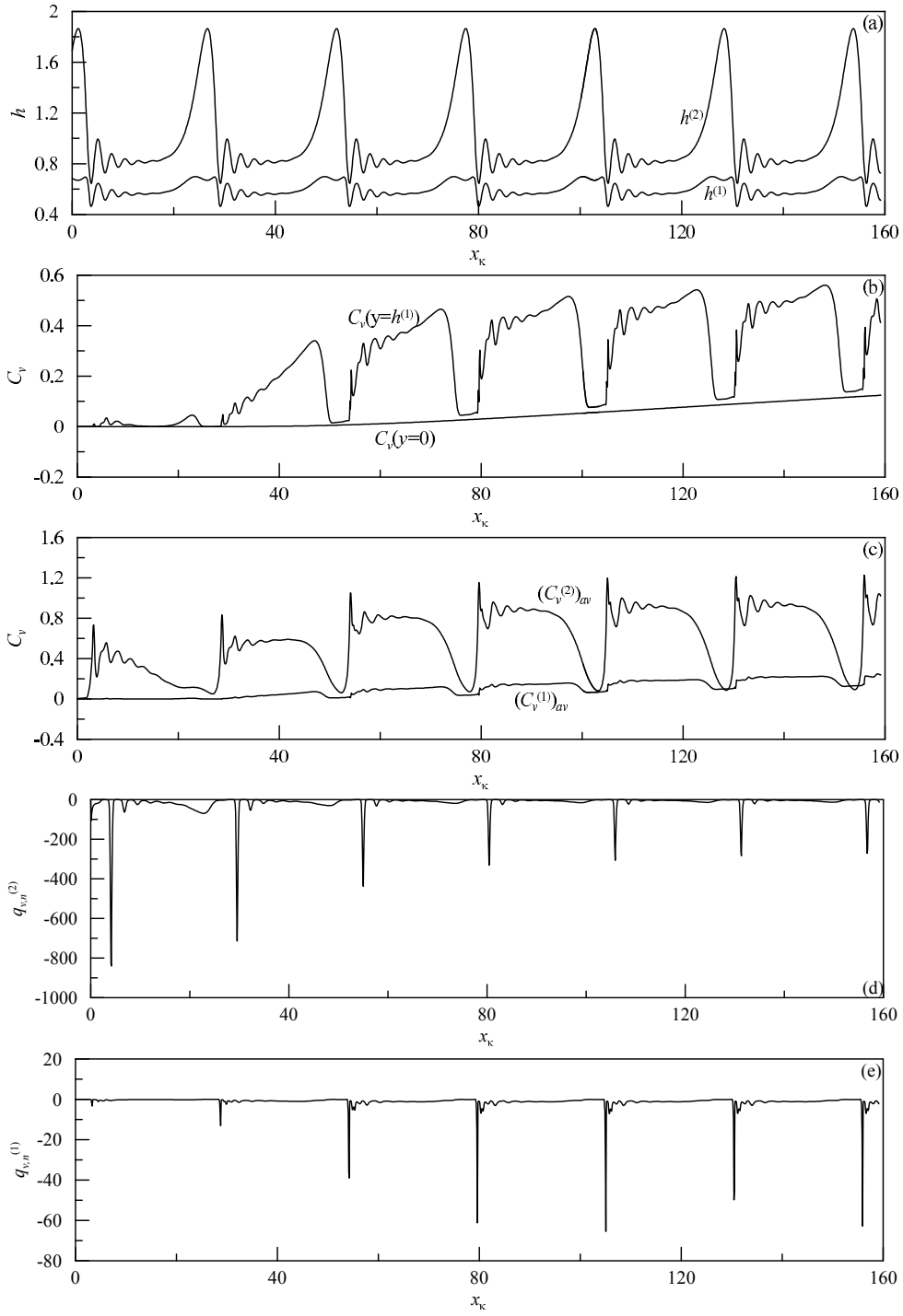

Figure 5.12: Instant profiles of the interface and surface (a), the interface and wall concentrations (b), the average concentrations in the layers (c), the local fluxes at the surface (d) and interface (e) at $H = 0.6$ and $s = 0.2$.

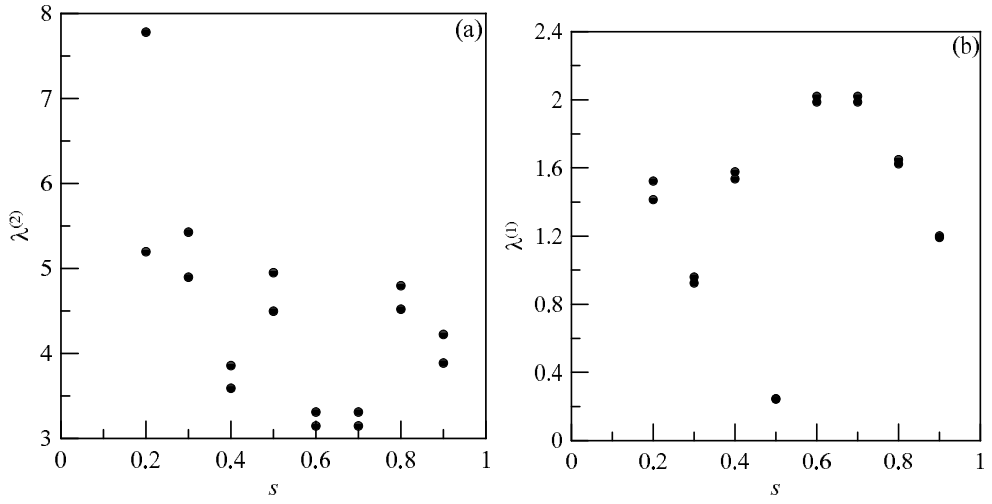

Figure 5.13: Minimum and maximum values of $\lambda^{(2)}$ (a) and $\lambda^{(1)}$ (b) at $H = 0.6$.

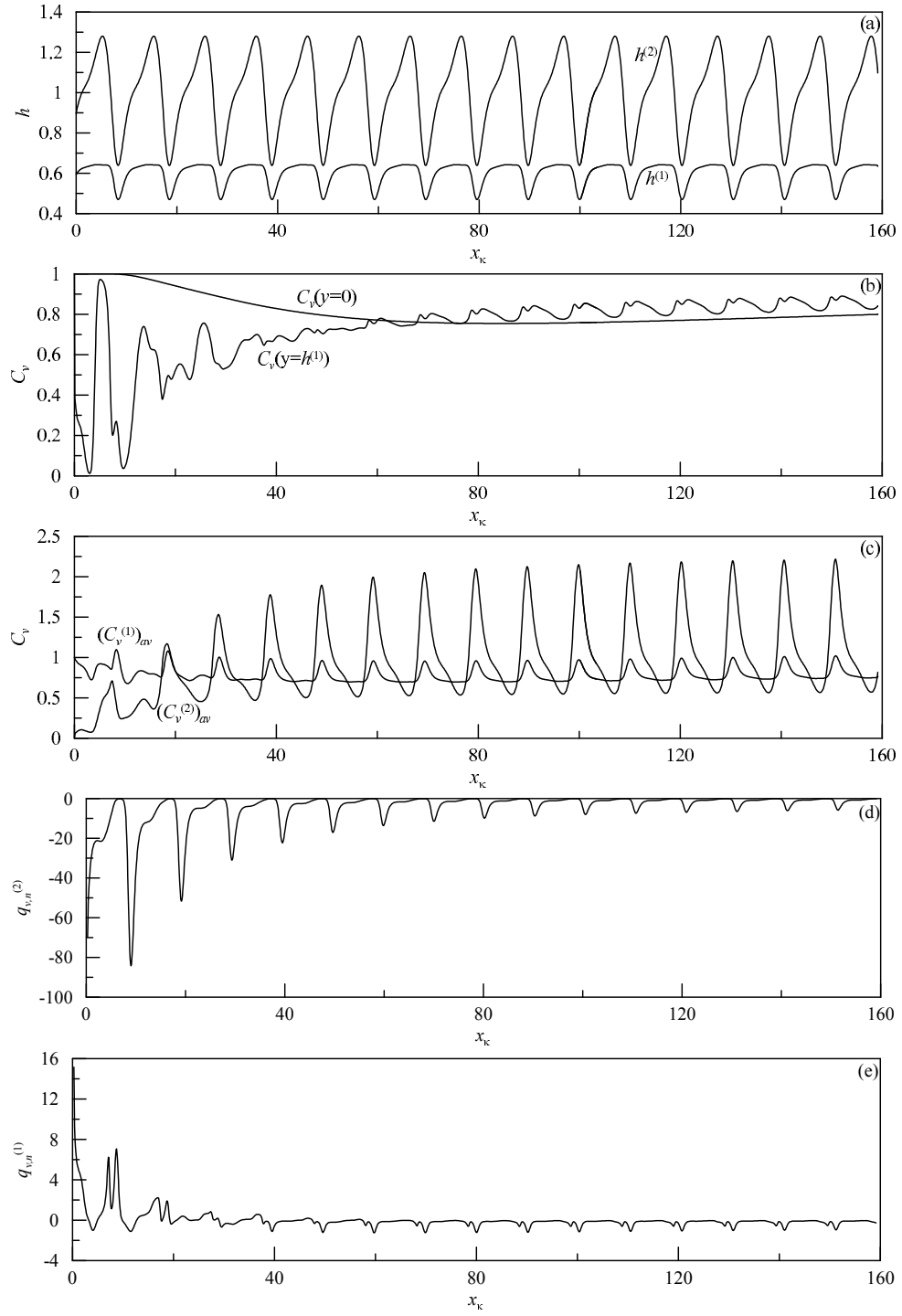

Figure 5.14: Instant profiles of the interface and surface (a), the interface and wall concentrations (b), the average concentrations in the layers (c), the local fluxes at the surface (d) and interface (e) at $\delta = 0.1$, $H = 0.6$ and $s = 0.5$ at the initial conditions with $C^{(1)}(y) = 1$, $C^{(2)}(y) = 0$.

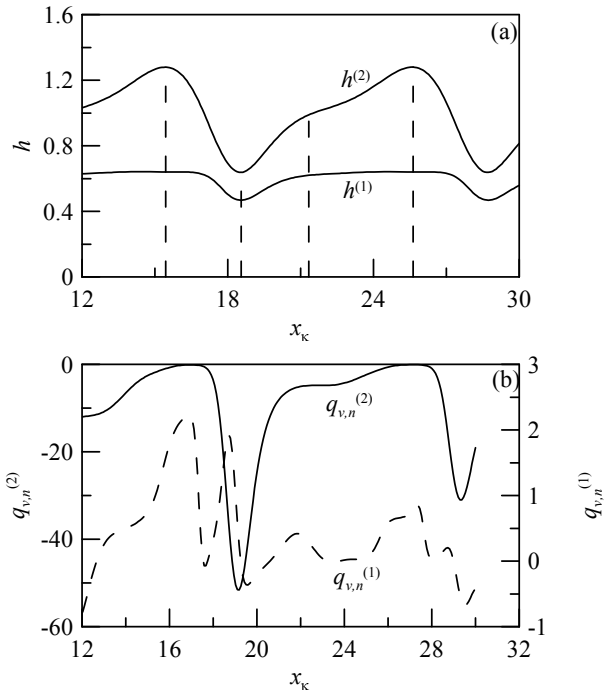

Figure 5.15: Instant profiles of the interface and surface (a) and the local fluxes (b) at the inlet area in the case shown in Fig. 5.14.

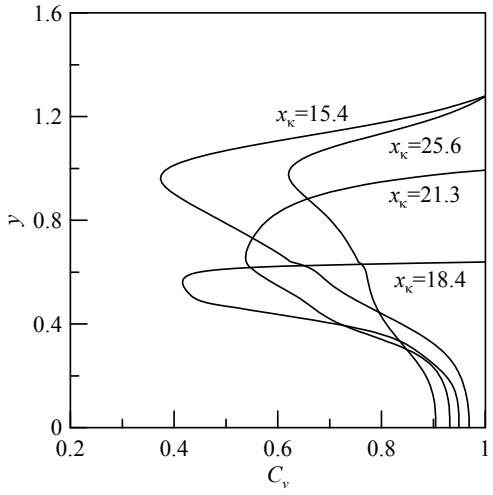

Figure 5.16: Instant profiles of concentration at the inlet area in the case shown in Fig. 5.14.

Chapter 6

Conclusion

In this thesis, we use approximate evolution equations to model a two-layer film flowing down a vertical wall and compute the absorption of a weakly soluble gas into the film.

To derive the evolution equations, the full Navier-Stokes problem for the two-layer film flow is firstly simplified for long-wave flows when the longitudinal length scale is much larger than the cross length scale. Then, the integral method with the parabolic approximation of the longitudinal velocity is used to derive evolution equations for the film thickness, the first layer thickness and flow rates in the first layer and the whole film.

The linear analysis of the waveless flow in the framework of the evolution equations has been carried out and compared with results of the generalized Orr-Sommerfeld problem obtained earlier. The comparison of the linear spectra verified the model.

In contrast to the case of one-layer film flows, two-layer films possess two unstable modes. One mode corresponds to the film surface and it is similar to the mode in the one-layer film. Another mode with very small amplification factors is associated with the interface. The domain of instability of the interface mode is localized at small values of the wavenumbers.

For the first time, strongly nonlinear waves in a two-layer falling liquid film have been calculated at real-life values of the similarity parameters. The bifurcation schemes of the

wave families have been calculated for different values of the similarity parameters. In particular, the role of the interface location has been revealed.

Non-uniqueness of the solutions raises a question of how to select solutions which can be used for comparison with experimental data. Transient numerical computations have been carried out to find attracting flow regimes, so-called dominating waves in two-layer films. It has been shown that in most cases, the developing wave regimes are oscillating regimes in neighbourhoods of steady-travelling space-periodic waves with maximum film thickness and wave velocity. In the corresponding phase space, these attracting waves are two-dimensional tori. Predominance of oscillating regimes developing in the two-layer film flow differ from one-layer film flows where the dominating waves are steady-travelling waves, or the limit cycles in the phase space in a wide range of wavenumbers. As follows from the examples shown in Chapter 4, the oscillating regimes are characterized by absence of coherence of waves at the surface and interface.

These results are applied to select wave regimes that could be used to model experiments, in particular, mass transfer of a weakly soluble gas in the film.

It has been shown that, similar to the one-layer film flow, the absorption rate is increased in wavy regimes in comparison with the waveless flow, and this amplification has a place at the interface between liquids as well as at the film surface. Numerous transient computations have demonstrated that the growth of the absorption rate is explained by nonuniform distribution of the concentration gradient along the film surface and the interface. The largest gradients and thus local gas fluxes at the surface and interface are observed at wave troughs where thicknesses of the first layer and the whole film have minimums.

In future work, small wave numbers will be investigated for the unsteady dynamics. Also, the existence of solitary waves in two-layer films will be analysed to understand the behaviour of very long waves. Such waves have special dynamics in the case of the

one-layer film and the dynamics of the two-layer film is also affected by the interface instability existing only in this domain.

Appendix A

Numerical algorithm to solve the Orr-Sommerfeld problem

To solve the eigenvalue problem (2.9), we represent solutions in each layer in the form:

$$\vec{w}^{(1)} = A^{(1,1)}\vec{w}^{(1,1)} + A^{(1,2)}\vec{w}^{(1,2)}, \quad \vec{w}^{(2)} = A^{(2,1)}\vec{w}^{(2,1)} + A^{(2,2)}\vec{w}^{(2,2)}. \tag{A.1}$$

Here the functions $w^{(1,1)}(y)$ and $w^{(1,2)}(y)$ are particular linearly independent solutions in layer 1, and they satisfy the boundary conditions at $y = 0$. Similar, $w^{(2,1)}(y)$ and $w^{(2,2)}(y)$ are particular linearly independent solutions in layer 2, and they satisfy the boundary conditions at $y = 1$.

Then, the boundary conditions at $y = H$ give us a system of linear algebraic equations for the coefficients $A^{(1,1)}$, $A^{(1,2)}$, $A^{(2,1)}$, $A^{(2,2)}$. The characteristic equation for calculating an eigenvalue c as function of the similarity parameters and the wavenumber follows from the condition that the system determinant is zero.

The numerical algorithm to compute an eigenvalue c is reduced to solve the following equation $F(c; \alpha, \mathrm{Re}, \mathrm{We}, \rho_0, \nu_0, \sigma_0, H) = 0$ where the function F is calculated as follows:

1. Two Cauchy's problems for (2.9) are solved with the corresponding initial conditions

at $y = 0$

$$w_1^{(1,1)} = 0, \quad w_2^{(1,1)} = 0, \quad w_3^{(1,1)} = 1, \quad w_4^{(1,1)} = 0,$$
$$w_1^{(1,2)} = 0, \quad w_2^{(1,2)} = 0, \quad w_3^{(1,2)} = 0, \quad w_4^{(1,2)} = 1,$$

and the velocity profile

$$U = \frac{1}{\varphi\nu_0}\left(a^{(1)}y - \frac{y^2}{2}\right), \quad U' = \frac{1}{\varphi\nu_0}\left(a^{(1)} - y\right), \quad U'' = -\frac{1}{\varphi\nu_0}.$$

2. Two Cauchy's problems for (2.9) are solved with the corresponding initial conditions at $y = 1$

$$w_1^{(2,1)} = 1, \quad w_2^{(2,1)} = 0, \quad w_3^{(2,1)} = -\left(\alpha^2 - \frac{U''}{U-c}\right),$$
$$w_4^{(2,1)} = -\left[\frac{i\alpha}{U-c}\frac{\alpha^2\mathrm{Re}}{\mathrm{We}} + \left(i\alpha\mathrm{Re} + \frac{2\alpha^2}{U-c}\right)U'\right];$$
$$w_1^{(2,2)} = 0, \quad w_2^{(2,2)} = 1, \quad w_3^{(2,2)} = 0, \quad w_4^{(2,2)} = 3\alpha^2 + i\alpha\mathrm{Re}(U-c),$$

and the velocity profile

$$U = \frac{1}{\varphi}\left(a^{(2)} + y - \frac{y^2}{2}\right), \quad U' = \frac{1}{\varphi}\left(1 - y\right), \quad U'' = -\frac{1}{\varphi}.$$

3. The function F is computing from the boundary conditions (2.9) at $y = H$:

$$F\left(\alpha, c; \delta, \rho_0, \nu_0, \sigma_0, H\right) \equiv \det\left(L_{mn}\right) = 0,$$

where the entries of the matrix (L_{mn}) are computed at $y = H$ as

$$
\begin{aligned}
k = 1, 2 \quad : \quad & L_{1,k} = w_1^{(1,k)}, \quad L_{2,k} = w_2^{(1,k)} - \frac{U'}{U-c} w_1^{(1,k)}, \\
& L_{3,k} = \rho_0 \nu_0 \left\{ w_3^{(1,k)} + \left(\alpha^2 - \frac{U''}{U-c} \right) w_1^{(1,k)} \right\}, \\
& L_{4,k} = \rho_0 \nu_0 \Bigg\{ w_4^{(1,k)} - \left[3\alpha^2 + \frac{i\alpha \mathrm{Re}}{\nu_0} (U-c) \right] w_2^{(1,k)} + \\
& \qquad \left[\frac{i\alpha \mathrm{Re} U'}{\nu_0} + \frac{1}{U-c} 2\alpha^2 U' \right] w_1^{(1,k)} \Bigg\} + \frac{i\alpha^3 \sigma_0 \mathrm{Re}}{\mathrm{We}\,(U-c)} w_1^{(1,k)}, \\
& L_{1,k+2} = -w_1^{(2,k)}, \quad L_{2,k+2} = -w_2^{(2,k)} + \frac{U'}{U-c} w_1^{(2,k)}, \\
& L_{3,k+2} = - \left[w_3^{(2,k)} + \left(\alpha^2 - \frac{U''}{U-c} \right) w_1^{(2,k)} \right], \\
& L_{4,k+2} = - \Bigg\{ w_4^{(2,k)} - \left[3\alpha^2 + i\alpha \mathrm{Re}(U-c) \right] w_2^{(2,k)} + \\
& \qquad \left[i\alpha \mathrm{Re} U' + \frac{1}{U-c} 2\alpha^2 U' \right] w_1^{(2,k)} \Bigg\}.
\end{aligned}
$$

If an eigenfunction corresponding to an eigenvalue c has to be found from the linear system

$$
\begin{aligned}
L_{11} A^{(1,1)} + L_{12} A^{(1,2)} + L_{13} A^{(2,1)} + L_{14} A^{(2,2)} = 0, \\
L_{21} A^{(1,1)} + L_{22} A^{(1,2)} + L_{23} A^{(2,1)} + L_{24} A^{(2,2)} = 0, \\
L_{31} A^{(1,1)} + L_{32} A^{(1,2)} + L_{33} A^{(2,1)} + L_{34} A^{(2,2)} = 0, \\
L_{41} A^{(1,1)} + L_{42} A^{(1,2)} + L_{43} A^{(2,1)} + L_{44} A^{(2,2)} = 0,
\end{aligned}
$$

we can take $A^{(2,2)} = \epsilon$, where ϵ is an arbitrary value, and then the coefficients $A^{(1,1)}$, $A^{(1,2)}$

and $A^{(2,1)}$ are calculated from the system

$$L_{11}A^{(1,1)} + L_{12}A^{(1,2)} + L_{13}A^{(2,1)} = -L_{14}A^{(2,2)},$$
$$L_{21}A^{(1,1)} + L_{22}A^{(1,2)} + L_{23}A^{(2,1)} = -L_{24}A^{(2,2)},$$
$$L_{31}A^{(1,1)} + L_{32}A^{(1,2)} + L_{33}A^{(2,1)} = -L_{34}A^{(2,2)}.$$

Then, (A.1) gives us solutions in each layer.

The method was developed in [62].

Appendix B

Nonlinear system for Fourier coefficients of steady-travelling space-periodic waves

To apply Newton's iteration method, new variables

$$
\begin{aligned}
&y_{2n-1} = \left(a_n^{\left(h^{(1)}\right)}\right)_r, \quad y_{2n} = \left(a_n^{\left(h^{(1)}\right)}\right)_i, \quad n = 1, \ldots, N-1, \\
&y_{2N-2+2n-1} = \left(a_n^{\left(h^{(2)}\right)}\right)_r, \quad y_{2N-2+2n} = \left(a_n^{\left(h^{(2)}\right)}\right)_i, \quad n = 1, \ldots, N-1, \\
&y_{4N-3} = p^{(j_1)}, \quad y_{4N-2} = p^{(j_2)}, \quad y_{4N-1} = p^{(j_3)},
\end{aligned}
$$

are defined, where $p^{(j_1)}$, $p^{(j_2)}$ and $p^{(j_3)}$ are three variables of c, $q_0^{(1)}$, $q_0^{(2)}$ and s. Since one of the variables c, $q_0^{(1)}$, $q_0^{(2)}$ and s is arbitrary, we obtained one-parametric family of solutions.

For finding steady-travelling waves, we get nonlinear algebraic system of order $4N-1$ for $y_1, \ldots, y_{4N-1}$:

$$
\begin{aligned}
&\left(f_n^{(1)}\right)_r = 0, \quad \left(f_n^{(1)}\right)_i = 0, \quad n = 1, \ldots, N-1, \\
&\left(f_n^{(2)}\right)_r = 0, \quad \left(f_n^{(2)}\right)_i = 0, \quad n = 1, \ldots, N-1,
\end{aligned}
\tag{B.1}
$$

$$\left(f_N^{(1)}\right)_r = 0, \quad \left(f_N^{(2)}\right)_r = 0,$$
$$y_{4N-5}\tan\eta_0 + y_{4N-4} = 0,$$

where $f_n^{(1)}$ and $f_n^{(2)}$ are coefficients of the Fourier series

$$f^{(1)} = \sum_{n=1}^{2N} f_n^{(1)} e^{i(N-n)\eta}, \quad f_n^{(1)} = \overline{f_{2N-n}^{(1)}}, n = 1, \ldots, N, \quad f_{2N}^{(1)} = 0$$
$$f^{(2)} = \sum_{n=1}^{2N} f_n^{(2)} e^{i(N-n)\eta}, \quad f_n^{(2)} = \overline{f_{2N-n}^{(2)}}, n = 1, \ldots, N, \quad f_{2N}^{(2)} = 0$$

of the left-hand sides of equations (3.3) after substitution of the solutions.

The last equation in (B.1) corresponds to a given phase η_0 of the first harmonic of $h^{(2)}$:

$$\begin{aligned}
h^{(2)}(\eta) &= \sum_{n=1}^{2N} a_n^{\left(h^{(2)}\right)} e^{i(N-n)\eta} \\
&= \sum_{n=1}^{N-2} a_n^{\left(h^{(2)}\right)} e^{i(N-n)\eta} + a_{N-1}^{\left(h^{(2)}\right)} e^{i\eta} + 1 + a_{N+1}^{\left(h^{(2)}\right)} e^{-i\eta} + \sum_{n=N+2}^{2N} a_n^{\left(h^{(2)}\right)} e^{i(N-n)\eta} \\
&= \sum_{n=1}^{N-2} a_n^{\left(h^{(2)}\right)} e^{i(N-n)\eta} + \left[\left(a_{N-1}^{\left(h^{(2)}\right)}\right)_r + i\left(a_{N-1}^{\left(h^{(2)}\right)}\right)_i\right](\cos\eta + i\sin\eta) + 1 \\
&+ \left[\left(a_{N+1}^{\left(h^{(2)}\right)}\right)_r + i\left(a_{N+1}^{\left(h^{(2)}\right)}\right)_i\right](\cos\eta - i\sin\eta) + \sum_{n=N+2}^{2N} a_n^{\left(h^{(2)}\right)} e^{i(N-n)\eta} \\
&= \sum_{n=1}^{N-2} a_n^{\left(h^{(2)}\right)} e^{i(N-n)\eta} + \left[\left(a_{N-1}^{\left(h^{(2)}\right)}\right)_r + i\left(a_{N-1}^{\left(h^{(2)}\right)}\right)_i\right](\cos\eta + i\sin\eta) + 1 \\
&+ \left[\left(a_{N-1}^{\left(h^{(2)}\right)}\right)_r - i\left(a_{N-1}^{\left(h^{(2)}\right)}\right)_i\right](\cos\eta - i\sin\eta) + \sum_{n=N+2}^{2N} a_n^{\left(h^{(2)}\right)} e^{i(N-n)\eta} \\
&= 1 + 2\left[\left(a_{N-1}^{\left(h^{(2)}\right)}\right)_r \cos\eta - \left(a_{N-1}^{\left(h^{(2)}\right)}\right)_i \sin\eta\right] + \sum_{n=1}^{N-2} a_n^{\left(h^{(2)}\right)} e^{i(N-n)\eta} \\
&+ \sum_{n=N+2}^{2N} a_n^{\left(h^{(2)}\right)} e^{i(N-n)\eta}
\end{aligned}$$

$$
\begin{aligned}
&= 1 + 2\sqrt{\left(a_{N-1}^{\left(h^{(2)}\right)}\right)_r^2 + \left(a_{N-1}^{\left(h^{(2)}\right)}\right)_i^2} \\
&\times \left[\frac{\left(a_{N-1}^{\left(h^{(2)}\right)}\right)_r}{\sqrt{\left(a_{N-1}^{\left(h^{(2)}\right)}\right)_r^2 + \left(a_{N-1}^{\left(h^{(2)}\right)}\right)_i^2}} \cos\eta - \frac{\left(a_{N-1}^{\left(h^{(2)}\right)}\right)_i}{\sqrt{\left(a_{N-1}^{\left(h^{(2)}\right)}\right)_r^2 + \left(a_{N-1}^{\left(h^{(2)}\right)}\right)_i^2}} \sin\eta \right] \\
&+ \sum_{n=1}^{N-2} a_n^{\left(h^{(2)}\right)} e^{i(N-n)\eta} + \sum_{n=N+2}^{2N} a_n^{\left(h^{(2)}\right)} e^{i(N-n)\eta} \\
&= 1 + 2\sqrt{\left(a_{N-1}^{\left(h^{(2)}\right)}\right)_r^2 + \left(a_{N-1}^{\left(h^{(2)}\right)}\right)_i^2} \cos\left(\eta - \eta_0\right) + \sum_{n=1}^{N-2} a_n^{\left(h^{(2)}\right)} e^{i(N-n)\eta} \\
&+ \sum_{n=N+2}^{2N} a_n^{\left(h^{(2)}\right)} e^{i(N-n)\eta}
\end{aligned}
$$

where

$$
\sin\eta_0 = -\frac{\left(a_{N-1}^{\left(h^{(2)}\right)}\right)_i}{\sqrt{\left(a_{N-1}^{\left(h^{(2)}\right)}\right)_r^2 + \left(a_{N-1}^{\left(h^{(2)}\right)}\right)_i^2}}, \quad \cos\eta_0 = \frac{\left(a_{N-1}^{\left(h^{(2)}\right)}\right)_r}{\sqrt{\left(a_{N-1}^{\left(h^{(2)}\right)}\right)_r^2 + \left(a_{N-1}^{\left(h^{(2)}\right)}\right)_i^2}},
$$

and thus

$$
\tan\eta_0 = -\frac{\left(a_{N-1}^{\left(h^{(2)}\right)}\right)_i}{\left(a_{N-1}^{\left(h^{(2)}\right)}\right)_r} = -\frac{y_{4N-4}}{y_{4N-5}}.
$$

Appendix C

Velocity of harmonics

We consider the projection of a phase trajectory onto the complex plane of the Fourier coefficient of $h^{(1)}(\eta,\tau)$ or $h^{(2)}(\eta,\tau)$:

$$a_n^{(h)}(\tau) \equiv a_{n,r}^{(h)}(\tau) + i a_{n,i}^{(h)}(\tau) = \rho_n^{(h)}(\tau) e^{i\psi_n^{(h)}(\tau)},$$

where $\rho_n^{(h)}$ and $\psi_n^{(h)}$ are the amplitude and phase of nth harmonics. Then,

$$\rho_{2N-n}^{(h)} = \rho_n^{(h)}, \quad \psi_{2N-n}^{(h)} = -\psi_n^{(h)}.$$

We can rewrite the thickness as follows:

$$\begin{aligned}
h(\eta,\tau) &= \sum_{n=1}^{2N} \rho_n^{(h)} e^{i\left[\psi_n^{(h)} + (N-n)(\eta-\eta_0)\right]} \\
&= \sum_{n=1}^{N-1} \rho_n^{(h)} e^{i\left[\psi_n^{(h)} + (N-n)(\eta-\eta_0)\right]} + \rho_N^{(h)} e^{i\psi_N^{(h)}} + \sum_{n=N+1}^{2N-1} \rho_n^{(h)} e^{i\left[\psi_n^{(h)} + (N-n)(\eta-\eta_0)\right]} \\
&= \sum_{n=1}^{N-1} \rho_n^{(h)} e^{i\left[\psi_n^{(h)} + (N-n)(\eta-\eta_0)\right]} + \rho_N^{(h)} e^{i\psi_N^{(h)}} + \sum_{n=1}^{N-1} \rho_{2N-n}^{(h)} e^{i\left[\psi_{2N-n}^{(h)} - (N-n)(\eta-\eta_0)\right]} \\
&= \sum_{n=1}^{N-1} \rho_n^{(h)} e^{i\left[\psi_n^{(h)} + (N-n)(\eta-\eta_0)\right]} + \rho_N^{(h)} e^{i\psi_N^{(h)}} + \sum_{n=1}^{N-1} \rho_n^{(h)} e^{-i\left[\psi_n^{(h)} + (N-n)(\eta-\eta_0)\right]}
\end{aligned}$$

$$= 2\sum_{n=1}^{N-1} \rho_n^{(h)} \cos\left[\psi_n^{(h)} + (N-n)(\eta - \eta_0)\right] + \rho_N^{(h)} e^{i\psi_N^{(h)}}.$$

In plane (η, τ), the equation

$$\psi_n^{(h)}(\tau) + (N-n)(\eta - \eta_0) = \text{constant}$$

determines a curve of the permanent phase of nth harmonics. By the definition, the velocity of nth harmonics is the velocity along this curve, that is

$$c_n(\tau) \equiv \frac{d\eta}{d\tau} = -\frac{1}{N-n}\frac{d\psi_n^{(h)}}{d\tau}.$$

To calculate the velocity, we can write by definition, tangent of the phase and then differentiate it:

$$\tan\psi_n^{(h)} = \frac{a_{n,i}^{(h)}}{a_{n,r}^{(h)}}, \quad \frac{d\psi_n^{(h)}}{d\tau} = \frac{\cos^2\psi_n^{(h)}}{\left(a_{n,r}^{(h)}\right)^2}\left(a_{n,r}^{(h)}\frac{da_{n,i}^{(h)}}{d\tau} - a_{n,i}^{(h)}\frac{da_{n,r}^{(h)}}{d\tau}\right).$$

Then, the velocity of nth harmonics is found as

$$c_n(\tau) = -\frac{1}{N-n}\frac{1}{\left(a_{n,r}^{(h)}\right)^2 + \left(a_{n,i}^{(h)}\right)^2}\left(a_{n,r}^{(h)}\frac{da_{n,i}^{(h)}}{d\tau} - a_{n,i}^{(h)}\frac{da_{n,r}^{(h)}}{d\tau}\right).$$

This formula derived in [55] allows us to compute velocities of the harmonics in transient computations.

Appendix D

Solving diffusion problem

We solve the equations (5.6) using the following algorithms:

$$
\begin{aligned}
&\check{C}_{v,1,m} = C_{v,l}\left(\zeta_M, \tau_v\right), \quad m = 1, \ldots, M^{(2)},\\
&\check{C}_{v,n,M^{(2)}} = C_{v,s}\left(\xi_{v,n}, \tau_v\right), \quad n = 1, \ldots, N,\\
&\check{C}_{v,n,m} = \left(1 + \frac{\triangle\tau_v}{2\triangle\xi_v}u^{(2)}\Big|_{\xi_{v,n},\zeta_m,\tau_v} - \frac{\triangle\tau_v}{2\triangle\zeta^{(2)}}V^{(2)}\Big|_{\xi_{v,n},\zeta_m,\tau_v}\right)^{-1} \times\\
&\quad\left[C_{v,n,m} + \frac{\triangle\tau_v}{2\triangle\xi_v}u^{(2)}\Big|_{\xi_{v,n},\zeta_m,\tau_v}\check{C}_{v,n-1,m} - \frac{\triangle\tau_v}{2\triangle\zeta^{(2)}}V^{(2)}\Big|_{\xi_{v,n},\zeta_m,\tau_v}\check{C}_{v,n,m+1}\right.\\
&\quad\left.+\frac{\triangle\tau_v}{2}\left(\chi^{(2)}\frac{\partial^2 C_v}{\partial\zeta^2}\right)\Big|_{\xi_{v,n},\zeta_m,\tau_v}\right],\\
&\quad m = M^{(2)} - 1, \ldots, M^{(1)}, \quad n = 2, \ldots, N,\\
&\check{C}_{v,n,m} = \left(1 + \frac{\triangle\tau_v}{2\triangle\xi_v}u^{(1)}\Big|_{\xi_{v,n},\zeta_m,\tau_v} - \frac{\triangle\tau_v}{2\triangle\zeta^{(1)}}V^{(1)}\Big|_{\xi_{v,n},\zeta_m,\tau_v}\right)^{-1} \times\\
&\quad\left[C_{v,n,m} + \frac{\triangle\tau_v}{2\triangle\xi_v}u^{(1)}\Big|_{\xi_{v,n},\zeta_m,\tau_v}\check{C}_{v,n-1,m} - \frac{\triangle\tau_v}{2\triangle\zeta^{(1)}}V^{(1)}\Big|_{\xi_{v,n},\zeta_m,\tau_v}\check{C}_{v,n,m+1}\right.\\
&\quad\left.+\frac{\triangle\tau_v}{2}\left(\chi^{(1)}\frac{\partial^2 C_v}{\partial\zeta^2}\right)\Big|_{\xi_{v,n},\zeta_m,\tau_v}\right],\\
&\quad m = M^{(1)} - 1, \ldots, 1 \quad n = 2, \ldots, N.
\end{aligned}
$$

We solve the diffusion equations (5.7) with the following boundary conditions:

$$\begin{aligned}
&\frac{\hat{C}_{v,n,2}-\hat{C}_{v,n,1}}{\triangle\zeta}=0,\\
&D_0^{(2)}\frac{\hat{C}_{v,n,M^{(1)}+1}-\hat{C}_{v,n,M^{(1)}}}{\triangle\zeta^{(2)}}=D_0^{(1)}\frac{\hat{C}_{v,n,M^{(1)}}-\hat{C}_{v,n,M^{(1)}-1}}{\triangle\zeta^{(1)}},\\
&\hat{C}_{v,n,M^{(2)}}=C_{v,s}\left(\xi_{v,n},\tau_v\right),\quad n=1,\ldots,N.
\end{aligned}$$

Combining the equations and these boundary conditions, we arrive at the following algorithm:

$$\begin{aligned}
&n=1:\quad \hat{C}_{v,1,m}=C_{v,l}\left(\zeta_m,\tau_v+\triangle\tau_v\right),\quad m=1,\ldots,M^{(2)},\\
&n=2,\ldots,N:\\
&\quad A_m\hat{C}_{v,n,m-1}-B_m\hat{C}_{v,n,m}+C_m\hat{C}_{v,n,m+1}=D_m,\quad m=1,\ldots,M^{(2)},\\
&\qquad m=1:\quad A_m=0,\quad B_m=1,\quad C_m=1,\quad D_m=0,\\
&\qquad m=2,\ldots,M^{(1)}-1:\\
&\qquad\quad A_m=\frac{\triangle\tau_v}{2\left(\triangle\zeta^{(1)}\right)^2}\lambda\chi^{(1)}\Big|_{\xi_{v,n},\tau_v+\triangle\tau_v},\\
&\qquad\quad B_m=1+\frac{\triangle\tau_v}{\left(\triangle\zeta^{(1)}\right)^2}\lambda\chi^{(1)}\Big|_{\xi_{v,n},\tau_v+\triangle\tau_v},\\
&\qquad\quad C_m=\frac{\triangle\tau_v}{2\left(\triangle\zeta^{(1)}\right)^2}\lambda\chi^{(1)}\Big|_{\xi_{v,n},\tau_v+\triangle\tau_v},\\
&\qquad\quad D_m=-\left(1-\lambda\right)\frac{\triangle\tau_v}{2\left(\triangle\zeta^{(1)}\right)^2}\chi^{(1)}\Big|_{\xi_{v,n},\tau_v+\frac{\triangle\tau_v}{2}}\left(\check{C}_{v,n,m+1}+\check{C}_{v,n,m-1}\right)\\
&\qquad\qquad-\left[1-\left(1-\lambda\right)\frac{\triangle\tau_v}{\left(\triangle\zeta^{(1)}\right)^2}\chi^{(1)}\Big|_{\xi_{v,n},\tau_v+\frac{\triangle\tau_v}{2}}\right]\check{C}_{v,n,m}\\
&\qquad\qquad+\frac{\triangle\tau_v}{2}\left(u^{(1)}\frac{\partial C_v}{\partial\xi_v}+V^{(1)}\frac{\partial C_v}{\partial\zeta}\right)\Big|_{\xi_{v,n},\zeta_m,\tau_v+\frac{\triangle\tau_v}{2}},
\end{aligned}$$

$$
\begin{aligned}
&m = M^{(1)}: \quad A_m = \frac{D_0^{(1)}}{D_0^{(2)}} \frac{\triangle \zeta^{(1)}}{\triangle \zeta^{(2)}}, \quad B_m = 1 + \frac{D_0^{(1)}}{D_0^{(2)}} \frac{\triangle \zeta^{(1)}}{\triangle \zeta^{(2)}}, \quad C_m = 1, \quad D_m = 0, \\
&m = M^{(1)} + 1, \ldots, M^{(2)} - 1: \\
&\quad A_m = \frac{\triangle \tau_v}{2 \left(\triangle \zeta^{(2)} \right)^2} \lambda \chi^{(2)} \Big|_{\xi_{v,n}, \tau_v + \triangle \tau_v}, \\
&\quad B_m = 1 + \frac{\triangle \tau_v}{\left(\triangle \zeta^{(2)} \right)^2} \lambda \chi^{(2)} \Big|_{\xi_{v,n}, \tau_v + \triangle \tau_v}, \\
&\quad C_m = \frac{\triangle \tau_v}{2 \left(\triangle \zeta^{(2)} \right)^2} \lambda \chi^{(2)} \Big|_{\xi_{v,n}, \tau_v + \triangle \tau_v}, \\
&\quad D_m = -(1-\lambda) \frac{\triangle \tau_v}{2 \left(\triangle \zeta^{(2)} \right)^2} \chi^{(2)} \Big|_{\xi_{v,n}, \tau_v + \frac{\triangle \tau_v}{2}} \left(\check{C}_{v,n,m+1} + \check{C}_{v,n,m-1} \right) \\
&\qquad - \left[1 - (1-\lambda) \frac{\triangle \tau_v}{\left(\triangle \zeta^{(2)} \right)^2} \chi^{(2)} \Big|_{\xi_{v,n}, \tau_v + \frac{\triangle \tau_v}{2}} \right] \check{C}_{v,n,m} \\
&\qquad + \frac{\triangle \tau_v}{2} \left(u^{(2)} \frac{\partial C_v}{\partial \xi_v} + V^{(2)} \frac{\partial C_v}{\partial \zeta} \right) \Big|_{\xi_{v,n}, \zeta_m, \tau_v + \frac{\triangle \tau_v}{2}}, \\
&m = M^{(2)}: \quad A_m = 0, \quad B_m = 1, \quad C_m = 0, \quad D_m = -C_{v,s} \left(\xi_{v,n}, \tau_v \right).
\end{aligned}
$$

Tridiagonal matrix is solved by the shooting method.

To calculate coefficients D_m the following formulas are used:

$$
\left. \frac{\partial C_v}{\partial \xi_v} \right|_{\xi_{v,n}, \zeta_m, \tau_v + \frac{\triangle \tau_v}{2}} = \begin{cases} \frac{1}{2 \triangle \xi_v} \left(\check{C}_{v,n+1,m} - \check{C}_{v,n-1,m} \right), & n = 2, \ldots, N-1, \\ \frac{1}{\triangle \xi_v} \left(\frac{1}{2} \check{C}_{v,N-2,m} - 2 \check{C}_{v,N-1,m} + \frac{3}{2} \check{C}_{v,N,m} \right), & n = N. \end{cases}
$$

List of References

[1] D. J. Acheson. *Elementary Fluid Dynamics*. Oxford University Press, 1990.

[2] C. Albert, H. Marschall, and D. Bothe. Direct Numerical Simulation of interfacial mass transfer into falling films. *International Journal of Heat and Mass Transfer*, 69:343–357, 2014.

[3] S. V. Alekseenko, V. E. Nakoryakov, and B. T. Pokusaev. *Wave Flow of Liquid Films*. Begel House, Inc., New York, 1994.

[4] D. D. Back and M. G. McCready. Theoretical study of interfacial transport in gas-liquid flows. *AIChE Journal*, 34(11):1789–1802, 1988.

[5] T. B. Benjamin. Wave formation in laminar flow down an inclined plane. *Journal of Fluid Mechanics*, 2:554–574, 1957.

[6] A. V. Bunov, E. A. Demekhin, and V. Ya. Shkadov. On the nonuniqueness of nonlinear wave solutions in a viscous layer. *Journal of Applied Mathematics and Mechanics*, 48(4):691–696, 1984.

[7] P. Carreau, D. D. Kee, and M. Daroux. An analysis of the viscous behaviour of polymeric solutions. *Canadian Journal of Chemical Engineering*, 57:135–140, 1979.

[8] G. Cekic. Two-layer falling film, 2013. MRes(qual).

[9] H.-C. Chang and E. A. Demekhin. *Complex Wave Dynamics on Thin Films*. Elsevier, Amsterdam, 2002.

[10] Hsueh-Chang Chang, E. A. Demekhin, and D. L. Kopelevich. Nonlinear evolution of waves on a vertically falling film. *Journal of Fluid Mechanics*, 250:433–480, 1993.

[11] K. P. Chen. Wave formation in the gravity-driven low-Reynolds number flow of two liquid films down an inclined plane. *Physics of Fluids A*, 5(12):3038–3048, 1993.

[12] P. V. Danckwerts. Significance of liquid-film coefficients in gas absorption. *Industrial and Engineering Chemistry*, 43(6):1460–1467, 1951.

[13] E. A. Demekhin and V. Ya. Shkadov. On nonstationary waves in the layer of liquid layer. *Fluid Dynamics*, 16(3):151–154, 1981.

[14] P. G. Drazin. *Introduction to Hydrodynamic Stability*. Cambridge University Press, Cambridge, 2002.

[15] R. E. Emmert and R. L. Pigford. A study of gas absorption in falling liquid films. *Chemical Engineering Progress*, 50(2):87–93, 1954.

[16] G. P. Galdi. *An Introduction to the Mathematical Theory of the Navier-Stokes Equations*, volume 2. Springer-Verlag, New York, 1994.

[17] C. T. Gallagher, D. T. Leighton, and M. J. McCready. Experimental investigation of a two-layer shearing instability in a cylindrical couette cell. *Physics of Fluids*, 8(9):2385–2392, 1996.

[18] P. Gao and X.-Y. Lu. Mechanism of the long-wave inertialess instability of a two-layer film flow. *Journal of Fluid Mechanics*, 608:379–391, 2008.

[19] S. L. Goren and R. V. S. Mani. Mass transfer through horizontal liquid films in wavy motion. *AIChE Journal*, 14(1):57–61, 1968.

[20] W. H. Henstock and T. J. Hanratty. Gas absoption by a liquid layer flowing on the wall of a pipe. *AIChE Journal*, 25(1):122–131, 1979.

[21] R. Higbie. The rate of absorption of pure gas into a still liquid during short periods of exposure. *Transactions of the American Institute of Chemical Engineers*, 31:365–389, 1935.

[22] E. J. Hinch. A note on the mechanism of the instability at the interface between two shearing fluids. *Journal of Fluid Mechanics*, 144:463–465, 1984.

[23] A. P. Hooper. Long-wave instability at the interface between two viscous fluids: thin layer effects. *Physics of Fluids*, 28(6):1613–1618, 1985.

[24] A. P. Hooper and W. G. C. Boyd. Shear-flow instability at the interface between two viscosity fluids. *Journal of Fluid Mechanics*, 128:507–528, 1983.

[25] A. P. Hooper and R. Grimshaw. Nonlinear instability at the interface between two viscous fluids. *Physics of Fluids*, 28(1):37–45, 1985.

[26] J. Hu, S. Millet, V. Botton, H. B. Hadid, and D. Henry. Inertialess temporal and spatio-temporal stability analysis of the two-layer film flow with density stratification. *Physics of Fluids*, 18:104101, 2006.

[27] J. Hu, X. Y. Yin, H. B. Hadid, and D. Henry. Linear temporal and spatiotemporal stability analysis of the two-layer falling film flows with density stratification. *Physical Review E*, 77:026302, 2008.

[28] J. C. Jepsen, O. K. Crosser, and R. H. Perry. The effect of wave induced turbulence on the rate of absorption of gases in falling liquid films. *AIChE Journal*, 12(1):186–192, 1966.

[29] W. Y. Jiang, B. Helenbrook, and S. P. Lin. Inertialess instability of a two-layer liquid film flow. *Physics of Fluids*, 16:652–663, 2004.

[30] W. Y. Jiang and S. P. Lin. Enhancement or suppression of instability in a two-layered liquid film flow. *Physics of Fluids*, 17:1–8, 2005.

[31] T. W. Kao. Role of the interface in the stability of stratified flow down an inclined plane. *Physics of Fluids*, 8:2190–2194, 1965.

[32] T. W. Kao. Stability of two-layer viscous stratified flow down an inclined plane. *Physics of Fluids*, 8:812, 1965.

[33] T. W. Kao. Role of viscosity stratification in the stability of two-layer flow down an incline. *Journal of Fluid Mechanics*, 33:561–572, 1968.

[34] P. L. Kapitza. Wave flow of a thin viscous fluid layer. I. Free flow. *Journal of Experimental and Theoretical Physics*, 18(1):3–20, 1948.

[35] P. L. Kapitza and S. P. Kapitza. Wave flow of thin viscous liquid films. III. Experimental study of wave regime of a flow. *Journal of Experimental and Theoretical Physics*, 19(2):105–120, 1949.

[36] L. P. Kholpanov and V. Ya. Shkadov. *Hydrodynamics and Heat and Mass Transfer at Interfaces*. Nauka, Moscow, 1990.

[37] J. D. Killion and S. Garimella. A critical review of models of coupled heat and mass transfer in falling-film absoption. *International Journal of Refrigeration*, 24:755–797, 2001.

[38] D. S. Loewenherz and C. J. Lawrence. The effect of viscosity stratification on the instability of a free surface flow at low reynolds number. *Physics of Fluids A*, 1:1686–1693, 1989.

[39] M. J. McCready and T. J. Hanratty. Effect of air shear on gas absorption by a liquid film. *AIChE Journal*, 31(12):2066–2074, 1985.

[40] S. Millet, V. Botton, H. B. Hadid, D. Henry, and F. Rousset. Stability of two-layer shear-thinning film flows. *Physical Review E*, 88:043004, 2013.

[41] K. Muenz and J. M. Marchello. Surface motion and gas absorption. *AIChE Journal*, 12(2):249–253, 1966.

[42] D. R. Oliver and T. E. Atherinos. Mass transfer to liquid films on an inclined plane. *Chemical Engineering Science*, 23:525–536, 1968.

[43] A. A. Rastaturin, E. A. Demekhin, and E. N. Kalaidin. Optimum regimes of mass transfer in fluid films. *Doklady-Physics*, 50(2):115–117, 2005.

[44] M. Renardy and Y. Y. Renardy. Derivation of amplitude equations and analysis of sideband instabilities in two-layer flows. *Physics of Fluids A*, 5:2738–2762, 2005.

[45] R. M. Roberts, Y. Ye, E. A. Demekhin, and H.-C. Chang. Wave dynamics in two-layer couette flow. *Chemical Engineering Science*, 55:345–362, 2000.

[46] Z. Rotem and J. E. Neilson. Exact solution for diffusion to flow down an incline. *Canadian Journal of Chemical Engineering*, 47(4):341–346, 1969.

[47] E. Ruckenstein and C. Berbente. Mass transfer in wave flow. *Chemical Engineering Science*, 20:795–801, 1965.

[48] C. Ruyer-Quil and P. Manneville. Improved modeling of flows down inclined planes. *The European Physical Journal B*, 15:357–369, 2000.

[49] C. Ruyer-Quil and P. Manneville. Further accuracy and convergence results on the modelling of flows down inclined planes by weighted-residual approximations. *Physics of Fluids*, 14(1):170–183, 2002.

[50] T. R. Salamon, R. C. Armstrong, and R. A. Brown. Travelling waves on inclined films: numerical analysis by the finite element method. *Physics of Fluids*, 6:2202–2220, 1994.

[51] P. J. Schmid and D. S. Henningson. On the stability of a falling liquid curtain. *Journal of Fluid Mechanics*, 463:163–171, 2002.

[52] V. Ya. Shkadov. Wave flow regimes of a thin layer of viscous fluid subject to gravity. *Fluid Dynamics*, 2(1):29–34, 1967.

[53] V. Ya. Shkadov and G. M. Sisoev. Wavy falling liquid films: theory and computation instead of physical experiment. In *IUTAM Symposium on Nonlinear Waves in Multi-Phase Flow*, pages 1–10, Notre Dame, USA, 2000. Notre Dame University.

[54] V. Ya. Shkadov and G. M. Sisoev. On the theory of solitary waves in flowing-down layer of viscous fluid. *Doklady-Physics*, 46(10):760–764, 2001.

[55] V. Ya. Shkadov and G. M. Sisoev. Waves induced by instability in falling films of finite thickness. *Fluid Dynamics Research*, 35(5):357–389, 2004.

[56] V. Ya. Shkadov and G. M. Sisoev. Numerical bifurcation analysis of the travelling waves for a falling liquid film. *Computers and Fluids*, 34(2):151–168, 2005.

[57] G. M. Sisoev. Bifurcation of attractor in falling film problem. *International Journal on Non-Linear Mechanics*, 43:246–263, 2008.

[58] G. M. Sisoev and C. J. Bennett. Solitary and transitional waves in gravity-driven two-layer microchannel flow. *Fluid Dynamics Research*, 45:015503, 2013.

[59] G. M. Sisoev and C. J. Bennett. Solitary and transitional waves in pressure-driven two-layer microchannel flow. *Fluid Dynamics Research*, 46:025504, 2014.

[60] G. M. Sisoev, O. K. Matar, and C. J. Lawrence. Absorption of gas into a wavy falling film. *Chemical Engineering Science*, 60:827–838, 2005.

[61] G. M. Sisoev, O. K. Matar, and C. J. Lawrence. Gas absorption into a wavy film flowing over a spinning disc. *Chemical Engineering Science*, 60:2049–2058, 2005.

[62] G. M. Sisoev and V. Ya. Shkadov. Instability of two-layer film flow along an inclined surface. *Fluid Dynamics*, 27(2):160–165, 1992.

[63] G. M. Sisoev and V. Ya. Shkadov. Development of dominating waves from small disturbances in falling viscous-liquid films. *Fluid Dynamics*, 32(6):784–792, 1997.

[64] G. M. Sisoev and V. Ya. Shkadov. Dominant waves in a viscous liquid flowing in a thin sheet. *Doklady-Physics*, 42(12):683–686, 1997.

[65] G. M. Sisoev and V. Ya. Shkadov. A two-parameter manifold of wave solutions to an equation for a falling film of a viscous fluid. *Doklady-Physics*, 44(7):454–459, 1999.

[66] M. K. Smith. The mechanism for the long-wave instability in thin liquid films. *Journal of Fluid Mechanics*, 217:469–485, 1990.

[67] Yu. Ya. Trifonov and O. Yu. Tsvelodub. Nonlinear waves on the surface of a falling liquid film. Part 1. Waves of the first family and their stability. *Journal of Fluid Mechanics*, 229:531–554, 1991.

[68] O. Yu. Tsvelodub and Yu. Ya. Trifonov. On steady-state travelling solutions of an evolution equation describing the behavior of disturbances in an active dissipative media. *Physica D:Nonlinear Phenomena*, 39:336–351, 1989.

[69] O. Yu. Tsvelodub and Yu. Ya. Trifonov. Nonlinear waves on the surface of a falling liquid film. Part 2. Bifurcations of the first-family waves and other types of nonlinear waves. *Journal of Fluid Mechanics*, 244:149–169, 1992.

[70] Z. Wang, S. P. Lin, and Z. Zhou. Spatio-temporal instability of two-layer liquid film at small reynolds numbers. *Applied Mathematics and Mechanics*, 31:1–12, 2010.

[71] M. H. Ward. Interfacial thin films rupture and self-similarity. *Physics of Fluids*, 23:062105, 2011.

[72] F. K. Wasden and A. E. Dukler. A numerical study of mass transfer in free falling wavy films. *AIChE Journal*, 36(9):1379–1390, 1990.

[73] Y. S. Won and A. F. Mills. Correlation of the effects of viscosity and surface tension on gas absorption rates into freely falling turbulent liquid films. *International Journal of Heat and Mass Transfer*, 25(2):223–229, 1982.

[74] Z. F. Xu, B. C. Khoo, and N. E. Wijeysundera. Mass transfer across the falling film:simulations and experiments. *Chemical Engineering Science*, 63:2559–2575, 2008.

[75] C. S. Yih. Stability of parallel laminar flow with a free surface. In *Proceedings of the second U. S. national congress of applied mechanics*, pages 623–628, New York, 1955. American Society of Mechanical Engineers.

[76] C. S. Yih. Stability of liquid flow down an inclined plane. *Physics of Fluids*, 6(3):321–334, 1963.

[77] C.-S. Yih. Instability due to viscosity stratification. *Journal of Fluid Mechanics*, 27(2):337–352, 1967.

[78] P. N. Yoshimura, T. Nosoko, and T. Nagata. Enhancement of mass transfer into a falling laminar liquid film by two-dimensional surface waves - some experimental observations and modeling. *Chemical Engineering Science*, 51(8):1231–1240, 1996.

[79] Y. Zhao, G. Chen, and Q. Yuan. Liquid-liquid two-phase flow patterns in a rectangular microchannels. *AIChE Journal*, 52(12):4052–4060, 2006.